

FRAME SYNCHRONIZATION FOR PSAM IN AWGN AND RAYLEIGH FADING CHANNELS

A Thesis Submitted to the College of
Graduate Studies and Research
In Partial Fulfillment of the Requirements
for the Degree of Master of Science
in the Department of Electrical Engineering
University of Saskatchewan
Saskatoon

By

Haozhang Jia

Saskatoon, Saskatchewan, Canada

© Copyright Haozhang Jia, August, 2005. All rights reserved.

PERMISSION TO USE

In presenting this thesis in partial fulfillment of the requirements for a degree of Master of Science from the University of Saskatchewan, the author agrees that the libraries of this university may make it freely available for inspection. The author further agrees that permission for copying of this thesis in many manners, in whole or in part, for scholarly purpose may be granted by the professor or professors who supervised this thesis work or, in their absence, by the head of Department or the Dean of the College of Graduate Studies and Research. It is understood that any copying or publication or use of this thesis or part for financial gain shall not be allowed without the author's written permission. It is also understood that recognition shall be given to the author and to the University of Saskatchewan in any scholarly use which may be made of any material in this thesis.

Requests for permission to copy or to make other use of material in this thesis in whole or part should be addressed to:

Head of the Department of Electrical Engineering,
57 Campus Drive
University of Saskatchewan,
Saskatoon, Saskatchewan.
Canada, S7N 5A9

ABSTRACT

Pilot Symbol Assisted Modulation (PSAM) is a good method to compensate for the channel fading effect in wireless mobile communications. In PSAM, known pilot symbols are periodically inserted into the transmitted data symbol stream and the receiver uses these symbols to derive amplitude and phase reference.

One aspect of this procedure, which has not received much attention yet, is the frame synchronization, i.e. the method used by the receiver to locate the time position of the pilot symbols. In this study, two novel non-coherent frame synchronization methods are introduced in which only the magnitude of received signal is used to obtain the timing of the pilot symbol. The methods are evaluated for both additive white Gaussian noise (AWGN) and frequency non-selective slow Rayleigh fading channels.

One synchronization technique is derived by standard maximum likelihood (ML) estimation formulation, and the other is obtained by using maximum a posteriori probability (MAP) with a threshold test. Signal processing in the receiver uses simplifying approximations that rely on relatively high signal-to-noise ratio (SNR) as consistent with the reception of 16-QAM. Computer simulation has been used to test the acquisition time performance and the probability of false acquisition. Several lengths and patterns of pilot symbol sequences were tested where every 10th symbol was a pilot symbol and all other symbols were randomly selected data symbols. When compared with the other published synchronizers, results from this study show better performance in both AWGN and fading channels. Significantly better performance is observed in the presence of receiver frequency offsets. Moreover, this method leads to simpler analysis and is somewhat easier to implement.

ACKNOWLEDGEMENTS

I want to express my most special gratitude to my supervisor Professor David E. Dodds, for his intelligent and patient guidance and for providing me financial support from a NSERC Discovery Grant.

I want to acknowledge Mr. Q. Zhang for his previous work on this project. I want to thank all the professors who have taught me classes. Their knowledge is an invaluable resource to me not only for my school life but also for my future career life.

I would also like to give my most particular thanks to my parents and my fiancée Ying Zhang for supporting me in all ways. Their love and patience give me the strength to make this thesis possible.

Finally, thanks are given to the Department of Electrical Engineering, College of Engineering and College of Graduate Studies & Research, University of Saskatchewan, for providing computer facilities support during this study.

DEDICATION

To my father Yuchun Jia and my mother Fenge Wang

TABLE OF CONTENTS

| | |
|---|-------------|
| PERMISSION TO USE | i |
| ABSTRACT..... | ii |
| ACKNOWLEDGEMENTS | iii |
| DEDICATION..... | iv |
| TABLE OF CONTENTS..... | v |
| LIST OF FIGURES..... | viii |
| LIST OF TABLES | xii |
| LIST OF ABBREVIATIONS | xiii |
| Chapter 1 Introduction..... | 1 |
| 1.1 Introduction of Frame Synchronization..... | 1 |
| 1.2 Review of Frame Synchronization Techniques | 3 |
| 1.3 Pilot Assisted Modulation..... | 5 |
| 1.3.1 Pilot Tone Assisted Modulation (PTAM)..... | 6 |
| 1.3.2 Pilot Symbol Assisted Modulation (PSAM)..... | 6 |
| 1.4 Objective of Thesis | 8 |
| 1.5 Thesis Organization | 8 |
| Chapter 2 Background Theory | 10 |

| | | |
|---|--|-----------|
| 2.1 | 16 State Quadrature Amplitude Modulation (16-QAM) | 10 |
| 2.2 | Nyquist Filtering (Squared Root Raised Cosine Filter)..... | 15 |
| 2.3 | Transmission Channel..... | 19 |
| 2.3.1 | Additive White Gaussian Noise Channel..... | 19 |
| 2.3.2 | Multi-path Rayleigh Fading Channel..... | 20 |
| 2.3.3 | Characterization of Fading Channel | 21 |
| 2.3.4 | Frequency Non-Selective Slow Fading..... | 24 |
| 2.4 | PSAM and Pilot Symbol Mapping | 27 |
| Chapter 3 Frame Synchronization..... | | 31 |
| 3.1 | Design Considerations | 31 |
| 3.2 | Non-Coherent Synchronizer | 32 |
| 3.3 | Channel Fading Estimation..... | 34 |
| 3.4 | Data Model | 37 |
| 3.5 | Maximum Likelihood Frame Synchronization..... | 40 |
| 3.5.1 | Synchronization in AWGN..... | 42 |
| 3.5.2 | Synchronization in Fading | 50 |
| 3.6 | Maximum A Posteriori Probability Frame Synchronization | 51 |
| 3.6.1 | Synchronization in AWGN..... | 51 |
| 3.6.2 | Synchronization in Fading | 51 |
| Chapter 4 Simulation Implementation..... | | 60 |
| 4.1 | Simulink® Introduction | 60 |
| 4.2 | System Overview | 61 |
| 4.2.1 | Transmitter Overview | 62 |

| | | |
|--|---|------------|
| 4.2.2 | Channel Model Overview | 66 |
| 4.2.3 | Receiver Overview..... | 72 |
| 4.2.4 | Frame Synchronizer Overview | 72 |
| Chapter 5 Simulation Results and Discussions..... | | 77 |
| 5.1 | Simulation System Description | 77 |
| 5.2 | Simulation Test Bench..... | 79 |
| 5.3 | Simulation Results and Performance Analysis | 81 |
| 5.3.1 | Performance in AWGN Channel | 81 |
| 5.3.2 | Performance in Fading Channel..... | 83 |
| 5.4 | Comparison to Existing Synchronizers..... | 86 |
| Chapter 6 Conclusions and Future Work..... | | 103 |
| 6.1 | Conclusions..... | 103 |
| 6.2 | Future Work..... | 104 |
| References | | 107 |
| Appendix A..... | | 111 |
| Appendix B..... | | 115 |

LIST OF FIGURES

| | | |
|----------|---|----|
| Fig. 1.1 | Block diagram of a general frame structure | 3 |
| Fig. 1.2 | Block diagram of a general PSAM system | 7 |
| Fig. 1.3 | Frame structure with pilot symbol inserted..... | 7 |
| Fig. 2.1 | A typical QAM system..... | 12 |
| Fig. 2.2 | 16-QAM square constellation using Gray encoding..... | 13 |
| Fig. 2.3 | Nyquist pulse and raised cosine spectrum (Taken from [20]) | 17 |
| Fig. 2.4 | A simple multi-path channel model | 20 |
| Fig. 2.5 | Response of a time-variant multi-path fading channel to a pulse | 21 |
| Fig. 2.6 | Transmission channel model..... | 26 |
| Fig. 2.7 | Frame structure for PSAM input signal | 27 |
| Fig. 2.8 | Pilot symbol mapping into 16-QAM..... | 29 |
| Fig. 3.1 | Components of the power of squared magnitude of the received signal $ r(k) ^2$ | 36 |
| Fig. 3.2 | PSAM transmitter and receiver structure | 37 |
| Fig. 3.3 | Different magnitudes in a square 16-QAM constellation | 44 |
| Fig. 3.4 | Input signal structure of for a PSAM system | 47 |
| Fig. 3.5 | Thresholds illustration..... | 58 |
| Fig. 4.1 | System structure (top level) | 61 |

| | | |
|--------------|--|----|
| Fig. 4.2 | Simulink block diagram of transmitter | 63 |
| Fig. 4.3 | Constellation of 16-QAM from Simulink | 63 |
| Fig. 4.4 | Mapping of a pilot sequence into 16-QAM symbols from Simulink..... | 64 |
| Fig. 4.5 | Pilot (BK7) + Data composite input signal | 65 |
| Fig. 4.6 | Pulse shaping block..... | 65 |
| Fig. 4.7 | Input signal and output of transmitter SRRC filter | 66 |
| Fig. 4.8 | Multi-path propagation channel | 67 |
| Fig. 4.9 | 16-QAM signal corrupted by a multi-path Rayleigh fading | 68 |
| Fig. 4.10 | 16-QAM signal corrupted by an AWGN channel..... | 69 |
| Fig. 4.11 | 16-QAM signal corrupted by multi-path Rayleigh fading and AWGN... | 70 |
| Fig. 4.12 | Simulation of frequency offset..... | 71 |
| Fig. 4.13 | Effect of fading and frequency offset to 16-QAM points | 71 |
| Fig. 4.14 | Simulink receiver block diagram | 72 |
| Fig. 4.15 | Simulink block diagram of non-coherent frame synchronizer..... | 73 |
| Fig. 4.16 | ML frame synchronization simulator..... | 74 |
| Fig. 4.17 | MAP frame synchronization simulator | 75 |
| Fig. 5.1 | Test bench for simulation..... | 79 |
| Fig. 5.2 (a) | ML, false acquisition in AWGN channel without frequency offset.... | 88 |
| Fig. 5.2 (b) | ML, false acquisition in AWGN channel with frequency offset = 0.02 f_{sy} | 88 |
| Fig. 5.2 (c) | ML, mean time to acquisition in AWGN channel without frequency offset..... | 89 |

| | |
|---|----|
| Fig. 5.2 (d) ML, mean time to acquisition in AWGN channel with frequency offset =0.02 f_{sy} | 89 |
| Fig. 5.3 (a) MAP, false acquisition in AWGN channel without frequency offset . | 90 |
| Fig. 5.3 (b) MAP, false acquisition in AWGN channel with frequency offset = 0.02 f_{sy} | 90 |
| Fig. 5.3 (c) MAP, mean time to acquisition in AWGN channel without frequency offset..... | 91 |
| Fig. 5.3 (d) MAP, mean time to acquisition in AWGN channel with frequency offset =0.02 f_{sy} | 91 |
| Fig. 5.4 (a) AWGN performance degradation of ML and MAP synchronizers vs. f_0 | 92 |
| Fig. 5.4 (b) AWGN performance degradation of ML synchronizer vs. f_0 | 92 |
| Fig. 5.4 (c) AWGN performance degradation of MAP synchronizer vs. f_0 | 93 |
| Fig. 5.5 (a) ML, false acquisition in fading channel with $f_d = 0.01$ and $f_0 = 0$.. | 94 |
| Fig. 5.5 (b) ML, false acquisition in fading channel with $f_d = 0.01$ and $f_0 = 0.02 f_{sy}$ | 94 |
| Fig. 5.5 (c) ML, mean time to synchronization in fading channel with $f_d = 0.01$ and $f_0 = 0$ | 95 |
| Fig. 5.5 (d) MAP, mean time to synchronization in fading channel with $f_d = 0.01$ and $f_0 = 0$ | 95 |

| | |
|--|-----|
| Fig. 5.6 (a) MAP, false acquisition of in fading channel with $f_d = 0.01$ and $f_0 = 0$ | 96 |
| Fig. 5.6 (b) MAP, false acquisition in fading channel with $f_d = 0.01$ and $f_0 = 0.02f_{sy}$ | 96 |
| Fig. 5.6 (c) Mean time to synchronization of MAP frame synchronizers in fading channel no freq. offset..... | 97 |
| Fig. 5.6 (d) Mean time to synchronization of MAP frame synchronizers in fading channel with freq. offset..... | 97 |
| Fig. 5.7 (a) Performance of ML and MAP synchronizers in fading channel vs. f_0 . | 98 |
| Fig. 5.7 (b) Performance of ML synchronizer in fading channel vs. f_0 and β | 98 |
| Fig. 5.7 (c) Performance of MAP synchronizer in fading channel vs. f_0 and β | 99 |
| Fig. 5.8 ML frame synchronizer under different fading rates | 100 |
| Fig. 5.9 MAP frame synchronizer under different fading rates | 100 |
| Fig. 5.10 Comparison of synchronizers in AWGN channel without carrier frequency offset and pilot sequence BK11 | 101 |
| Fig. 5.11 Comparison of synchronizers in AWGN channel with frequency offset = 1% and pilot sequence BK11 | 101 |
| Fig. 5.12 Comparison of synchronizers in fading channel with $f_d = 1\%$ of the. symbol rate without frequency offset and pilot sequence is BK11..... | 102 |

LIST OF TABLES

| | |
|--------------------------------------|----|
| Table 1 List of pilot sequences..... | 30 |
|--------------------------------------|----|

LIST OF ABBREVIATIONS

| | |
|--------|-------------------------------------|
| AWGN | Additive White Gaussian Noise |
| BER | Bit Error Rate |
| BK | Barker Code |
| FIR | Finite Impulse Response |
| GUI | Graphical User Interface |
| I-axis | In-Phase axis |
| I.I.D | Independent, Identical Distribution |
| ISI | Intersymbol Interference |
| LOS | Line of Sight |
| ML | Maximum Likelihood |
| MAP | Maximum A Posteriori Probability |
| N-H | Neuman-Hoffman |
| PAM | Pulse Amplitude Modulation |
| PDF | Probability Density Function |
| PN | Pseudorandom Noise |
| PSAM | Pilot Symbol Assisted Modulation |
| PSD | Power Spectral Density |
| PSK | Phase Shift Keying |

| | |
|------|---------------------------------|
| PTAM | Pilot Tone Assisted Modulation |
| QAM | Quadrature Amplitude Modulation |
| QPSK | Quadrature Phase Shift Keying |
| SNR | Signal to Noise Ratio |
| SRRC | Squared Root Raised Cosine |
| TDMA | Time-Division Multiple Access |
| TTIB | Transparent Tone In-Band |

Chapter 1 Introduction

Today, the technology of synchronization has become a foundation of modern digital communications. However, in terms of technologies in 16th century, it was a really difficult job for Charles V to make two clocks agree to each other, although he was an intelligent and powerful man.

“When Charles V retired in weariness from the greatest throne in the world to the solitude of this monastery at Yuste, he occupied his leisure for some weeks in trying to regulate two clocks. It proved very difficult. One day, it is recorded, he turned to his assistant and said: ‘To think that I attempted to force the reason and conscience of thousands of men into one mold, and I cannot make two clocks agree!’” (Ellis: The Task of Social Hygiene) [1].

1.1 Introduction of Frame Synchronization

Synchronization refers to the process of making two or more events occur at the same time [2]. Generally there are three levels of synchronization in a complete communication system: carrier synchronization, symbol synchronization and frame synchronization.

Carrier synchronization, in radio communications, refers to the process of generating a reference carrier with frequency and phase that is close to the frequency and phase of a received noisy carrier [2]. The process of carrier synchronization begins with frequency and phase acquisition and continues with phase tracking. Frequency acquisition is a problem in mobile radio applications due to the Doppler Effect, which causes an offset in the frequency of the received

carrier. While received frequency varies slowly, it is more difficult to extract carrier phase from the distorted received signal, because carrier phase can vary rapidly.

Symbol synchronization refers to the process of deriving timing signals at the receiver which indicate where, in time, the transmitted symbols are located. Symbol synchronization is one of the most significant functions performed at the receiver in a synchronous digital communication system. Because the data available to the receiver is always noisy and distorted, perfect timing information is hard to obtain in practice, although practical systems can come reasonably close.

Once symbol synchronization is accomplished, the next synchronization level is frame synchronization. Frame synchronization is necessary in systems for which the unit of information is not a symbol, but rather a sequence of symbols. Such systems are, for instance, systems where the unit of information is a codeword, or a frame that consists of a number of symbols. In this case, it is clear that knowing where the symbols are is not enough. Further knowledge of the frame boundary is required. It is easily seen that achievement of frame synchronization automatically implies symbol synchronization, but the converse is not true. Therefore, one might attempt to achieve frame synchronization thus achieving symbol synchronization at the same time. Such an approach, although in theory results in good performance, has the disadvantage of requiring more complex processing than the approach of first achieving lower level synchronization before higher ones are achieved. In practice, the latter approach is almost always used. In a standard frame synchronization method, the transmitter inserts a special synchronization pattern at the start of every frame and, at the receiver, frame boundaries are located through the detection of these synchronization patterns.

In this study we want to develop the frame synchronization technique to operate appropriately in wireless land mobile communication environments. It is required that this frame synchronizer works properly in wireless transmission channels when there is a range of frequency and phase errors. It is our purpose to improve the frame synchronizer's tolerance to frequency and phase errors to avoid

providing another accurate carrier synchronizer as part of frame synchronizer. Carrier synchronization is assumed to be approximately recovered; however, a small frequency error exists. Symbol synchronization is assumed perfectly recovered before frame synchronization is investigated. Based on these assumptions, only frame synchronization approaches will be discussed in the subsequent chapters.

1.2 Review of Frame Synchronization Techniques

In recent decades, there has been much research on frame synchronization techniques. The widely used technique for providing frame synchronization in a binary signaling system is to insert a fixed binary synchronization pattern or “syncword” periodically into the data stream [3]. Based on the assumption that symbol synchronization has already been obtained, and the receiver obtains frame synchronization by locating the position of the syncword in the received data stream. Fig. 1.1 is a general frame structure illustrating this method.

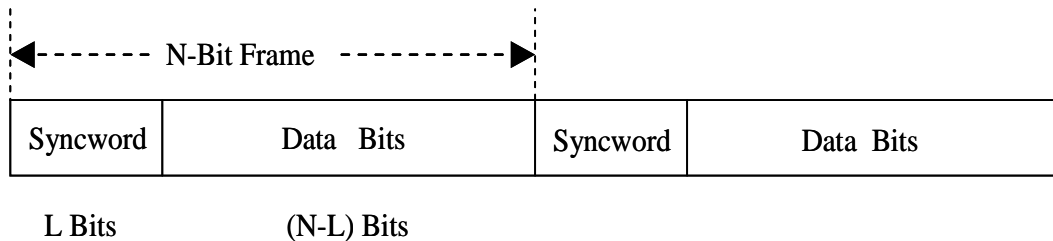


Fig. 1.1 Block diagram of a general frame structure [3]

In his pioneering work on frame synchronization, Barker [4] assumed that by passing the received signal through a “pattern recognizer”, which was simply a correlator that correlates consecutive L-digit segments of the received signal with the L-digit syncword, the segments that give the maximum correlation would be taken as the syncword and the location of the syncword is therefore identified. Subsequent to Barker’s work, Massey [5] derived the optimum maximum likelihood (ML) frame synchronization rule, the high and low SNR approximations of the ML

rule for the Gaussian noise channel with coherent BPSK modulation. This ML rule has much better performance than the correlation rule concluded by Barker. More importantly, Massey's work showed that the high SNR approximation of ML rule yields a performance virtually indistinguishable from that of the optimum ML rule. Later, in [6], Lui and Tan extended Massey's work from BPSK modulation to general M-ary phase-coherent and phase non-coherent signaling over the additive white Gaussian noise channel. They derived the optimum ML frame synchronization rule, high SNR ML rule, and correlation rule for the AWGN channel as well. Moon and Soliman [7] derived the ML frame synchronization method for a time variant AWGN channel with intersymbol interference (ISI).

All the frame synchronization techniques reviewed above have been investigated assuming an AWGN channel. However, with the development and deployment of wireless mobile communication nowadays, the fading effect has become a significant and dominant phenomenon. In most wireless communication circumstances it degrades the transmitted signal much more devastatingly than Gaussian noise and makes the reception of the transmitted signal difficult.

The rapid development of wireless mobile communication has stimulated a great deal of interest in fading channels. Also, research on frame synchronization techniques in a fading channel has attracted much attention. In [8], Robertson derived a maximum likelihood frame synchronization rule for the Rayleigh fading channel with coherent M-ary signaling. In his work, a simpler high SNR frame synchronizer sync rule performs as well as the optimal rules even at low SNR. In [9], Gansman presented two frame synchronization techniques for the Rayleigh fading channel and the AWGN channel. One frame synchronization rule is based on a standard maximum likelihood formulation and the other is a sequential testing algorithm.

Given the importance of wireless mobile communications for cellular personal communication and wireless networking, it is important and necessary for us to focus on this aspect. As frame synchronization is a crucial part in these digital

communication processes, in this study we intend to develop frame synchronization techniques suitable for the land mobile wireless environment.

1.3 Pilot Assisted Modulation

A fundamental aspect of wireless communication systems is the reliability and integrity of the data that are being communicated. Ideally, the data that are being transmitted from a transmitter in a mobile radio communication system should be identical to the data, which are being received at a receiver. Practically, however, the data that are received at the receiver have often been corrupted with respect to the original data transmitted from the transmitter. Such data communication errors may be attributed to several factors. One especially typical and important effect among all factors is the fading. In the multi-path propagation scenario, the received signals usually are made up of a group of reflections from objects, and none of the reflected signal paths is any more dominant than the other ones. The different signals, which were reflected by different paths, arrive at receiver at slightly different times, with different amplitudes, and with different phases. Because there are many different signal paths, constructive and destructive interference can result in, namely, multi-path fading. Furthermore, this effect also prevents proper signal sampling and in turn negatively affects the bit error rate (BER), which is directly related to the signal quality of a transmission path assigned to a particular user.

Rapid fading effect not only degrades the bit error rate (BER) severely, but also inhibits the use of multilevel modulation formats, such as QAM, a modulation format that has greater spectral efficiency. To overcome the impact of fading and to facilitate the use of QAM schemes, a good way is to estimate the channel fading signal and use this information to reverse the effect of fading. The estimation of fading signal can be achieved with the aid of a reference signal (or a pilot signal). In pilot signal assisted fading estimation, a pilot signal is transmitted along with the data signal. The receiver stores an original copy of the pilot signal. It compares the received copy of the pilot signal with the original copy to calculate the distortion

caused by fading and then to obtain the estimate of channel information. Such an approach is commonly used in today's wireless communications, where the motivation is to minimize the complexity of implementation and the time required to get a good channel estimate for receiver.

There are two powerful pilot assisted approaches generally referred to in literatures to ensure adequate QAM operation in fading environment. They are called Pilot Tone Assisted Modulation (PTAM) and Pilot Symbol Assisted Modulation (PSAM).

1.3.1 Pilot Tone Assisted Modulation (PTAM)

In PTAM, as introduced in [10], pilot tones are inserted at nulls of the spectrum of the signal that carries the information. After propagation over the multi-path fading channel, each path has some Doppler shift and this generates frequency-shifted versions of the original pilot tone. These received versions of the original pilot tone are different from each other because they have different frequency shifts and phase distortion. All these frequency-shifted versions of the pilot tone together form a spectrum that reflects the fading effect. Fading signal therefore can be extracted from the received signal by using a narrow bandpass filter with the passband located around each pilot tone.

Pilot tone assisted modulation has been proposed by several authors [10 -13]. The tone provides the receiver with an explicit amplitude and phase reference for detection, and thereby suppresses the error caused by fading. However, it requires relatively complex signal processing and expands the spectral occupancy.

1.3.2 Pilot Symbol Assisted Modulation (PSAM)

In PSAM systems [14, 15], the transmitter periodically inserts known pilot symbols into data stream, from which the receiver derives its amplitude and phase

reference. As in PTAM, PSAM also suppresses the error caused by fading effect and enables multilevel modulation. However, it does so with no change to the transmitted pulse shape and has lower complexity. Extensive studies from [14 - 16] show that PSAM is a promising method to reduce fading effect in land mobile communications. A general block diagram of PSAM system adapted from [16] is illustrated in Fig. 1.2,

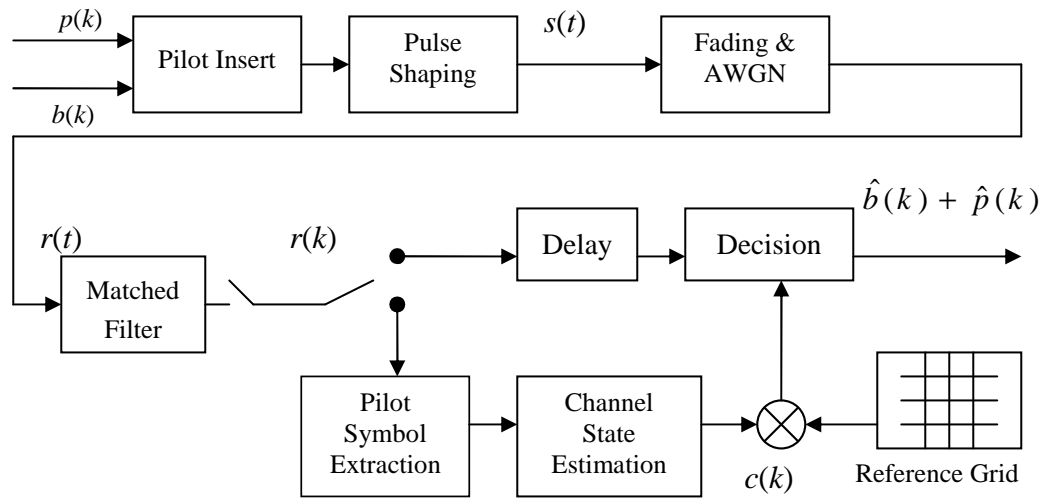


Fig. 1.2 Block diagram of a general PSAM system [16]

Known pilot symbols are periodically inserted into the data sequence prior to pulse shaping, and the composite signal is transmitted in the usual way over a channel characterized by fading and additive white Gaussian noise. The resulting frame structure is illustrated in Fig. 1.3.

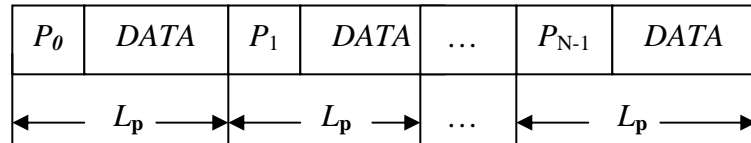


Fig. 1.3 Frame structure with pilot symbol inserted

After matched filter detection, the receiver splits the symbol samples into two streams. The reference branch decimates the samples to extract only those due to the pilot symbols, and interpolates these symbols to form an estimate of channel state. It then uses the estimate to scale and rotate a reference decision grid (such as a 16-QAM grid), and feeds the modified decision boundaries to the data branch.

1.4 Objective of Thesis

Synchronization plays a very important role for the proper operation of a PSAM system [17]. One practical problem in designing a PSAM receiver is how the receiver can distinguish between pilot and data symbols, in other words, how the receiver can identify and locate the position of pilot symbols in distorted received signals. Because this technique of identifying pilot symbols is similar to the technique of frame synchronization in digital communications, we call this procedure as “frame synchronization for PSAM”.

Although many traditional frame synchronization techniques have been developed, frame synchronization for PSAM is often neglected in most literatures. Through literature search, we find the most applicable publication on this aspect is proposed by Prof. J. Gansman [9]. In his work, Gansman presented two frame synchronization techniques for PSAM based on coherent signal detection. Motivated by his original work, we think it is valuable to do further research on the frame synchronization algorithm and design an improved frame synchronizer for PSAM. Compared with the frame synchronization methods developed by Gansman, this work solves the problem in a different way and two novel frame synchronization approaches based on non-coherent detection have been developed.

1.5 Thesis Organization

This thesis is organized in 6 chapters.

Chapter 1 provides a brief history of frame synchronization techniques and an introduction of the PSAM system. The motivation and the objective of this thesis are presented as well.

Chapter 2 describes the background theories that are important to this study. This chapter introduces the preliminary knowledge such as 16-QAM modulation scheme, band-limited Nyquist pulse shaping filter (squared root cosine filter), transmission channels and pilot symbol sequences. The detailed description of the fading channel provides a theoretical foundation for the development of frame synchronization techniques.

Chapter 3 presents how the frame synchronization criteria are developed for this study. The non-coherent scheme is introduced first and then the maximum likelihood (ML) and maximum a Posteriori probability (MAP) frame synchronization techniques for an AWGN channel and a Rayleigh fading channel are presented.

Chapter 4 provides a description of the prototype of the simulation system in Simulink® and shows how the performance is tested through computer simulations.

Chapter 5 describes the simulation parameters and the performance of frame synchronizers is evaluated. Simulation results for both AWGN and frequency non-selective Rayleigh fading channels are illustrated in figures.

Chapter 6 presents the conclusions of this study based on the results obtained from computer simulations. It also identifies some directions for further study.

Chapter 2 Background Theory

In this chapter, the essential background knowledge on modulation schemes and transmission channel models is presented. Pilot symbol assisted modulation (PSAM) and some pilot sequences are also introduced.

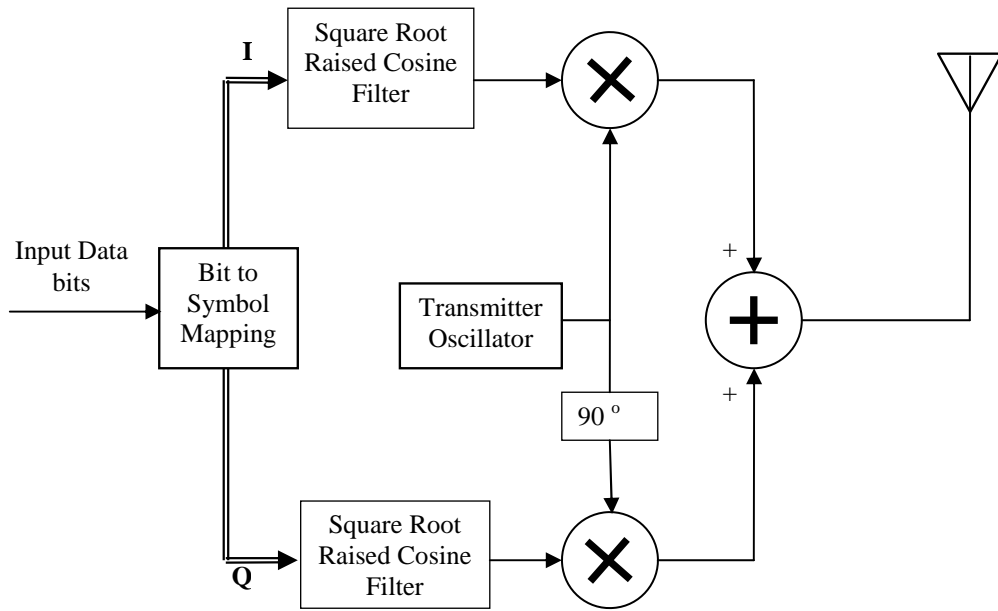
2.1 16 State Quadrature Amplitude Modulation (16-QAM)

To transmit data and voice information from one location to another without physically connecting together, as in wireless mobility, it is important to choose a suitable modulation scheme to accomplish this purpose. A modulation scheme is a process that uses an information signal to alter some properties of a higher frequency carrier waveform. By modulating each information signal into a different carrier frequency, many information signals can be communicated between distant sender and receiver. Radio waves are used as the transmission medium between the sender and receiver. The choice of modulation and demodulation used for the radio communication system is dependent on the required information transfer rate, the available spectrum to convey the information, and the cost.

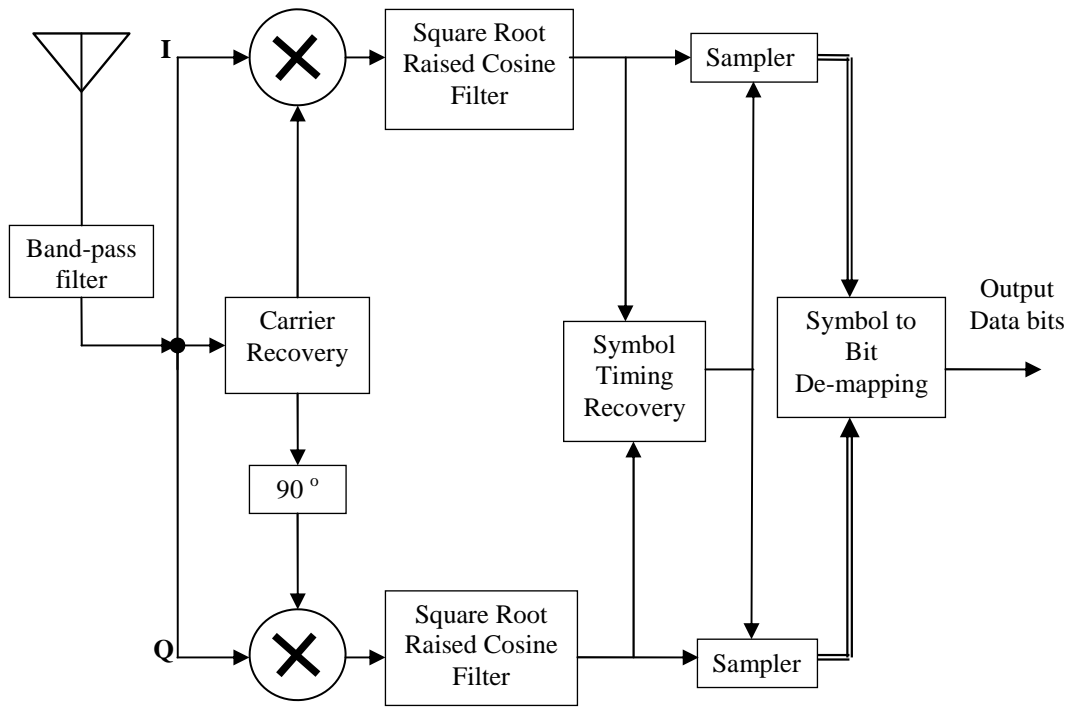
There are many types of modulation formats used for the transportation of information. Three fundamental modulations techniques are used mostly: amplitude modulation (AM), phase modulation (PM) and frequency modulation (FM). In AM, the magnitude of carrier is varied according to the magnitude of message signal. While in PM and FM modulations, the angle of the carrier are varied with the magnitude of message signal and the magnitude of carrier is constant.

AM has many unique qualities with it. However, this form of communication is not used directly in mobile wireless communication system primarily because it is more susceptible to noise. However, a variant of AM, quadrature amplitude modulation (QAM) is recently used predominantly for the demand of higher bandwidth efficiency. The major difficulty of using bandwidth-efficient multi-level QAM schemes is that, over fading channels, the transmitted signal magnitude is attenuated and the phase is rotated by channel, which causes big trouble for signal reception. As introduced in Chapter 1, by using a PSAM system, the impact from fading can be reduced and it makes the use of QAM possible. In this study we choose 16-QAM as the modulation format. 16-QAM is one of the simpler forms in the QAM family and it provides more capacity by transmitting 4 bits per information symbol and hence it increases bandwidth efficiency relative to binary phase shift keying (BPSK) or quadrature phase shift keying (QPSK). A simple block diagram of a 16-QAM system is presented in Fig. 2.1.

In the QAM system illustrated in Fig. 2.1, it is assumed that the input information is a stream of random binary bits. This bit stream is first mapped into I and Q QAM symbols. In a 16-QAM system, the binary bit stream is mapped into 4-bit symbols and the square constellation using Gray coding is illustrated in Fig. 2.2,



(a) QAM Transmitter



(b) QAM Receiver

Fig. 2.1 A typical QAM system

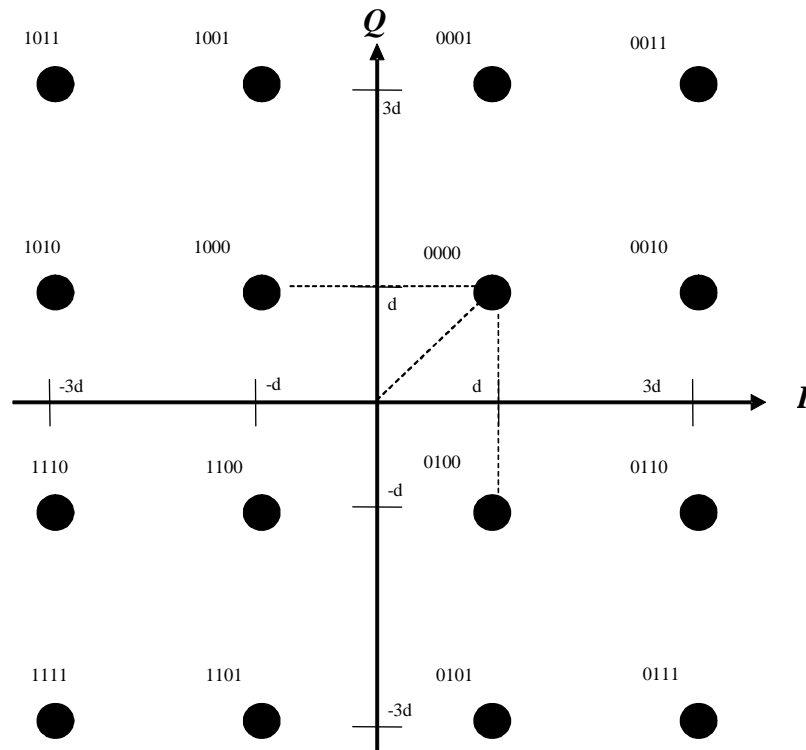


Fig. 2.2 16-QAM square constellation using Gray encoding [18]

In this square 16-QAM constellation, each point represents a 4-bit symbol, which is constituted by two in-phase bits on I axis and two Quadrature bits on Q axis. On the quaternary quadrature components I and Q axis, Gray encoding is performed by assigning the bits 01 , 00 , 10 , 11 to the levels $3d$, d , $-d$, $-3d$, respectively.

It is noted that in Fig. 2.2, the Hamming distance between any two neighboring code points is always one. For example, points 0101 and 0111 would have a Hamming distance 1. The Hamming distance between any two points other than neighboring points is larger than one. For example, points 0101 and 0011 would have a Hamming distance 2. This is a fundamental feature of Gray coding process so that when a received symbol is corrupted by noise and it is misinterpreted into a neighboring constellation point, it ensures the demodulator will only make a single bit error. This minimizes the error probability.

There are many possibilities for selecting 16-QAM constellations. In practice, this square constellation in Fig. 2.2 is widely used. According to the discussion of Proakis [20], this square constellation has the advantage of being easily generated as two PAM signals impressed on phase-quadrature carriers. In addition, they are easily demodulated. Compared with other commonly used 16-QAM constellations, this square constellation has higher minimum distance at the same average phasor energy and thus it is frequently used in an AWGN channel, where noise is the dominant channel impairment.

In this study, random binary bits are used as the input information signal. The input data represent a discrete time, complex random process. Given the random characteristics of the input bit stream, each 4-bit symbol will fall on each point of this square 16-QAM constellation with equal probability. The probability density functions for each symbol are independent, identically distributed (i.i.d). As in [19], the mean and variance of constellation points are:

$$\begin{aligned}\mu_x &= \sum_{i=1}^{\infty} x_i p_i \\ &= \left\{ \left[d\left(\frac{4}{16}\right) - d\left(\frac{4}{16}\right) + 3d\left(\frac{4}{16}\right) - 3d\left(\frac{4}{16}\right) \right] + j \left[d\left(\frac{4}{16}\right) - d\left(\frac{4}{16}\right) + 3d\left(\frac{4}{16}\right) - 3d\left(\frac{4}{16}\right) \right] \right\} \\ &= 0 + j0 = 0\end{aligned}$$

$$\begin{aligned}\sigma_x^2 &= \sum (x_i - \mu_x)^2 p_i \\ &= (d^2 + d^2) \left(\frac{4}{16} \right) + [(3d)^2 + d^2] \left(\frac{8}{16} \right) + [(3d)^2 + (3d)^2] \left(\frac{4}{16} \right) \\ &= 10d^2\end{aligned}$$

In frequency domain, the power spectrum of input data has a constant value of $10d^2$ over $(-1/2T_s, 1/2T_s)$, where T_s is the symbol time.

2.2 Nyquist Filtering (Square Root Raised Cosine Filter)

Rectangular pulses are used as input data to the 16-QAM modulator because in the time domain, this pulse shape is convenient because it is wholly contained within its allocated interval and does not interfere with pulses in adjacent intervals. However, the frequency content of a rectangular pulse has a $\sin x/x$ shape and the tails of the $\sin x/x$ function decay very slowly, thus a very wide bandwidth is needed to ensure a rectangular pulse is transmitted without adjacent symbol interference. However, this is not applicable for most communication channels that are bandwidth-constrained. Therefore, if these rectangular pulses are not pulse shaped appropriately, it may cause severe intersymbol interference (ISI) with adjacent pulses. Hence, proper pulse shaping is important and this process is well known as Nyquist filtering.

A comprehensive theoretical description of Nyquist filtering is provided in references [20], [25] and [26]. Hence here we restrict our discussion to a rudimentary introduction. An ideal linear low-pass filter (LPF) has a cut-off frequency of $f_N = f_s/2$, where $f_s = 1/T_s$ is the symbol rate, T_s is the symbol interval duration and $f_N = 1/(2T_s)$ is the so-called Nyquist frequency. Such a filter usually has a $(\sin x)/x$ shaped impulse response with equidistant zero-crossings at the sampling instants $n \cdot T_s$. When sampled at the correct instants, this low-pass filter avoids intersymbol interference (ISI) between consecutive symbols.

A particular pulse shape that satisfies the above-mentioned ideal low-pass filter characteristic and has been widely used in practice is the Nyquist raised cosine pulse. The raised cosine frequency characteristic is described by Proakis [20] and Barry [25] as

$$X_{rc}(f) = \begin{cases} T_s & 0 \leq |f| \leq \left(\frac{1-\beta}{2T_s}\right) \\ \frac{T_s}{2} \left\{ 1 + \cos \left[\frac{\pi T_s}{\beta} \left(|f| - \frac{1-\beta}{2T_s} \right) \right] \right\} & \left(\frac{1-\beta}{2T_s}\right) \leq |f| \leq \left(\frac{1+\beta}{2T_s}\right) \\ 0 & |f| > \left(\frac{1+\beta}{2T_s}\right) \end{cases} \quad (2.1)$$

where T_s is the symbol duration, and β is the roll-off factor which takes values in the range $[0,1]$.

The corresponding time domain impulse response of a raised cosine filter above is given as in [20]:

$$x_{rc}(t) = \frac{\text{sinc}\left(\frac{\pi t}{T_s}\right) \cos\left(\frac{\pi \beta t}{T_s}\right)}{1 - 4\left(\frac{\beta t}{T_s}\right)^2}. \quad (2.2)$$

The raised cosine pulse spectral characteristics and corresponding pulses for $\beta = 0, 0.5$, and 1 are illustrated in Fig. 2.3.

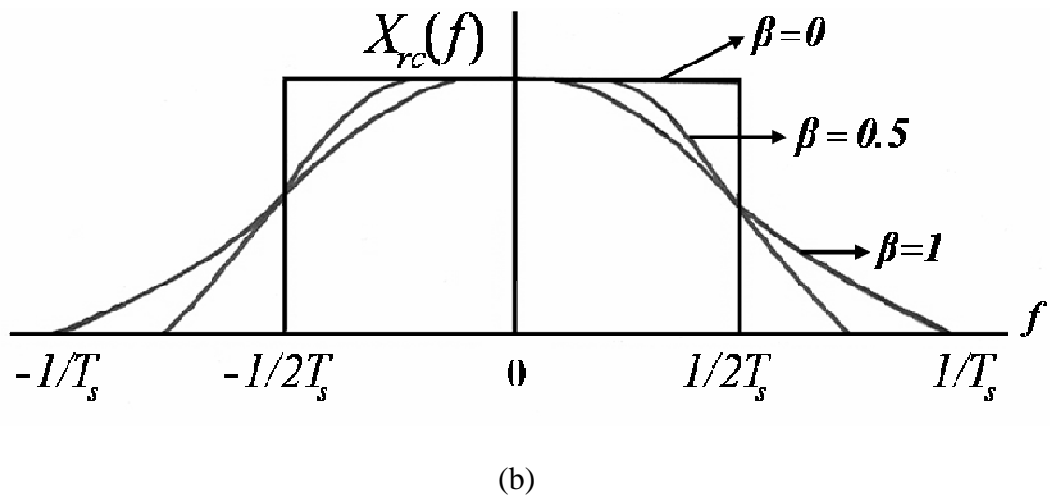
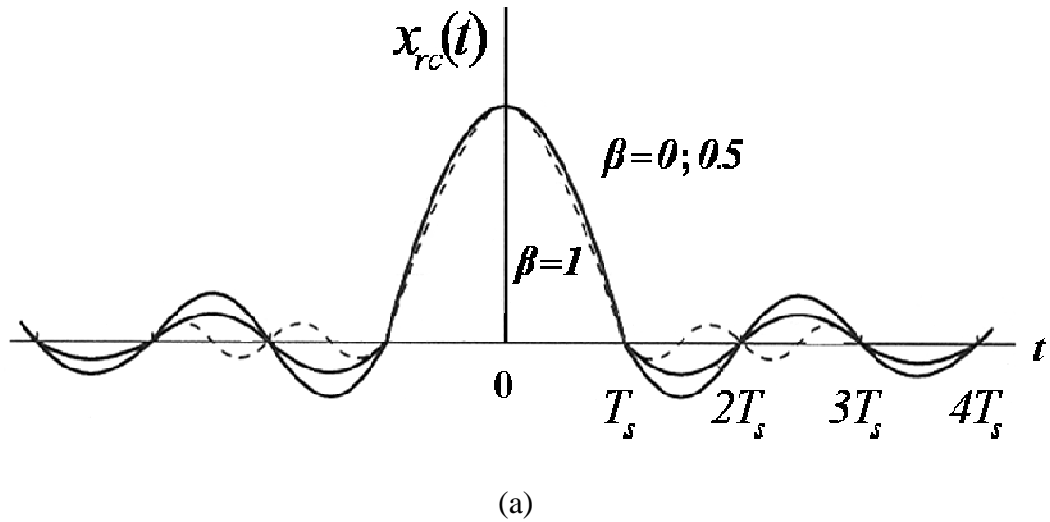


Fig. 2.3 Nyquist pulse and raised cosine spectrum (adapted from [20])

Because of the smooth characteristics of the raised cosine frequency response, it is possible to design practical filters for the transmitter and the receiver that approximate the desired frequency response. In the special case that channel is ideal, we have

$$X_{rc}(f) = G_T(f)G_R(f). \quad (2.3)$$

where $G_T(f)$ and $G_R(f)$ are the filter frequency responses at the transmitter and at

the receiver respectively. In this case, according to optimum detection theory from [27], if the filter for receiver is matched to the filter for transmitter, we have

$$X_{rc}(f) = G_T(f)G_R(f) = |G_T(f)|^2. \quad (2.4)$$

ideally,

$$G_T(f) = \sqrt{|X_{rc}(f)|} e^{-j2\pi f t_0}.$$

and $G_R(f) = G_T^*(f)$, where t_0 is some nominal delay that is required to ensure physical realization of the filter. Thus, the overall raised cosine Nyquist filter is split evenly into the cascade of two identical filters, a transmitter filter and a receiver filter, each characterized by a square root of raised cosine shape, as illustrated in Fig. 2.1. In an ideal channel, i.e. no distortion and ISI, two square root raised cosine filters in combination have the same performance as one raised cosine filter.

The frequency response of a square root raised cosine filter is given in [25] [26] and expressed as:

$$X_{srrc}(f) = \begin{cases} \sqrt{T_s} & 0 \leq |f| \leq \left(\frac{1-\beta}{2T_s}\right) \\ \sqrt{\frac{T_s}{2} \left[1 + \cos \left[\frac{\pi T_s}{\beta} \left(|f| - \frac{1-\beta}{2T_s} \right) \right] \right]} & \left(\frac{1-\beta}{2T_s}\right) \leq |f| \leq \left(\frac{1+\beta}{2T_s}\right) \\ 0 & |f| > \left(\frac{1+\beta}{2T_s}\right) \end{cases}. \quad (2.5)$$

A finite impulse response (FIR) square root raised cosine filter in the time domain may be synthesized directly from the impulse response, which is also given in [25] as:

$$x_{srrc}(t) = \frac{4\beta}{\pi\sqrt{T_s}} \frac{\cos\left(\frac{(1+\beta)\pi t}{T_s}\right) + \frac{T_s}{4\beta t} \sin\left(\frac{(1-\beta)\pi t}{T_s}\right)}{1 - \left(\frac{4\beta t}{T_s}\right)^2}. \quad (2.6)$$

2.3 Transmission Channel

Once I and Q baseband signals have been generated and filtered by the band-limited Nyquist squared root raised cosine filter, they are modulated by an I - Q modulator with two quadrature carriers as illustrated in Fig. 2.1. This process allows these two signals to be transmitted and received over a single channel within the same bandwidth.

The transmission channel is often the limiting factor that influences the performance of any communication system. The objective of this study is to develop frame synchronization techniques operating in the land mobile communication environment, thus mobile radio channel is the emphasis of our discussion. Two commonly used channel models are introduced in this section. They are the additive white Gaussian noise channel and the multi-path Rayleigh fading channel. The latter will be introduced in more detail, because it is the dominant case in a land mobile communication system. This channel model is fundamental to the development of frame synchronization criteria.

2.3.1 Additive White Gaussian Noise Channel

The simplest type of channel is the Gaussian channel. It is often referred to the additive white Gaussian noise (AWGN) channel. Basically, it is the noise generated in the receiver side if we assume that the transmitter is ideal and noiseless. This type of noise is assumed to have a constant power spectral density over the whole channel bandwidth and its amplitude probability density function (PDF) obeys the statistics of a Gaussian distribution.

Gaussian noise is very important in the analysis of communication system performance. The classical AWGN channel is always considered as the starting point to develop basic systems performance. Also, according to central limit theorem [22], even when there are a larger number of non-Gaussian independent noise sources, the mobile channel noise may still be approximated with a Gaussian distribution. This feature allows for simpler analysis of the communication system.

2.3.2 Multi-Path Rayleigh Fading Channel

In a mobile radio communication system, one of the most devastating phenomena is fading. Fading is the direct result of multi-path propagation where radio waves propagate along different paths before arriving at the receiver antenna. These radio waves may arrive at receiver after different delays, with different amplitudes, and with different phases. Because there are so many different received signal components, constructive and destructive interference results in fading. This sort of channel is called a multi-path fading channel, which is illustrated in Fig. 2.4.

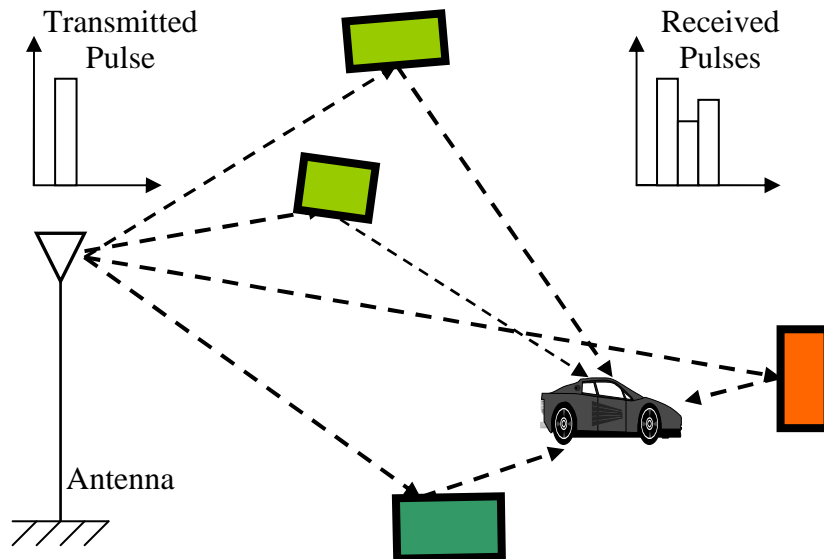


Fig. 2.4 A simple multi-path channel model

Thus, in a multi-path fading channel, when a signal pulse is transmitted, the mobile receives the superposition of many pulses. These multi-paths cause a wide fluctuation in the received signal magnitude, which makes reliable transmission of information a challenge. The received pulses shown on the Fig. 2.4 makes a good illustration, however, multiple received pulses are not the problem that is being addressed. The problem is the path length difference causes destructive interference and very small received signal.

There are extensive introductions of multi-path fading channel in many text books such as [20], [24] and [27]. In the following subsections, rudimentary knowledge about the statistical characterization of multi-path fading channel is briefly presented. The definition of frequency non-selective, slow fading is given as well.

2.3.3 Characterization of Fading Channel

As mentioned previously, if an extreme short pulse, ideally an impulse is transmitted over a time-varying multi-path fading channel, the received signal might be a series of pulses as illustrated in Fig. 2.5.

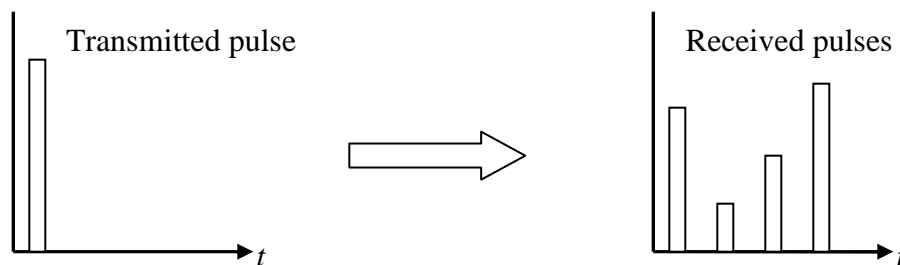


Fig. 2.5 Response of a time-variant multi-path fading channel to a pulse

The time variations of the received pulses train appear to be unpredictable and random to the user of this multi-path channel. Thus it is important to characterize

this channel statistically. For this purpose, first we examine the effects of the channel on a transmitted signal in general as:

$$s_p(t) = \text{Re}[s(t) e^{j2\pi f_c t}]. \quad (2.7)$$

where $\text{Re}[\]$ means the real part of a complex signal, $s_p(t)$ is the bandpass transmitted signal, $s(t)$ is the baseband input signal band-limited by the transmitter filter and f_c is the carrier frequency. Assuming that there are multiple propagation paths and associated with each path there are a propagation time delay $\tau(t)$ and an amplitude attenuation factor $a(t)$. Both propagation delays and amplitude attenuation factors are time-variant because of changes in the structure of the medium in the wireless mobile communications system. Thus the received bandpass signal after multi-path propagation may be expressed as the sum of signals from different paths in the form of:

$$x(t) = \sum_n a_n(t) s_p[t - \tau_n(t)]. \quad (2.8)$$

where $a_n(t)$ is the amplitude attenuation factor of the received signal in the n^{th} path and $\tau_n(t)$ is the propagation time delay for n^{th} path. Substitution for $s_p(t)$ from equation (2.7) into equation (2.8) yields the result

$$x(t) = \text{Re} \left\{ \sum_n a_n(t) s[t - \tau_n(t)] e^{j2\pi f_c [t - \tau_n(t)]} \right\}. \quad (2.9)$$

and therefore the equivalent low-pass baseband received signal is obtained as

$$r(t) = \sum_n a_n(t) e^{-j2\pi f_c \tau_n(t)} s[t - \tau_n(t)]. \quad (2.10)$$

Since $r(t)$ is the response of an equivalent low-pass baseband channel to the equivalent low-pass baseband input signal $s(t)$, the equivalent low-pass channel can be described by using the time-variant impulse response as $h(\tau, t)$ and it is given as

$$h(\tau, t) = \sum_n a_n(t) e^{-j2\pi f_c \tau_n(t)} \delta[t - \tau_n(t)]. \quad (2.11)$$

When an unmodulated carrier at frequency f_c is transmitted, and if $s(t) = 1$ for all t , then the received signal in equation (2.10) reduces to

$$r(t) = \sum_n a_n(t) e^{-j2\pi f_c \tau_n(t)} = \sum_n a_n(t) e^{-j\theta_n(t)}. \quad (2.12)$$

where $\theta_n(t) = 2\pi f_c \tau_n(t)$. Thus, it is clear that the received signal is composed of different time-variant vectors that have different amplitude factors and phases. Because the change of $a_n(t)$ and $\theta_n(t)$ is in a random manner, this multi-path propagation model in the above equation (2.12) results in severe signal fading when the random changing vectors add destructively. When this situation occurs, the received signal is very small or nearly zero. It is called fade. Due to the randomness of $a_n(t)$ and $\theta_n(t)$, the received signal $r(t)$ can be modeled as a random process too. We rewrite the fading channel response equation (2.11) to

$$h(\tau, t) = \sum_n a_n(t) e^{-j\theta_n(t)} \delta[t - \tau_n(t)]. \quad (2.13)$$

This means the time-variant fading response $h(\tau, t)$ is a random process of variable t too. According to central limit theorem in [22], when there are a large number of paths, the $r(t)$ may be simplified to a complex-valued Gaussian random process. Thus the channel fading response is a complex-valued Gaussian random process based on t variable as well.

The random process of multi-path channel fading can be modeled by several probability density functions [24]. Some of the most common models in the literatures are Rayleigh distribution and Rician distribution. For example, when the process is modeled as a zero mean complex-valued Gaussian process, the envelope of such a received signal is usually described by Rayleigh probability density function (PDF) and the channel is said to be a Rayleigh fading channel. This mostly

happens in urban areas, where there are multiple reflective paths and no direct path, i.e., no line-of-sight (LOS) between the transmitter and the receiver. While the process is modeled as a non-zero mean complex-valued Gaussian process, the envelope of such a received signal is statistically described by Rician probability density function (PDF) and the channel is said to be a Rician fading channel. This mostly happens in rural areas, where there is a direct path, i.e., line-of-sight (LOS) between transmitter and receiver [19].

Although in practice, there are more models than the two mentioned above [20], in this work we will model the fading process as a Rayleigh fading, since it is typical for the urban environment.

2.3.4 Frequency Non-Selective Slow Fading

When the transmitter, receiver and all other objects in the multi-path environment are fixed, the fading channel is time invariant. While all or some objects in this communication system are in motion, which is the most possible situation in wireless communication, the channel becomes time variant. Doppler shift is introduced in at least some of the signal paths when the length of a propagation path is changing.

Radio waves with different Doppler shifts can combine destructively to cancel at one time and combine constructively at another time, and this produces a time-variant channel fading. Simply, time-variant channel fading can be classified into fast and slow fading based on the normalized maximum fading rate f_d , which is described in [23] as:

$$f_d = \frac{f_m}{B} = \frac{f_c v \cos \alpha}{Bc}. \quad (2.14)$$

where f_m is the maximum Doppler shift, B is the bandwidth of the baseband signal, v is the velocity of the mobile user, f_c is the carrier frequency, α is the arrival

angle of the path that has maximum Doppler shift, and c is the constant of light speed. Slow fading refers to fading rate $f_d \ll 1$, which means the Doppler frequency shift is much smaller than the bandwidth of the signal. Typical fading rate for slow fading is less than 5% of the symbol rate according to Cavers paper [23]. The slow fading implies that the fading process may be regarded as a constant during at least one signaling interval.

Channel fading can also be classified as frequency selective fading or frequency non-selective (flat) fading. As indicated in Proakis [20], if the maximum difference of any two path delays is T_m in a fading multi-path channel, the coherence bandwidth of the channel, denoted by $(\Delta f_{coh.})$ can be expressed as

$$(\Delta f_{coh.}) = \frac{1}{T_m}.$$

If the coherence bandwidth $(\Delta f_{coh.})$ of the fading channel is less than the bandwidth of the transmitted signal, the channel is said to have frequency selective fading. In this case, the signal is severely distorted by the channel and may cause intersymbol interference. On the other hand, if the coherence bandwidth of fading channel is larger than the bandwidth of the transmitted signal, the channel is said to be frequency non-selective. In a frequency non-selective fading channel all frequency components in the transmitted signal undergo approximately the same attenuation and phase shift.

According to Proakis [20] and Cavers [23], in such a frequency non-selective fading channel, the received signal appears to arrive at the receiver via a single fading path and therefore the received signal can be simplified as the multiplication of transmitted signal with a random process, which models the time-variant characteristics of the fading multi-path channel.

It is necessary to note that in previous discussions, the noise term is missed. It is left out for the simplification of analysis. Also, unlike the signal, noise does not

necessarily propagate along multiple paths of the fading channel. Usually we think that it comes into the system at the front end of the receiver since most noise is thermal noise from electronic circuits. In this communications system, we assume additive white Gaussian noise (AWGN), which has a flat power spectrum, and shifts of the center frequency of it will not change its statistical properties. It is generally assumed that bandpass complex Gaussian noise has circular symmetry, i.e. the real and imaginary parts of random variable are independent with identical Gaussian distribution. The carrier frequency and phase offset will not change its statistical properties. Consequently, noise can be expressed as an additive term in the expression of received signal. Hence, we can first leave it out of our discussion and consider it at last.

Given all the discussions above, the frequency non-selective and slow Rayleigh fading channel can be approximated into a multiplicative factor of the transmitted signal. Therefore, with the noise, the received signal can be expressed as

$$r(t) = c(t)s(t) + n(t). \quad (2.15)$$

where $r(t)$ is the baseband received signal, $c(t)$ denotes the multiplicative fading distortion and its envelope has a Rayleigh distribution, $s(t)$ is the transmitted baseband signal and $n(t)$ is the additive white Gaussian noise with zero mean and power spectral density N_0 . In this study, our development of frame synchronization will consider only this type of fading channel. The channel model also can be illustrated as in Fig. 2.6.

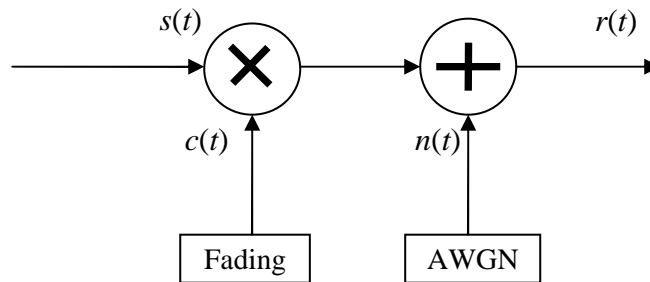


Fig. 2.6 Transmission channel model

2.4 PSAM and Pilot Symbol Mapping

Pilot symbol assisted modulation (PSAM) is used to ease the application of bandwidth-efficient QAM scheme in this study. As mentioned in Chapter 1, PSAM is effective to compensate the fading effect in land mobile communication and can make the use of multilevel modulation format QAM possible. A PSAM system block diagram is introduced in Chapter 1 and illustrated in Fig. 1.2.

According to the PSAM system model in Fig. 1.2, known pilot symbol sequences are periodically inserted into the data sequence prior to pulse shaping, and the composite signal is transmitted over a channel characterized by frequency non-selective, slow fading and additive white Gaussian noise.

After passing through matched filter detection, the received per-symbol samples are split into data and pilot paths, as seen in Fig. 1.2. The pilot path decimates the samples to extract the pilot symbols, and then interpolates the sequence of pilot symbols in order to derive a channel state estimation. Decisions are carried out against a decision reference grid that has been scaled and rotated according to the instantaneous channel estimate.

In this PSAM system, a sequence of pilot symbols is inserted into the 16-QAM data symbol stream and then transmitted together with data symbols through the fading and noisy channel. A general PSAM frame structure is depicted in Fig. 2.7.

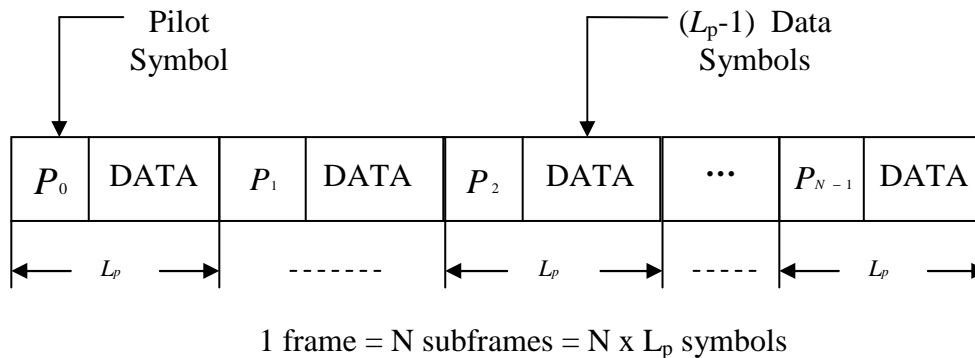


Fig. 2.7 Frame structure for PSAM input signal

In Gansman's paper [9], frame synchronization techniques for PSAM were developed based on coherent detection. A 16-QAM modulated data set and an 8-PSK pilot symbol set were combined together. Because in the coherent communications system, both phase and magnitude information of received data is needed to achieve the estimate of channel state, this algorithm is somewhat complicated.

In contrast to a coherent communication system, a non-coherent receiver does not require the knowledge of the carrier phase and can tolerate small inaccuracies in the carrier frequency [25]. By using a non-coherent receiver, the magnitude of the information is transmitted without being affected by phase errors. If we apply this idea on frame synchronization, it is possible to design a frame synchronizer based on non-coherent detection that is independent of phase and frequency errors. To implement such a non-coherent frame synchronizer, a pilot symbol must be identified only based on its amplitude. Once you have identified the pilot symbols, you can use both their magnitude and phase information to obtain accurate estimate of channel state information.

From the square constellation of 16-QAM in Fig. 2.8, we find that there are only three different levels of amplitude. This gives us an inspiration on how to identify the pilot symbols by transmitting a pattern in magnitudes. As discussed below, we use one of the several binary sequences for synchronization. As illustrated in Fig. 2.8, we select the innermost circle contain 16-QAM codes 0000, 0100, 1000 and 1100 to represent logic **0** in the binary sequence. Similarly, we select any one of the symbol codes 0011, 0111, 1011 and 1111 from the outermost circle to represent logic **1** in the binary pilot sequence.

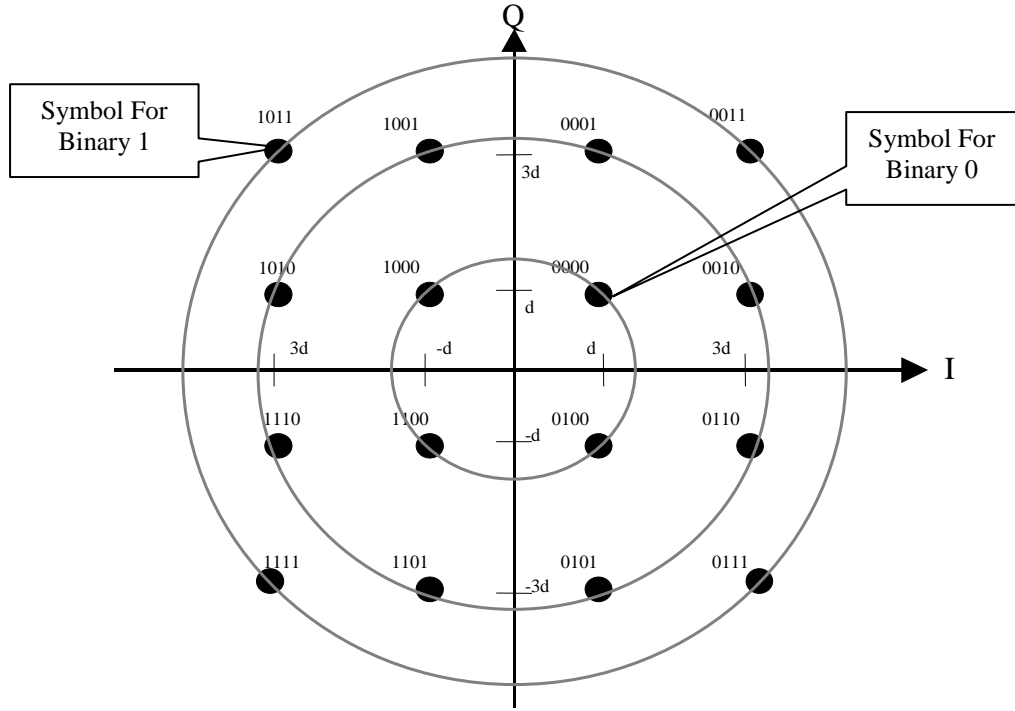


Fig. 2.8 Pilot symbol mapping into 16-QAM

Since the pilot symbols can be looked as a subset of all 16-QAM symbols, a pilot sequence can be easily introduced into a sequence of 16-QAM data symbols.

It is generally desirable to choose a pilot symbol pattern with good autocorrelation properties. Usually in the techniques of frame synchronization, special PN sequences, such as Barker sequences [26], are used for frame synchronization in digital communication systems. They are applied in Massey [5], Liu and Tan [6] and Moon [7]. In these papers, 7-bit Barker sequence (-1, -1, -1, 1, 1, -1, 1), 13-bit Barker sequence (-1, -1, -1, -1, -1, 1, 1, -1, -1, 1, -1, 1, -1) and 13-bit Neuman-Hofman sequence (1, 1, 1, 1, 1, 1, -1, -1, 1, 1, -1, 1, -1) are used as syncword pattern in frame structures. The autocorrelation function of the pilot sequences (without ISI) is given by

$$\varphi_j = \sum_{k=1}^{N-j} X_j X_{j+k} . \quad (2.16)$$

where X_j is an individual code symbol taking values +1 or -1, for $1 \leq j \leq N$ and $0 \leq k \leq N - j$. The correlation values of the Baker sequences and the Neuman-Hofman sequence have a high peak value at $j = 0$ and very low sidelobe values.

In this study we will use 7-bit Barker sequence (BK7), 13-bit Barker sequence (BK13) and 13-bit Neuman-Hofman (NH13) sequence as in [5 - 7], and also introduce 11-bit Barker sequence (BK11) and a 15-bit PN (PN15) sequence as pilot sequences for the PSAM system. The 11-bit Barker code sequence and the 15-bit PN sequence also have good autocorrelation properties. We introduce these two sequences in order to investigate the performance of our system with more pilot sequences and find out in which case the performance of frame synchronizer works best. These pilot symbol sequences are listed in Table 1.

Table 1: List of Pilot Sequence

| Sequence | Polar Binary Sequences |
|----------|---|
| BK7 | [-1, -1, -1, 1, 1, -1, 1] |
| BK11 | [-1, -1, -1, 1, 1, 1, -1, 1, 1, -1, 1] |
| BK13 | [-1, -1, -1, -1, -1, 1, 1, -1, -1, 1, -1, 1, -1] |
| N-H13 | [1, 1, 1, 1, 1, 1, -1, -1, 1, 1, -1, 1, -1] |
| PN15 | [-1, 1, 1, 1, -1, -1, -1, -1, 1, -1, 1, -1, -1, 1, 1] |

Chapter 3 Frame Synchronization

In this chapter the mathematical relations for PSAM frame synchronization techniques in both AWGN and Rayleigh fading channels are presented. The requirements of design are first addressed, and it is followed by detailed discussions of how each requirement is accomplished. Two non-coherent frame synchronization approaches are proposed. One is a standard maximum likelihood (ML) formulation and the other is maximum a Posteriori (MAP) probability criterion.

3.1 Design Considerations

Pilot symbol assisted modulation (PSAM) is used to reduce the effect of channel fading in mobile communication. It tests the channel by periodically inserting known pilot symbols into the data stream. The receiver uses these pilot symbols to determine the channel state information. One of the most important aspects of this procedure is the method used by the receiver to locate timing position of the pilot symbols, i.e., frame synchronization.

The purpose of frame synchronization for PSAM is to identify pilot symbols among received data symbols. Since in wireless mobile communications, the received signals are distorted by noise, multi-path fading effect and carrier frequency error, it is important that this frame synchronization design can manage all these distortions and to properly identify the position of the pilot symbols amongst the data symbols.

As we have discussed, residual frequency errors are unavoidable even after good carrier recovery. Therefore, this design is also on improving the

invulnerability of frame synchronizer to the frequency error and avoiding the design of another superior carrier synchronizer inside this frame synchronizer. The frame synchronizer must have good performance in presence of a range of small frequency offsets.

The PSAM system is applied to combat the fading effect, thus this frame synchronization design should also work well under fading conditions. Since the channel is linear (properties do not change with changes in the signal amplitude), the channel can be denoted by the multiplicative factor $c(k)$. To obtain a good estimate of $c(k)$ and use it to reverse fading effect could result in a complicated algorithm. Therefore, this frame synchronization algorithm should have minimum complexity and be simple to implement.

3.2 Non-Coherent System

In [9], Gansman's frame synchronization techniques for a PSAM system are designed based on coherent detection. Both amplitude and the phase of pilot symbols are used to estimate the fading process and this estimation is used to achieve coherent demodulation and data symbol decision. Although this coherent approach shows great performance in locating the pilot symbols, the algorithm is somewhat complicated. In order to reduce the complexity of the frame synchronizer as well as to improve the immunity to frequency offset, a non-coherent frame synchronization scheme is proposed in this study.

As mentioned in Section 2.4, in a non-coherent system, information is transmitted independent of the absolute value of carrier phase; hence the receiver is not sensitive to any carrier phase and frequency error. In this PSAM system, the receiver only estimates the magnitude variation of received signal to obtain the frame synchronization. According to Fig. 2.9, this is not a problem for a 16-QAM scheme. We choose the symbols on the outermost circle of the 16-QAM square constellation or those on the innermost circle to be the pilot symbols. Thus, in this

frame synchronizer, pilot symbol and data information symbol are both selected from the same 16-QAM data set. This differs from the Gansman's work where pilot symbols are selected from 8 PSK data set and data symbols are transmitted using 16-QAM [9].

At the start of frame synchronization, the system is working in a partially functional state, in which only signal magnitude can be reliably transmitted and signal phase is not reliable. Therefore, it is reasonable to use only the reliable portion to achieve the time location of pilot symbols. One might think that a non-coherent scheme is a waste of system capacity for only carrying the magnitude information, and thus the non-coherent design is inherently inferior to the coherent one. However, the non-coherent detection is only used for the frame synchronizer and detection of each data symbol still makes use of both magnitude and phase information in the whole PSAM system.

According to equation (A.5) (see Appendix A), the sampled received signal with frequency error is given as

$$r(k) = c(k)e^{j2\pi f_0 T_s k} s(k) + n(k). \quad (3.1)$$

where f_0 is the frequency offset after carrier recovery. Taking the squared magnitude of the received signal, we obtain

$$|r(k)|^2 = \underbrace{|c(k)|^2 |s(k)|^2}_{\text{Term 1}} + \underbrace{2\text{Re}\{c(k)e^{j2\pi f_0 T_s k} s(k)n^*(k)\}}_{\text{Term 2}} + \underbrace{|n(k)|^2}_{\text{Term 3}}. \quad (3.2)$$

where $\text{Re}[\]$ indicates the real part of a complex signal. From equation (3.2), for the same value of $c(k)$, $s(k)$ and $n(k)$, the receiver will have different values of $|r(k)|^2$ when different frequency offsets f_0 are applied. It seems that a non-coherent frame synchronizer, which is expected to perform equally on different frequency errors, is an impossibility. However, if we combine $e^{j2\pi f_0 T_s k}$ and $n^*(k)$ in second term of equation (3.2) together, we can think $e^{j2\pi f_0 T_s k} n^*(k)$ as a frequency-shifted version

of noise $n^*(k)$. Let $n'(k)$ denotes $e^{j2\pi f_0 T_s k} n^*(k)$. This frequency shift transforms one random process to another random process. However, since $n(k)$ is zero mean Gaussian noise with white spectrum, it can be proven that $n(k)$ and $n'(k)$ have same power spectrum, i.e. they are statistically identical. Because $|n(k)|^2 = |n'(k)|^2$, substitution of $n'(k)$ into equation (3.2) gives,

$$|r(k)|^2 = |c(k)|^2 |s(k)|^2 + 2\text{Re}\{c(k)s(k)n'(k)\} + |n'(k)|^2. \quad (3.3)$$

Equation (3.3) shows that there is an equivalent combination of a receiver that has zero frequency error and a channel noise $n'(k)$ which can be used to replace the combination of the receiver that has a frequency error f_0 and a channel noise $n(k)$. As $n(k)$ and $e^{j2\pi f_0 T_s k} n^*(k)$ are identical random process, it is implied that a scheme with a certain average performance on a receiver without frequency error will have the same average performance on a receiver with frequency error f_0 over the same ensemble of $n(k)$. In other words, this non-coherent frame synchronization system is statistically immune to a range of carrier frequency error.

3.3 Fading Estimation

In the last section, we eliminated the effect of carrier frequency offset by using a non-coherent system and thus the equation (3.1) can be replaced with the equivalent equation as

$$r(k) = c(k)s(k) + n(k). \quad (3.4)$$

So the following problem is how to eliminate the fading effect of $c(k)$. Channel fading estimation is considered as a major task of the frame synchronizer. In this non-coherent scheme, we only need to estimate the channel fading signal magnitude, which means the computation requirements are not as large as those in a coherent system.

Assume a mobile communication scenario where a mobile unit moves to a fixed end point along the different route with different speed repetitively. Each time a random signal $s(k)$ is transmitted. The receiver records one sample for each run. This scenario has been repeated infinite times and finally we obtain an ensemble of all sample records $r(k)$. Using the channel model in equation (3.4), the ensemble $\mathbf{r}(\mathbf{k})$ can be expressed as

$$\mathbf{r}(\mathbf{k}) = \mathbf{c}(\mathbf{k})\mathbf{s}(\mathbf{k}) + \mathbf{n}(\mathbf{k}) . \quad (3.5)$$

where $\mathbf{r}(\mathbf{k})$, $\mathbf{c}(\mathbf{k})$, $\mathbf{s}(\mathbf{k})$ and $\mathbf{n}(\mathbf{k})$ are marked in boldface to indicate random process. Furthermore, since $\mathbf{c}(\mathbf{k})$, $\mathbf{s}(\mathbf{k})$ and $\mathbf{n}(\mathbf{k})$ are stationary random processes, $\mathbf{r}(\mathbf{k})$ is a stationary process too.

The baseband power spectrum of $|r(k)|^2$ adapted from [28] is developed in Appendix B and given as

$$S_{r^2}(f) = \underbrace{\sigma_s^4 [S_{c^2}(f) - \delta(f)]}_{\text{Term 1}} + \underbrace{(2\sigma_s^4 + 2\sigma_s^2\sigma_n^2 + \sigma_n^4)}_{\text{Term 2}} + \underbrace{(\sigma_s^2 + \sigma_n^2)^2 \delta(f)}_{\text{Term 3}}. \quad (3.6)$$

The first term in the equation above is a scaled version of the power spectrum of $|c(k)|^2$, which is to be estimated in the following discussion, so we call it fading signal spectrum. The second term is called the noise term because it represents the variation in $|r(k)|^2$ caused by $s(k)$ and $n(k)$. Finally, the third term represents a dc value, which is the dc component of the squared magnitude of the fading signal, $|c(k)|^2$, in time domain. The power spectrum of the squared magnitude of received signal is illustrated as in Fig. 3.1.

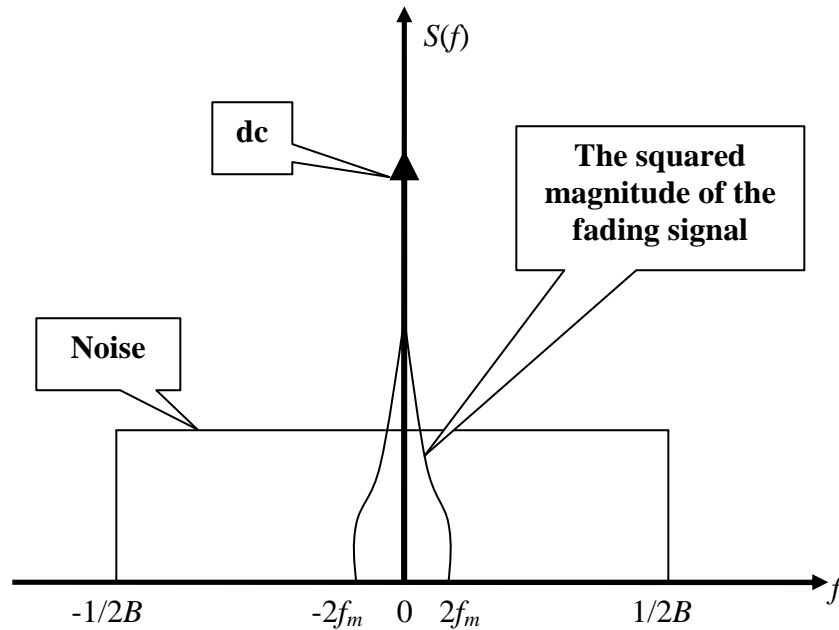


Fig. 3.1 Components of the power spectrum for $|r(k)|^2$ (with permission from [28])

where f_m is the maximum Doppler shift of the fading channel and the B is the bandwidth of transmitted signal.

Equation (3.6) shows that there is an additive relationship between the spectrum of $|c(k)|^2$ and that of noise. This additive relationship is only for the squared magnitude of the received signal $|r(k)|^2$, and this relationship implies that the components can be separated by proper linear filtering. From the spectrum of $|r(k)|^2$ in equation (3.6) and Fig. 3.1, we find that the power spectrum of $|c(k)|^2$ has a narrow band and is located at lower frequency, therefore an estimation of channel fading signal can be achieved by proper low-pass filtering of $|r(k)|^2$.

As illustrated in Fig. 3.1, the bandwidth of $|c(k)|^2$ is $4f_m$, four times the maximum Doppler shift, while the bandwidth of noise is spread over the entire signal. For a frequency non-selective slow fading channel, if a typical maximum fading rate is stated in Chapter 2 as 5%, then the normalized bandwidth of $|c(k)|^2$ is

20% (4 times 5%). This means by simply extracting the $|c(k)|^2$ from $|r(k)|^2$ using a low-pass filter, we obtain a reasonably low-noise estimate of the fading signal.

3.4 Data Model

In the PSAM system as illustrated in Fig. 3.2, the transmitter periodically inserts a specific pilot symbol into the data sequence at the interval of L_p symbols. With a specific sequence of N pilot symbols, this results in a combined pilot and data frame as illustrated in Fig. 2.7. The composite symbol sequence $s(k)$ is modulated by a square root Nyquist pulse, $p(t)$, and then transmitted over a channel characterized by flat slow fading and additive white Gaussian noise channel. Pilot symbols have the same pulse shape as the data symbols. The transmitted signal has a complex envelope given by,

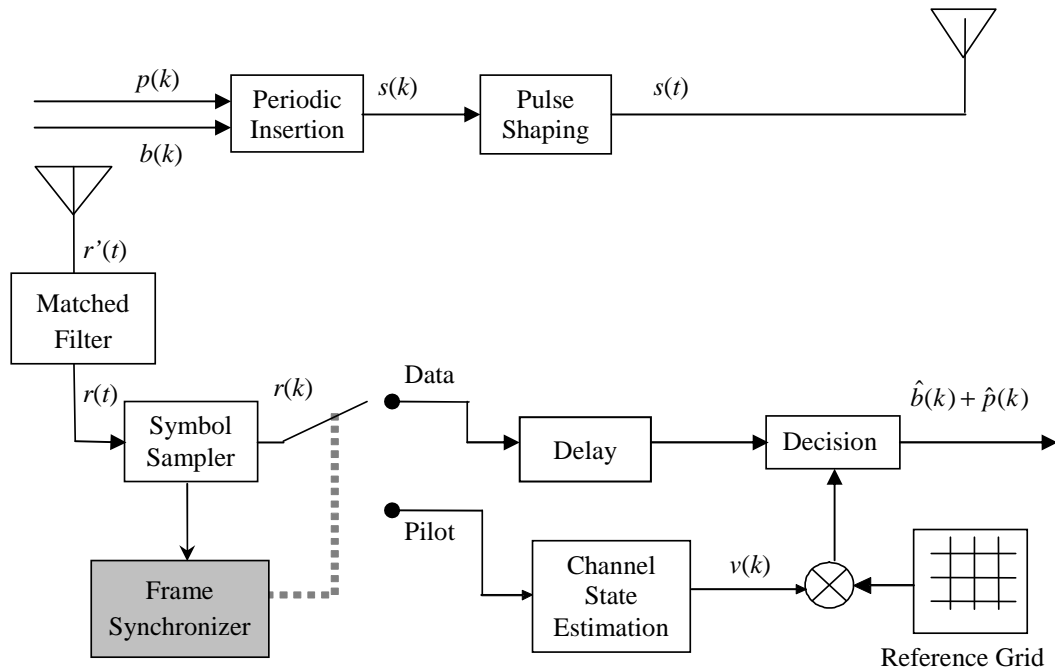


Fig. 3.2 PSAM transmitter and receiver structure [29]

$$s(t) = \sum_{k=-\infty}^{\infty} s(k) p(t - kT_s). \quad (3.7)$$

where $s(k)$ is the input pulse signal, T_s is the symbol time, and $p(t)$ is a unit energy pulse, which can be described in following equations:

$$\int_{-\infty}^{\infty} |p(t)|^2 dt = 1 \quad (3.8)$$

$$R_p(\tau) = \int_{-\infty}^{\infty} p(t) p^*(t - \tau) dt. \quad (3.9)$$

$$R_p(k) = R_p(kT_s) = \delta(k). \quad (3.10)$$

where $R_p(\tau)$ is the autocorrelation function of the pulse waveform $p(t)$ and $\delta(k)$ is the Kronecker delta function.

For frequency non-selective fading, the delay spread of the channel is much less than the symbol duration, i.e. all of the multi-paths arrive at receiver approximately at the same time. Therefore, the channel has no inherent intersymbol interference (ISI) and the multi-path distortion can be combined into one multiplicative distortion process $c(t)$ as we have discussed in Chapter 2. The received signal is then given by

$$r'(t) = c(t)s(t) + n(t). \quad (3.11)$$

where $n(t)$ is the zero mean AWGN with one-sided power spectral density $N_0/2$. As discussed in Section 2.2, passing this signal through a matched filter $p^*(-t)$ that is matched to the pulse shape $p(t)$ in the transmitter yields

$$r(t) = r'(t) * h(t). \quad (3.12)$$

where $*$ means the convolution operation and $h(t) = p^*(-t)$. Substituting equation (3.7) and equation (3.11) into (3.12), the output signal of the matched filter can be further given as

$$\begin{aligned}
r(t) &= \int_{-\infty}^{\infty} r'(\tau)h(t-\tau)d\tau \\
&= \int_{-\infty}^{\infty} c(\tau)s(\tau)p^*(\tau-t)d\tau + \int_{-\infty}^{\infty} n(\tau)p^*(\tau-t)d\tau \\
&= \int_{-\infty}^{\infty} \sum_{k=-\infty}^{\infty} s(k)c(\tau)p(\tau-kT_s)p^*(\tau-t)d\tau + n_c(t). \tag{3.13}
\end{aligned}$$

and sampling this received signal at the symbol time $t = nT_s$ gives,

$$r(n) = \sum_{k=-\infty}^{\infty} s(k) \int_{-\infty}^{\infty} c(\tau)p(\tau-kT_s)p^*(\tau-nT_s)d\tau + n_c(n). \tag{3.14}$$

where $r(n)$ is the response of the matched filter and symbol sampler. For slow fading, $c(t)$ is approximately constant over a symbol duration, so it may be pulled out of the integral. This yields

$$r(n) = \sum_{k=-\infty}^{\infty} s(k)c(\tau) \int_{-\infty}^{\infty} p(\tau-nT_s)p^*(\tau-kT_s)d\tau + n_c(n). \tag{3.15}$$

According to the properties of the Nyquist pulse in equation (3.8) to (3.10), we have

$$r(n) \approx \sum_{k=-\infty}^{\infty} s(k)c(k)R_p((k-n)T_s) + n_c(n). \tag{3.16}$$

when $n = k$, and because the property of noise does not change with these transformations, the equation (3.16) is finally simplified to

$$r(k) = s(k)c(k) + n(k) \tag{3.17}$$

This model is not strictly valid when variation in the received signal produces ISI; however, it is appropriate for a wide range of scenarios [23].

The synchronization structure developed later in this study is not limited to a specific fading process. In computer simulations the Rayleigh fading process is modeled as isotropic scattering,

$$E\{c_n c_{n-k}^*\} = \sigma_c^2 J_0(2\pi k f_d) \quad (3.18)$$

where $J_0(\bullet)$ is the zeroth order Bessel function, σ_c^2 is the variance of the fading component, and f_d is the maximum fading rate as stated in Chapter 2. This process is simulated based on Jakes' model [24].

With this data model, the basic idea behind PSAM is quite clear. If the fading component $c(t)$ can be estimated accurately, then this channel state estimation can be used to counteract the fading effect and make the data decision more accurate. Frame synchronization is required in order to implement such a process. As in Fig. 3.2, frame synchronization observes the received symbols and identifies the timing of the pilot symbols. Each pilot symbol gives a sample of channel state and these samples are then interpolated to form a continuous channel state estimation. This estimation is used to scale and rotate a reference decision grid and thus optimize the data output decision.

3.5 Maximum Likelihood Frame Synchronization

For a PSAM system, the frame synchronization must estimate the relative position of the first pilot symbol P_0 which corresponds to the start of a frame. Consider a full frame observation, \mathbf{x} , having length $L = L_p \times N$ with symbol index starting at 0,

$$\mathbf{x} = [x_0, x_1, x_2, \dots, x_n, \dots, x_{L-1}].$$

Let μ be the index of the pilot symbol P_0 within the full frame, where μ is an integer in the range $[0, L-1]$. The beginning of the frame (i.e., pilot symbol P_0) appears in any of the L positions in \mathbf{x} with equal probability. Therefore, the maximum likelihood estimation is to search for the value of $\hat{\mu}$ that maximizes the function $f_x(\mathbf{x} | \mu)$ as given by

$$\hat{\mu}_{ML} = \underset{\mu \in [0, L-1]}{\operatorname{argmax}} f_x(\mathbf{x} | \mu). \quad (3.19)$$

where $f_x(\mathbf{x} | \mu)$ assesses the similarity between the known pilot sequence \mathbf{P} and the N received pilot-spaced symbols denoted \mathbf{x}^p starting at position $\hat{\mu}$ and expressed as

$$\mathbf{x}^p = \sum_{k=0}^{N-1} x_{kL_p + \hat{\mu}} \quad (3.20)$$

The benefit of a precise estimate of channel fading signal is that, given channel state information, detection of pilot symbols could be achieved more easily and could be treated by using the traditional frame synchronization methods for AWGN channels. Assuming that we have perfect knowledge of channel fading signal, i.e. ignoring the error induced during the process of fading estimation, we can think of the fading channel as the combination of a hypothetical transmitter and a Gaussian noise channel. In this hypothetical transmitter, data symbols $|s(k)|$ are first modulated by fading signal $|c(k)|$, then the modified signal $|c(k)||s(k)|$ is transmitted over an AWGN channel. For simplicity, $|c(k)|$ is first dropped out in developing the PDF of $|r(k)|^2$. After the final expression is obtained, we substitute $|c(k)||s(k)|$ for $|s(k)|$ and give suitable results for a fading channel.

3.5.1 Synchronization in AWGN

Let \mathbf{r} denote the complex received signal, \mathbf{s} denotes the complex transmitted signal, and N_0 denotes the power spectral density of zero mean complex additive white Gaussian noise. Assuming the received signal is an N -dimensional vector and the components are assumed to be independent and identically distributed (i.i.d) to each other. It is well known that, for an AWGN channel [27], the joint conditional probability density function of the received signal is given as

$$f(\mathbf{r} | \mathbf{s}) = \prod_{i=0}^{N-1} f(r_i | s_i), \quad i = 0, 1, \dots, N-1 \quad (3.21)$$

where

$$f(r_i | s_i) = \frac{1}{\sqrt{\pi N_0}} \exp\left(-\frac{|r_i - s_i|^2}{N_0}\right) \quad (3.22)$$

For simplicity and convenience, we will denote the component r_i and s_i by r and s in the following discussion. After we obtain the desired probability density function of r , we will change it back with r_i . Some of the mathematic development is found in [28].

Let the component r and s be expressed in polar form as

$$\begin{cases} r = |r| \cdot \exp(j\theta_r) \\ s = |s| \cdot \exp(j\theta_s) \end{cases} \quad (3.23)$$

Expressing equation (3.22) in polar form yields

$$f((|r|, \theta_r) | (|s|, \theta_s)) = \frac{|r|}{\sqrt{\pi N_0}} \exp\left(-\frac{(|r|^2 + |s|^2)}{N_0}\right) \exp\left(\frac{2|r||s|\cos(\theta_r - \theta_s)}{N_0}\right) \quad (3.24)$$

Because pilot sequence is presented here in magnitude, our interest is the probability density function of $|r|$ conditioned on $|s|$. Integrating equation (3.24) over $\theta_r \in (0, 2\pi)$ for a specific value $\theta_s = \frac{\pi}{4}$, we obtain

$$\begin{aligned}
f(|r| | (|s|, \theta_s = \frac{\pi}{4})) &= \int_{2\pi} f(|r|, \theta_r | (|s|, \theta_s = \frac{\pi}{4})) d\theta_r \\
&= \int_{2\pi} \frac{|r|}{\sqrt{\pi N_0}} \exp\left(-\frac{(|r|^2 + |s|^2)}{N_0}\right) \exp\left(\frac{2|r||s|\cos(\theta_r - \frac{\pi}{4})}{N_0}\right) d\theta_r \\
&= \frac{|r|}{\sqrt{\pi N_0}} \exp\left(-\frac{(|r|^2 + |s|^2)}{N_0}\right) \int_{2\pi} \exp\left(\frac{2|r||s|\cos(\theta_r - \frac{\pi}{4})}{N_0}\right) d\theta_r. \quad (3.25)
\end{aligned}$$

Let $\theta_r' = \theta_r - \frac{\pi}{4}$ and then $d\theta_r' = d\theta_r$, also, because the cosine function in the above equation is a periodic function with a period of 2π and the interval of the integral is also 2π , θ_r' and $\theta_r - \frac{\pi}{4}$ have the same property as θ_r . Thus equation (3.25) is simplified to

$$f(|r| | (|s|, \theta_s = \frac{\pi}{4})) = \frac{|r|}{\sqrt{\pi N_0}} \exp\left(-\frac{(|r|^2 + |s|^2)}{N_0}\right) \int_{2\pi} \exp\left(\frac{2|r||s|\cos(\theta_r)}{N_0}\right) d\theta_r. \quad (3.26)$$

Using the modified Bessel function of the first kind and zero order from [30]

$$I_0(x) = \frac{1}{2\pi} \int_{2\pi} \exp(x \cos \theta) d\theta. \quad (3.27)$$

Substituting this modified Bessel function into the integral of equation (3.26) and let $x = \frac{2|r||s|}{N_0}$, the probability density function under the signal phase equal to $\pi/4$ becomes

$$f(|r||s|, \theta_s = \frac{\pi}{4}) = \frac{2\sqrt{\pi}|r|}{\sqrt{N_0}} \exp\left(-\frac{(|r|^2 + |s|^2)}{N_0}\right) I_0\left(\frac{2|r||s|}{N_0}\right). \quad (3.28)$$

In the similar way, we can show that the probability density functions for cases where phase θ_s is $3/4\pi$, $-4/\pi$, and $-3/4\pi$ are as same as the form in equation (3.28).

To derive the PDF of $f(|r||s|)$, we need to consider all the symbols with the same magnitude but different phases in the 16-QAM constellation. For convenience, we represent the constellation below in Fig. 3.3,

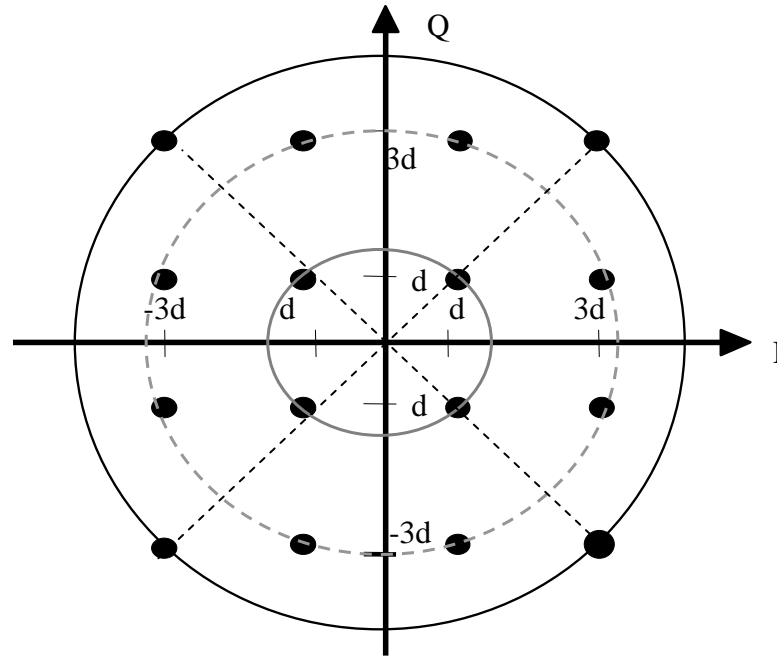


Fig. 3.3 Different magnitudes in a square 16-QAM constellation

Based on the assumption that all the symbols in 16-QAM constellation are equally likely to be sent, the probability of sending a symbol with a specific phase conditioned on same $|s|$ is equal. For instance, for the innermost circle when $|s|$ is $\sqrt{2}d$, as shown in the most inner circle on the constellation graph, the conditional probabilities for each possible phase are

$$\begin{aligned}
P\left(\theta_s = \frac{\pi}{4} \mid |s| = \sqrt{2}d\right) &= P\left(\theta_s = \frac{3\pi}{4} \mid |s| = \sqrt{2}d\right) \\
&= P\left(\theta_s = -\frac{\pi}{4} \mid |s| = \sqrt{2}d\right) \\
&= P\left(\theta_s = -\frac{3\pi}{4} \mid |s| = \sqrt{2}d\right) = \frac{1}{4}.
\end{aligned} \tag{3.29}$$

The PDF $f(|r| \mid |s|)$ for the $|s| = \sqrt{2}d$ is

$$\begin{aligned}
f(|r| \mid |s| = \sqrt{2}d) &= f\left(|r| \mid \left(|s| = \sqrt{2}d, \theta_s = \frac{\pi}{4}\right)\right) P\left(\theta_s = \frac{\pi}{4}\right) \\
&\quad + f\left(|r| \mid \left(|s| = \sqrt{2}d, \theta_s = \frac{3\pi}{4}\right)\right) P\left(\theta_s = \frac{3\pi}{4}\right) \\
&\quad + f\left(|r| \mid \left(|s| = \sqrt{2}d, \theta_s = -\frac{\pi}{4}\right)\right) P\left(\theta_s = -\frac{\pi}{4}\right) \\
&\quad + f\left(|r| \mid \left(|s| = \sqrt{2}d, \theta_s = -\frac{3\pi}{4}\right)\right) P\left(\theta_s = -\frac{3\pi}{4}\right) \\
&= f\left(|r| \mid \left(|s| = \sqrt{2}d, \theta_s = \frac{\pi}{4}\right)\right).
\end{aligned} \tag{3.30}$$

For the outermost circle when $|s|$ is $\sqrt{18}d$, the PDF $f(|r| \mid |s|)$ for the $|s| = \sqrt{18}d$ is

$$f(|r||s| = \sqrt{18d}) = f\left(|r||\left(|s| = \sqrt{18d}, \theta_s = \frac{\pi}{4}\right)\right). \quad (3.31)$$

It is clear that for each circle in Fig. 3.3, with the different magnitudes in the square 16-QAM constellation, no matter the value of signal phase, the probability density function of $f(|r||s|)$ is

$$f(|r||s|) = \frac{2\sqrt{\pi}|r|}{\sqrt{N_0}} \exp\left(-\frac{(|r|^2 + |s|^2)}{N_0}\right) I_0\left(\frac{2|r||s|}{N_0}\right). \quad (3.32)$$

Changing the random variable in equation (3.32) from $|r|$ into $|r|^2$ and $|s|$ into $|s|^2$ yields

$$f(|r|^2 |s|^2) = \sqrt{\frac{\pi}{N_0}} \exp\left(-\frac{(|r|^2 + |s|^2)}{N_0}\right) I_0\left(\frac{2|r||s|}{N_0}\right). \quad (3.33)$$

Under high SNR, from [6] the modified Bessel function in equation (3.27) can be approximated as

$$I_0(x) \approx \frac{\exp\left(|x| - \frac{1}{2} \ln|x|\right)}{\sqrt{2\pi}} \approx \frac{\exp(|x|)}{\sqrt{2\pi}}. \quad (3.34)$$

So the modified Bessel function in equation (3.34) is approximated to

$$I_0\left(\frac{2|r||s|}{N_0}\right) \approx \frac{\exp\left(\frac{2|r||s|}{N_0}\right)}{\sqrt{2\pi}}. \quad (3.35)$$

Thus, under high SNR, $f(|r||s|)$ can be simplified to

$$f(|r||s|) \approx \frac{2\sqrt{\pi}|r|}{\sqrt{2\pi N_0}} \exp\left(-\frac{(|r|^2 + |s|^2)}{N_0}\right) \exp\left(\frac{2|r||s|}{N_0}\right)$$

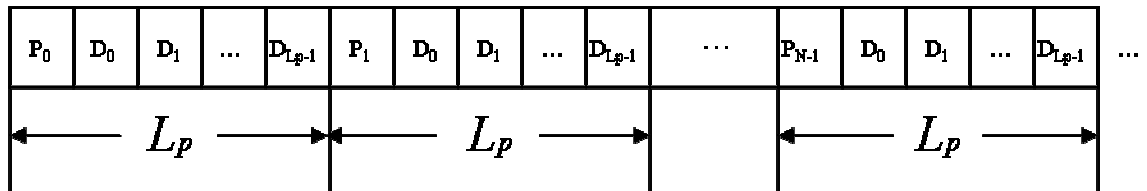
$$= \sqrt{\frac{2}{N_0}} |r| \exp\left(-\frac{(|r|-|s|)^2}{N_0}\right). \quad (3.36)$$

And therefore $f(|r|^2 ||s|^2)$ can be approximated as

$$f(|r|^2 ||s|^2) \approx \frac{1}{\sqrt{2N_0}} \exp\left(-\frac{(|r|-|s|)^2}{N_0}\right). \quad (3.37)$$

Equation (3.37) indicates that, under high SNR, the conditional probability function of the squared magnitude of the received signal $|r|^2$ is similar to the Gaussian density distribution in terms of symbol magnitude $|r|$. Note that this Gaussian function is not expressed in $|r|^2$. This function does not integrate to 1 and is therefore not, strictly speaking, a probability density function. However, it serves well in our study because this makes it very easy to simplify the computation and it approximates the conditional probability density function for a sequence of symbols.

As mentioned in Chapter 2, in this pilot symbol assisted modulation system, an interleaved frame format is used and it is illustrated in Fig. 3.4.



1 frame = N subframes = N x L_p symbols

Fig. 3.4 Input signal structure for a PSAM system

Pilot symbols are represented by P_i , where i is the index of pilot symbol into the pilot sequence P_0, P_1, \dots, P_{N-1} . A subframe is consisted of a pilot symbol and $L_p - 1$ data symbols. One frame contains N subframes. N is the length of a pilot sequence. Thus one frame has total $L = L_p \times N$ symbols. One frame of received symbols is called a full frame observation. If we space L_p symbols apart from each other, then we have pilot-spaced observations of a full frame observation. There are $N-1$ different pilot-spaced observations in a full frame. In simulation, every pilot symbol is inserted into the first position of every subframe at the transmitter as shown in Fig. 3.4.

To maximize the likelihood function, as in [31], the following notations are defined:

P --- Pilot symbol sequence

$$\mathbf{P} = [|P_0|^2, |P_1|^2, \dots, |P_{N-1}|^2]$$

d^p --- Random data symbols spaced L_p symbols apart from each other when they appear in a full frame observation. The superscript **p** stands for the pilot-spaced.

$$\mathbf{d}^p = [|d_0|^2, |d_1|^2, \dots, |d_{N-1}|^2]$$

r^p --- The pilot-spaced observation, which is the collection of symbols within a full received frame starting at the 1st position and spaced apart from each other by L_p symbols.

$$\mathbf{r}^p = [|r_0|^2, |r_1|^2, \dots, |r_{N-1}|^2]$$

Note that the elements in **P** must be the symbols located on the outermost circle or the innermost circle defined in the 16-QAM constellation. Both **r^p** and **d^p** are obtained by sampling the symbol stream at the pilot symbol spacing L_p .

Therefore, by equation (3.21) and equation (3.37), we can express the joint conditional probability density function of N -dimensional pilot-spaced random variable $\mathbf{r}^{\mathbf{P}}$ on N -dimensional pilot symbol \mathbf{P} as

$$\begin{aligned} f(\mathbf{r}^{\mathbf{P}} | \mathbf{P}) &= \prod_{i=0}^{N-1} f(|r_i|^2 | |P_i|^2) = \left(\left(\frac{1}{\sqrt{2N_0}} \right)^N \prod_{i=0}^{N-1} \exp \left(- \frac{(|r_i| - |P_i|)^2}{N_0} \right) \right) \\ &= \left(\frac{1}{\sqrt{2N_0}} \right)^N \exp \left(- \sum_{i=0}^{N-1} \frac{(|r_i| - |P_i|)^2}{N_0} \right). \end{aligned} \quad (3.38)$$

Then the frame synchronization problem of finding μ , the index of the pilot symbol P_0 within the full frame, becomes,

$$\hat{\mu}_{ML} = \arg \max \left(\left(\frac{1}{\sqrt{2N_0}} \right)^N \exp \left(- \sum_{i=0}^{N-1} \frac{(|r_i| - |P_i|)^2}{N_0} \right) \right). \quad (3.39)$$

where it is understood that pilot spaced sequence $r_0, r_1, r_2 \dots$ begins at the offset μ . The received symbol index $\mu + iL_p$ is modulo L and the pilot spaced symbols “wrap around” within the observed full frame.

By taking the logarithm of equation (3.39) and neglecting terms that are unrelated to $|P|$, we obtain the maximum likelihood criterion for the AWGN channel,

$$\hat{\mu}_{ML_AWGN} = \arg \max \left(\sum_{i=0}^{N-1} - (|r_i| - |P_i|)^2 \right). \quad (3.40 a)$$

or it is expanded as

$$\hat{\mu}_{ML_AWGN} = \arg \max \left(\sum_{i=0}^{N-1} (2|r_i||P_i| - |r_i|^2 - |P_i|^2) \right). \quad (3.40 b)$$

When viewed in N dimensional space, we select the received pilot-spaced sequence that has the minimum Euclidean distance to the pilot sequence.

3.5.2 Synchronization in Fading

We now consider the frame synchronization problem in a Rayleigh fading channel. As discussed in the beginning of Section 3.5, we assume a transmission model where data symbols $|s(k)|$ are first modulated by fading signal $|c(k)|$, then the modified signal $|c(k)||s(k)|$ is transmitted over AWGN channel. This gives the same received signal as if data signal has been transmitted over a fading and noisy channel and this is consistent with data model (equation 3.17). Thus, the probability density function suitable for fading, noisy channel is given as

$$f(|r|^2 | |c|^2; |P|^2) \approx \frac{1}{\sqrt{2N_0}} \exp\left(-\frac{(|r| - |c||P|)^2}{N_0}\right). \quad (3.41)$$

In the similar way, as in the development of maximum likelihood metric for the AWGN channel, we give the maximum likelihood metric for the Rayleigh fading channel as

$$\hat{\mu}_{ML_Fading} = \arg \max \left(\sum_{i=0}^{N-1} -(|r_i| - |c_i||P_i|)^2 \right) \quad (3.42 \text{ a})$$

or it is expanded as

$$\hat{\mu}_{ML_Fading} = \arg \max \sum_{i=0}^{N-1} \left((2|r_i||c_i||P_i| - |r_i|^2 - |c_i|^2|P_i|^2) \right). \quad (3.42 \text{ b})$$

In next chapter, Simulink® models are used to test the performance of both frame synchronizers with various pilot symbol sequences. The models implement the ML decision criteria above - an “argmax” structure indicates the most likely position of pilot symbol P_0 within a window length of L .

3.6 Maximum A Posteriori Probability Frame Synchronization

In order to design a frame synchronizer to make a good decision on the location of pilot symbols based on the pilot-spaced observation of received signal \mathbf{r}^p , we consider a rule based on the computation of the posterior probabilities defined as $P(\mathbf{P}|\mathbf{r}^p)$. This decision criterion is based on selecting the pilot symbol corresponding to the maximum of the set of the posterior probabilities $\{\mathbf{P} \text{ (pilot symbol was transmitted}|\mathbf{r}^p)\}$. Accordingly this criterion is called maximum a Posteriori probability (MAP) criterion.

Using Bayes' formula in [22], the posterior probabilities may be expressed as

$$f(\mathbf{P} | \mathbf{r}^p) = \frac{f(\mathbf{r}^p | \mathbf{P})P(\mathbf{P})}{f(\mathbf{r}^p)}. \quad (3.43)$$

where $f(\mathbf{r}^p | \mathbf{P})$ is the conditional probability density function (PDF) of the pilot-spaced observation of the received signal \mathbf{r}^p given pilot symbol sequence \mathbf{P} , and $P(\mathbf{P})$ is the a priori probability of the pilot signal being transmitted.

3.6.1 Synchronization in AWGN

Using the notations of \mathbf{r}^p , \mathbf{P} , and \mathbf{d}^p defined in section 3.5.1, the MAP formulation (3.43) may also be expressed as

$$\begin{aligned} f(\mathbf{P} | \mathbf{r}^p) &= \frac{f(\mathbf{r}^p | \mathbf{P})P(\mathbf{P})}{f(\mathbf{r}^p)} \\ &= \frac{f(\mathbf{r}^p | \mathbf{P})P(\mathbf{P})}{\sum_{All\ d} f(\mathbf{r}^p | \mathbf{d}^p)P(\mathbf{d}^p) + \sum_{All\ P_s} f(\mathbf{r}^p | \mathbf{P}_s)P(\mathbf{P}_s)P(\mathbf{P}_s) + f(\mathbf{r}^p | \mathbf{P})P(\mathbf{P})}. \end{aligned} \quad (3.44)$$

where the pilot spaced received signal \mathbf{r}^p may consist of pilot symbols \mathbf{P} , data symbols \mathbf{d}^p and in some cases \mathbf{P}_s , which is the shifted version of pilot symbol

sequence \mathbf{P} and can be expressed as $\mathbf{P}_s = [|P_a|^2, |P_{a+1}|^2, \dots, |P_{N-1}|^2, |P_0|^2, \dots, |P_{a-1}|^2]$. All the elements of the vectors in equation (3.44) are the squared magnitude of pilot-spaced observations. Before the development of this MAP decision criterion, we need to define several probabilities firstly. Since P_0 , the first symbol of a pilot-spaced observation, can fall in any position within a full frame observation of length $L = L_p \times N$ symbols with a uniform distribution, the probability of observing the pilot sequence is

$$P(\mathbf{P}) = \frac{1}{L_p N}, \quad (3.45)$$

The probability of observing a specific shifted pilot sequence is

$$P(\mathbf{P}_s) = \left(\frac{N-1}{L_p N} \right) \left(\frac{1}{N-1} \right) = \frac{1}{L_p N}, \quad (3.46)$$

And the probability of observing a specific data sequence $\mathbf{d}^{\mathbf{P}}$ is

$$P(\mathbf{d}^{\mathbf{P}}) = \left(\frac{L_p N - N}{L_p N} \right) \prod_{i=1}^N P(|d_i|^2). \quad (3.47)$$

where $P(|d_i|^2)$ is the prior probability of sending the squared symbol magnitude of $|d_i|^2$.

Dividing both numerator and denominator in the right side of equation (3.44) by the numerator gives

$$f(\mathbf{P} | \mathbf{r}^{\mathbf{P}}) = \frac{1}{\left(\frac{\sum_{all d} f(\mathbf{r}^{\mathbf{P}} | \mathbf{d}^{\mathbf{P}}) P(\mathbf{d}^{\mathbf{P}})}{f(\mathbf{r}^{\mathbf{P}} | \mathbf{P}) P(\mathbf{P})} \right) + \left(\frac{\sum_{all p_s} f(\mathbf{r}^{\mathbf{P}} | \mathbf{P}_s) P(\mathbf{P}_s)}{f(\mathbf{r}^{\mathbf{P}} | \mathbf{P}) P(\mathbf{P})} \right) + 1}. \quad (3.48)$$

Maximization of the posterior probabilities is equal to the maximization of the equation above and is equivalent to the minimization of the first two terms in the denominator. Considering that for a pilot symbol sequence that is long enough, there will be many data sequences that are closer to pilot symbol sequence than shifted pilot sequences in terms of Euclidean distance in the multidimensional signal space. Therefore correct detection of pilot symbols relies more on using the decision metric to exclude data sequences close to the pilot sequence rather than the shifted pilot sequences. Thus, the second term in the denominator of equation (3.48) can be ignored reasonably and rearranging the equation (3.48) gives

$$\frac{1}{f(\mathbf{P}|\mathbf{r}^p)} - 1 = \frac{\sum_{All d} f(\mathbf{r}^p | \mathbf{d}^p)P(\mathbf{d}^p)}{f(\mathbf{r}^p | \mathbf{P})P(\mathbf{P})} . \quad (3.49)$$

Inverting the equation (3.49) gives

$$\frac{f(\mathbf{P}|\mathbf{r}^p)}{1 - f(\mathbf{P}|\mathbf{r}^p)} = \frac{f(\mathbf{r}^p | \mathbf{P})P(\mathbf{P})}{\sum_{All d} f(\mathbf{r}^p | \mathbf{d}^p)P(\mathbf{d}^p)} . \quad (3.50)$$

Thus the maximization of posteriori probability $f(\mathbf{P}|\mathbf{r}^p)$ is equal to the maximization of the right side of equation (3.50).

The denominator in the equation above requires calculation over the set of all possible data symbols, which may be a terrible task for large frames. To further reduce computation, we notice that contributions from each term in the summation are not equal. The data symbol sequence that is closest to the pilot-spaced observation \mathbf{r}^p will contribute most significantly to the sum operation. We call this term the dominant term \mathbf{d}_{dom}^p , and use the dominant term as an approximation to the sum, i.e., sequence \mathbf{d}_{dom}^p generates the maximum value for the expression $f(\mathbf{r}^p | \mathbf{d}^p)P(\mathbf{d}^p)$ among all possible data sequences. This approximation gives good performance in high SNR conditions. Thus the right side of equation (3.50) is further reduced to

$$\frac{f(\mathbf{r}^p | \mathbf{P})P(\mathbf{P})}{f(\mathbf{r}^p | \mathbf{d}_{\text{dom}}^p)P(\mathbf{d}_{\text{dom}}^p)}. \quad (3.51)$$

In order to calculate this posteriori probability, there is only one remaining question: how to determine the dominant data sequence $\mathbf{d}_{\text{dom}}^p$. Since elements in $\mathbf{d}_{\text{dom}}^p$ are assumed to be independent random variables and in additive white Gaussian channel, we use the hard decision of data sequence s to replace it and calculate the likelihood ratio in equation (3.51). This is because the hard decision is supposed to be the data sequence closest to the received sequence, hence contributes predominately to the sum of all data sequence as $\mathbf{d}_{\text{dom}}^p$ does. We expand the abovementioned expression as

$$f(\mathbf{r}^p | \mathbf{d}_{\text{dom}}^p)P(\mathbf{d}_{\text{dom}}^p) = \prod_{i=0}^{N-1} f(|r_i|^2 | |d_{(dom)i}|^2)P(|d_{(dom)i}|^2). \quad (3.52)$$

Replacing the dominant data sequence $\mathbf{d}_{\text{dom}}^p$ with hard decision s and combining equation (3.38), the likelihood ratio (3.51) is finally given as

$$\frac{f(\mathbf{r}^p | \mathbf{P})P(\mathbf{P})}{f(\mathbf{r}^p | \mathbf{d}_{\text{dom}}^p)P(\mathbf{d}_{\text{dom}}^p)} = \frac{\prod_{i=0}^{N-1} f(|r_i|^2 | |P_i|^2) \cdot \left(\frac{1}{L_p N}\right)}{\prod_{i=0}^{N-1} f(|r_i|^2 | |s_i|^2) \cdot P(|s_i|^2)}. \quad (3.53)$$

Therefore, our next concern is that how to obtain the hard decision sequence s . As illustrated in Fig. 3.4, there are three levels of data symbol magnitude on the square 16-QAM constellation. The squared magnitude of these symbols are $2d^2$, $10d^2$ and $18d^2$ respectively. We define following hypotheses as

$$H_0: |s|^2 = 2d^2 \text{ was transmitted,}$$

$$H_1: |s|^2 = 10d^2 \text{ was transmitted,}$$

$$H_2: |s|^2 = 18d^2 \text{ was transmitted.}$$

Let \mathbf{R} denote the squared magnitude of the observed symbols $|r|^2$. The posteriori probabilities $P(H_0 | \mathbf{R})$, $P(H_1 | \mathbf{R})$ and $P(H_2 | \mathbf{R})$ are obtained in similar way as

$$\begin{aligned}
 P(H_0 | \mathbf{R}) &= \frac{f_{R|H_0}(\mathbf{R} | H_0)P(H_0)}{f_R(\mathbf{R})} \\
 &= \frac{\frac{1}{\sqrt{2N_0}} \exp\left(-\frac{(\sqrt{\mathbf{R}} - \sqrt{2}d)^2}{N_0}\right)P(H_0)}{f_R(\mathbf{R})}.
 \end{aligned} \tag{3.54}$$

$$\begin{aligned}
 P(H_1 | \mathbf{R}) &= \frac{f_{R|H_1}(\mathbf{R} | H_1)P(H_1)}{f_R(\mathbf{R})} \\
 &= \frac{\frac{1}{\sqrt{2N_0}} \exp\left(-\frac{(\sqrt{\mathbf{R}} - \sqrt{10}d)^2}{N_0}\right)P(H_1)}{f_R(\mathbf{R})}.
 \end{aligned} \tag{3.55}$$

$$\begin{aligned}
 P(H_2 | \mathbf{R}) &= \frac{f_{R|H_2}(\mathbf{R} | H_2)P(H_2)}{f_R(\mathbf{R})} \\
 &= \frac{\frac{1}{\sqrt{2N_0}} \exp\left(-\frac{(\sqrt{\mathbf{R}} - \sqrt{18}d)^2}{N_0}\right)P(H_2)}{f_R(\mathbf{R})}.
 \end{aligned} \tag{3.56}$$

It is assumed that the 16 symbols in the square 16-QAM constellation are equally likely to be transmitted, the probabilities of the three hypothesis are: $P(H_0) = P(H_2) = 1/4$ and $P(H_1) = 1/2$. Since $f_R(\mathbf{R})$ is a common denominator in the above three equations and only the relative values between three hypothesis are interested, these three a posteriori probabilities can be changed to

$$f_{R|H_0}(\mathbf{R} | H_0)P(H_0) = \frac{1}{\sqrt{2N_0}} \exp\left(-\frac{(\sqrt{\mathbf{R}} - \sqrt{2d})^2}{N_0}\right) \left(\frac{1}{4}\right), \quad (3.57)$$

$$f_{R|H_1}(\mathbf{R} | H_1)P(H_1) = \frac{1}{\sqrt{2N_0}} \exp\left(-\frac{(\sqrt{\mathbf{R}} - \sqrt{10d})^2}{N_0}\right) \left(\frac{1}{2}\right), \quad (3.58)$$

$$f_{R|H_2}(\mathbf{R} | H_2)P(H_2) = \frac{1}{\sqrt{2N_0}} \exp\left(-\frac{(\sqrt{\mathbf{R}} - \sqrt{18d})^2}{N_0}\right) \left(\frac{1}{4}\right). \quad (3.59)$$

These a posteriori probabilities diminish very quickly in high SNR conditions when the observation is far from the hypothesis value (i.e., the squared magnitude of the transmitted signal). This means that when an observed received signal magnitude value is between two adjacent hypothesis values, the third one has very little influence to the detection probability. Thus this three-hypothesis can be simplified to two threshold test. The first threshold test is between H_0 and H_1 when the observed value is less than $10d^2$. The second threshold test is between H_1 and H_2 when the observation is more than H_1 . The case where the observed values equals H_1 can be arbitrarily combined with either threshold test, the probability to combine with either of them is $1/2$. These thresholds can be obtained by following step:

If the a posterior probability $f_R(\mathbf{R} | H_0)P(H_0) > f_R(\mathbf{R} | H_1)P(H_1)$, we select H_0 as the transmitted signal; otherwise, we select H_1 , it may be expressed as

$$\frac{f_R(\mathbf{R} | H_1)P(H_1)}{f_R(\mathbf{R} | H_0)P(H_0)} \underset{H_0}{\overset{H_1}{\geq}} 1. \quad (3.60)$$

But, from equations (3.57) and (3.58),

$$\frac{f_R(\mathbf{R} | H_1)P(H_1)}{f_R(\mathbf{R} | H_0)P(H_0)} = 2 \cdot \exp\left(\frac{(\sqrt{\mathbf{R}} - \sqrt{2d})^2 - (\sqrt{\mathbf{R}} - \sqrt{10d})^2}{N_0}\right). \quad (3.61)$$

Replacing $\sqrt{\mathbf{R}}$ with $|r|$, the magnitude of received observation, thus equation (3.60) may be expressed as

$$\frac{2(\sqrt{10d} - \sqrt{2d})|r| - 8d^2}{N_0} \underset{H_0}{\overset{H_1}{\gtrless}} \text{Ln}\left(\frac{1}{2}\right) \quad (3.62)$$

Or equivalently,

$$|r| \underset{H_0}{\overset{H_1}{\gtrless}} \frac{N_0 \text{Ln}\left(\frac{1}{2}\right) + 8d^2}{2(\sqrt{10d} - \sqrt{2d})}. \quad (3.63)$$

Similarly, if the posteriori probability $f_R(\mathbf{R} | H_1)P(H_1) > f_R(\mathbf{R} | H_2)P(H_2)$, we select H_1 as transmitted signal; otherwise, we select H_2 . Comparing the ratio of these two probabilities, it can be derived in same process as we used to derive equation (3.63), so the other threshold can be expressed as

$$|r| \underset{H_1}{\overset{H_2}{\gtrless}} \frac{N_0 \text{Ln}(2) + 8d^2}{2(\sqrt{18d} - \sqrt{10d})}. \quad (3.64)$$

Therefore these two thresholds are listed below as

$$\left\{ \begin{array}{l} \text{Threshold 1} = \frac{N_0 \text{Ln}\left(\frac{1}{2}\right) + 8d^2}{2(\sqrt{10d} - \sqrt{2d})} \\ \text{Threshold 2} = \frac{N_0 \text{Ln}(2) + 8d^2}{2(\sqrt{18d} - \sqrt{10d})} \end{array} \right. \quad (3.65)$$

It is interesting to note that in order to compute these thresholds; we need the knowledge of value of power spectral density of additive Gaussian noise, or, equivalently, the signal-to-noise ratio SNR. Also, we note that the thresholds apply to the magnitude of the receiver observation instead of squared magnitude of the

received observation. This is because the independent variables in the posteriori probabilities are expressed in the magnitude of the received observation. To illustrate the use of equation (3.65), let consider a simple example. Assuming that d is equal to 1 and SNR is 20 dB, the thresholds in (3.65) are

$$\left\{ \begin{array}{l} \text{Threshold 1} = \frac{\frac{1}{10} \text{Ln}\left(\frac{1}{2}\right) + 8}{2(\sqrt{10} - \sqrt{2})} \approx 2.27 \\ \text{Threshold 2} = \frac{\frac{1}{10} \text{Ln}(2) + 8}{2(\sqrt{18} - \sqrt{10})} \approx 3.73 \end{array} \right. \quad (3.66)$$

And the thresholds value can be demonstrated in Fig. 3.5 as

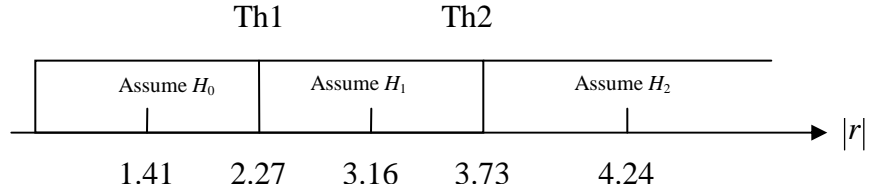


Fig. 3.5 Thresholds illustration

Using this two-threshold tester, the hard decision of data sequence is obtained to server for the maximization of the posteriori possibility. Expanding equation (3.53) with conditional probability in an AWGN channel gives

$$\frac{\prod_{i=0}^{N-1} f(r_i | P_i) \cdot \left(\frac{1}{L_p N}\right)}{\prod_{i=0}^{N-1} f(r_i | s_i) \cdot P(s_i)} = \frac{\left(\frac{1}{\sqrt{2N_0}}\right)^N \prod_{i=0}^{N-1} \exp\left(-\frac{(|r_i| - |P_i|)^2}{N_0}\right) \left(\frac{1}{L_p N}\right)}{\left(\frac{1}{\sqrt{2N_0}}\right)^N \prod_{i=0}^{N-1} \exp\left(-\frac{(|r_i| - |s_i|)^2}{N_0}\right) P(s_i)} \quad (3.67)$$

Taking the logarithm of the above equation, dropping constants and collecting terms gives the MAP synchronization criterion in the AWGN channel:

$$\hat{\mu}_{MAP_AWGN} = \arg \max \left\{ \sum_{i=0}^{N-1} \left(|s_i|^2 - |P_i|^2 \right) + 2|r_i|(|P_i| - |s_i|) - LnP(|s_i|^2) \right\}. \quad (3.68)$$

3.6.2 Synchronization in Fading

The thresholds expressions in equation (3.65) need to be modified to be suitable for the fading channel model. As we have discussed in the data model, we can replace data symbol d with $|c|d$, however, by this way, $|c|$ will appear in the denominator of the threshold equations. Because $|c|$ is the estimate of fading signal, estimation errors may cause it to take zero or negative value. Since $|c|$ is a magnitude and cannot be a negative value, we set $|c|$ to be very close to zero but larger than zero when it is estimated as a negative value or zero in simulation. By doing this restraint, we can always have positive estimation of fading signal $|c|$. Adding the fading signal $|c|$ into threshold functions and the MAP frame synchronization criterion (3.68), we have the suitable metric of MAP for Rayleigh fading channel,

$$\hat{\mu}_{MAP_Fading} = \arg \max \left\{ \sum_{i=0}^{N-1} \left(|c_i|^2 (|s_i|^2 - |P_i|^2) + 2|c_i||r_i|(|P_i| - |s_i|) - LnP(|s_i|^2) \right) \right\}. \quad (3.69)$$

This asymptotic function is a function of pilot-spaced observations and an “argmax” structure is used to indicate the most likely position of pilot symbol P_0 within a window length of L .

Chapter 4 Simulation Implementation

In this chapter, Matlab/Simulink®, computer simulation software for this study is briefly introduced. Then the system simulation models are described from top to bottom levels in hierarchy.

4.1 Simulink® Introduction

In this study, Simulink® was chosen as the simulation software to test the performance of frame synchronization scheme. Simulink is a program that runs as a companion to MATLAB®. As a very popular simulation software, Simulink is widely used in industry and academia.

Simulink® is used to model, simulate, and analyze systems that change over time [32]. These systems are usually dynamic systems such as electrical circuits, braking systems, and many other mechanical systems. Simulink supports linear and nonlinear systems modeled in continuous time, discrete time, or a hybrid of the two. These systems can also be multirate. Simulink provides a graphical user interface (GUI) for building models as block diagrams which means the models can be drawn as we do with pencil and paper. Compared with previous simulation programs such as C and C+ languages that require complicated programming and debugging to formulate equations, it is easier to model these equations with Simulink by using its block libraries. Models in Simulink are hierarchical and they can be built by using both top-down and bottom-up approaches. The system can be viewed at a high level, and then the increasing levels of model detail can be seen by double-click blocks to go down through the levels.

Generally, simulating a dynamic system is a two-step process with Simulink. First, a graphical model of the system is created by using integrated blocks. The model depicts the time-dependent mathematical relationships among the system's inputs, states, and outputs. Then, Simulink is run to simulate the behavior of the system over a specified time span. The simulation results can be viewed while Simulink is running. Because MATLAB and Simulink are integrated together, the models can be simulated, analyzed, and revised in either environment.

Although running Simulink sometimes means more machine time and higher demands to the power of the computer, when compared with the human time spent on building and debugging models in other program languages, Simulink is still an economical choice. The cost of human time is high and computers continue to become more powerful and cheaper.

4.2 System Overview

In this simulation system, our simulation model is built by top-down hierarchy. The block diagram of Fig. 4.1 shows the top-level of the simulation models.

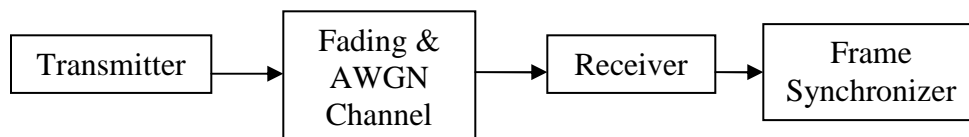


Fig. 4.1 System structure (top level)

At the top level of the simulation system structure, a signal is first generated and modulated in the transmitter and then transmitted over a frequency non-selective, slow and noisy fading channel. On the receiver side, assuming perfect symbol timing, the received signal is first processed through a matched filter and then sampled by the symbol sampler. These sampled discrete received signals go into the non-coherent frame synchronizer to be processed and then the corresponding statistical performance evaluations are calculated. Please note that in simulation we use baseband linear modulation and avoid the stages of high frequency carrier modulation and carrier recovery, therefore we can simplify the Simulink structure and make the simulation analysis easier. However, the carrier frequency and phase error cannot be neglected. Because, even after good carrier recovery, there is still some residual frequency error and this error will rotate the received signal and distort the received signal severely. In the subsequent discussion, the effect of frequency offset will be simulated and the impact of this error to the performance of frame synchronization algorithms will be tested.

4.2.1 Transmitter Overview

The first block in the top level system structure is the transmitter block. In the transmitter there are two general parts: the input signal generator and the Nyquist pulse shaping filter (square root raised cosine filter). A discrete uniform distributed random data sequence and a specific pilot sequence are generated in the signal generator first and are mapped into the 16-QAM data set respectively by using a 16-QAM mapper. These two sequences then interleave together and form the input frame structure as introduced in Fig. 3.4, in which every pilot symbol is located in the first position in every subframe. This serial sequence is input into the system as the raw input signal for the whole simulation. Since the data sequence and pilot sequence are all mapped by a 16-QAM mapper, they are all discrete complex signals. The Simulink block diagram for the transmitter is illustrated in Fig. 4.2.

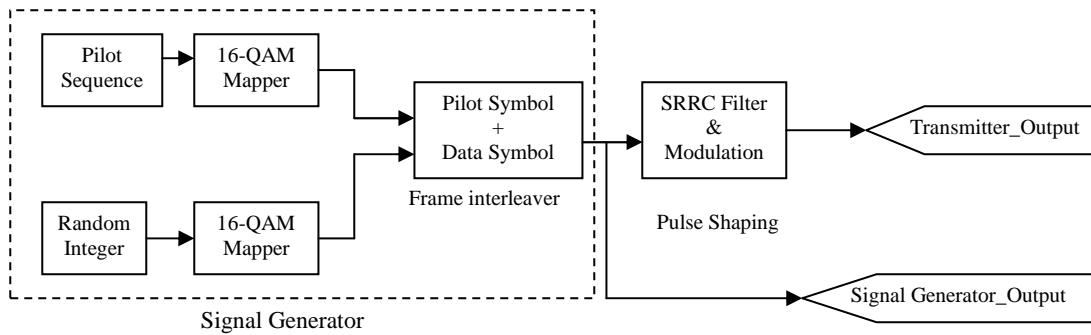


Fig. 4.2 Simulink block diagram of transmitter

The “random integer” block generates uniformly distributed integer data in the range of $[0, M-1]$, where M is the M-ary number. In this transmitter we use 16-QAM, so $M = 16$. The 16-QAM constellation of the random data simulated by Simulink is shown as follows in Fig. 4.3,

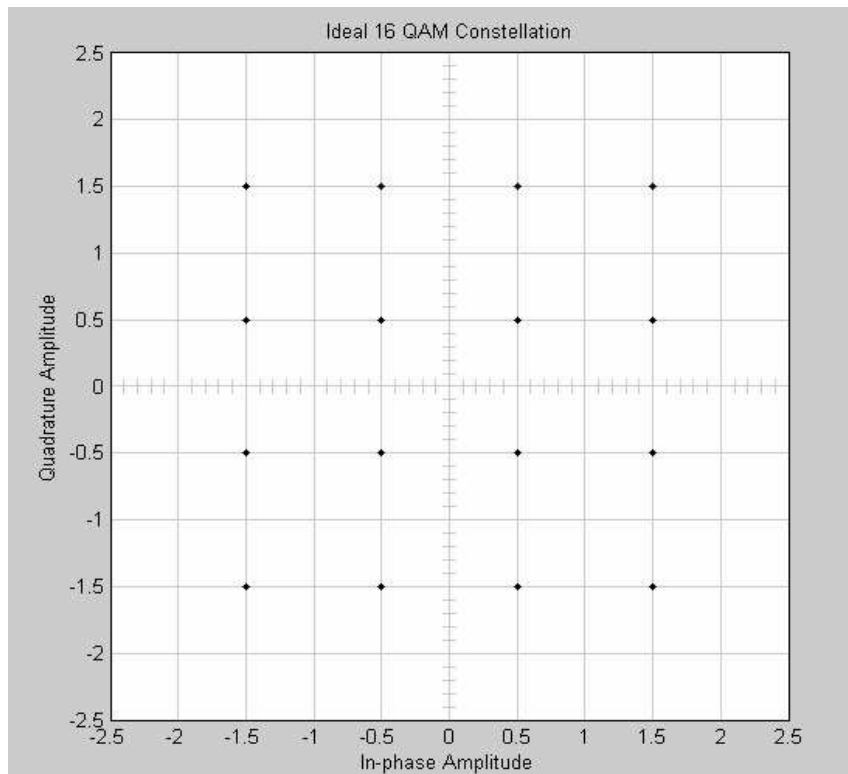


Fig. 4.3 Constellation 16 QAM from Simulink

In this square 16-QAM constellation, the distance between symbols is normalized to minimum 1. As illustrated in Fig. 4.4, there are three different levels of magnitude according to the constellation of 16-QAM. According to the discussion of pilot symbol mapping in Chapter 2, logic **1** in the pilot sequence is mapped to an outermost symbol, and Logic **0** in the pilot sequence is mapped to an innermost symbol.

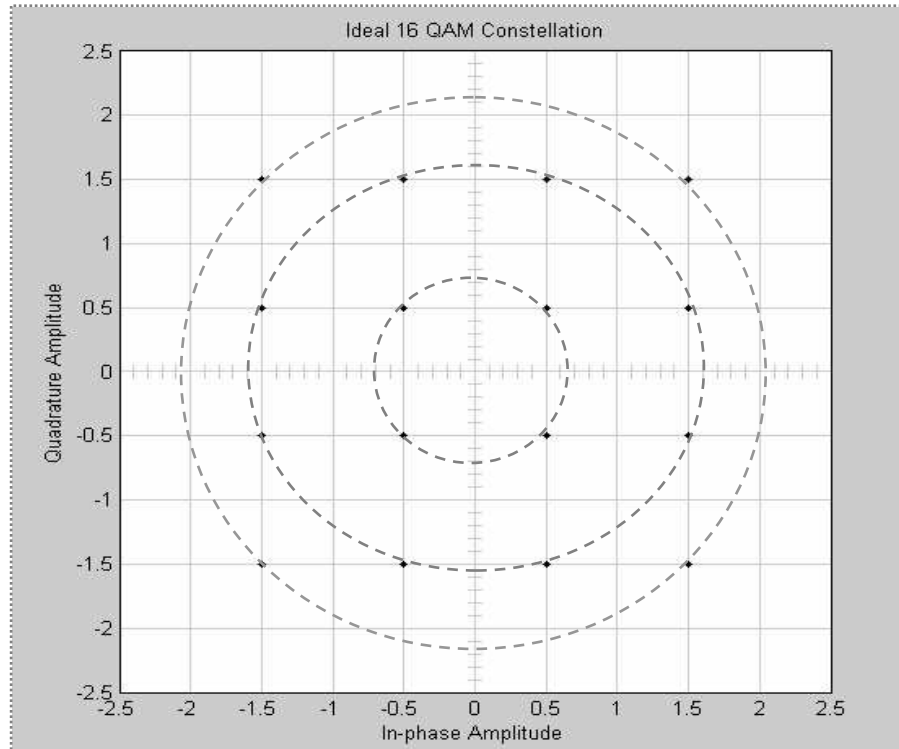


Fig. 4.4 Mapping of pilot sequence into 16-QAM symbols from Simulink

In the simulation process, we use 7-bit Barker code, 11-bit Barker code, 13-bit Barker code, 13-bit Neuman-Hoffman sequence and 15-bit PN sequence as pilot sequences. These sequences are combined with random 16-QAM data symbols. The insertion rate of pilot symbol is 1/10, which means pilot symbol is inserted every 10 symbols and the first symbol in each subframe is pilot symbol. For example, for pilot sequence 7-bit Barker code (-1, -1, -1, 1, 1, -1, 1), the length of a full frame observation is $7 \times 10 = 70$ symbols. A composite sequence of un-shaped symbols

from the signal generator is illustrated in Fig. 4.5. Pilot symbols occur at interval of 10 symbols and are indicated by a dot.

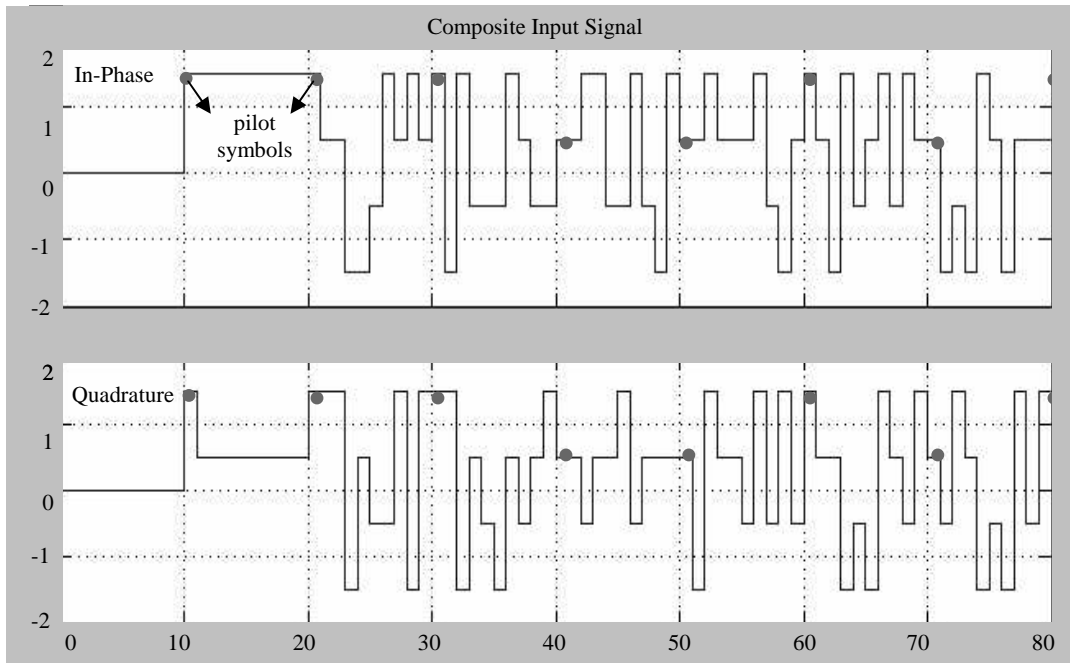


Fig. 4.5 Pilot (BK7) + Data composite input signal

The composite signal is first filtered by a band-limiting Nyquist filter. The baseband Nyquist pulse filtering is achieved by using a square root raised cosine (SRRC) filter. This Simulink block diagram is illustrated in Fig. 4.6



Nyquist Pulse Shaping

Fig. 4.6 Pulse shaping block

In this transmitter SRRC filter, the input signal is linearly modulated and upsampled by a factor of 16, the roll-off factor is set to 0.5. The output of SRRC filter is then ready to be transmitted over the communication channel. The quadrature signal of Fig. 4.5 is passed through the SRRC filter of Fig. 4.6 to produce the “Transmitter_Output” and this is presented in Fig. 4.7. The in-phase signal is similarly processed.

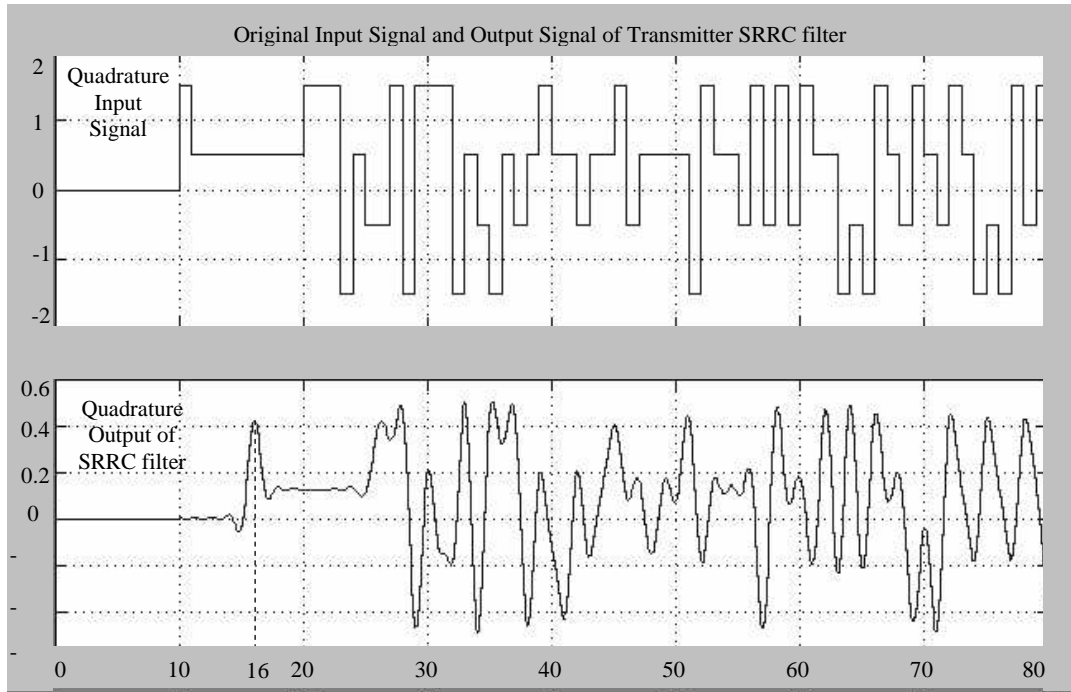


Fig. 4.7 Input signal and output of transmitter SRRC filter

4.2.2 Channel Overview

To simulate the effects of multi-path Rayleigh fading channel, the signal “Transmitter_Output” is used as the input of the channel block as illustrated in Fig. 4.8.

For the simplest case, we use the AWGN block in Simulink block library to simulate additive white Gaussian noise. The AWGN block in this simulation runs in

signal to noise ratio mode, i.e. E_s/N_0 . SNR is defined by the ratio of the average power of input signal to the noise power.

For the multi-path Rayleigh fading channel case, we will consider both fading and additive white Gaussian noise. Our channel is modeled as in equation $r(t) = c(t)s(t) + n(t)$, where $c(t)$ is the fading signal approximated as a multiplicative factor of the transmitted signal $s(t)$, and where $s(t)$ is from the data set of 16-QAM and $n(t)$ is the additive white Gaussian noise with zero mean and power spectral N_0 . According to the channel model, additive Gaussian noise is added to the baseband signal after it first passes through the multi-path Rayleigh fading channel. There is a “Multipath Rayleigh Fading Channel” block in the Simulink blockset which processes complex-valued baseband signals. Within this block, the magnitude of channel gain obeys a Rayleigh distribution. In a multi-path channel, relative motion between the transmitter and receiver causes Doppler shifts in the signal frequency. In this block, the power spectral density (PSD) of the Rayleigh distribution is determined by the Jakes Model [24]. Using this block, we can set the number of paths, the maximum Doppler shift of the channel, magnitude gain of each path and different time delay of different path. The channel model is given in Fig. 4.8

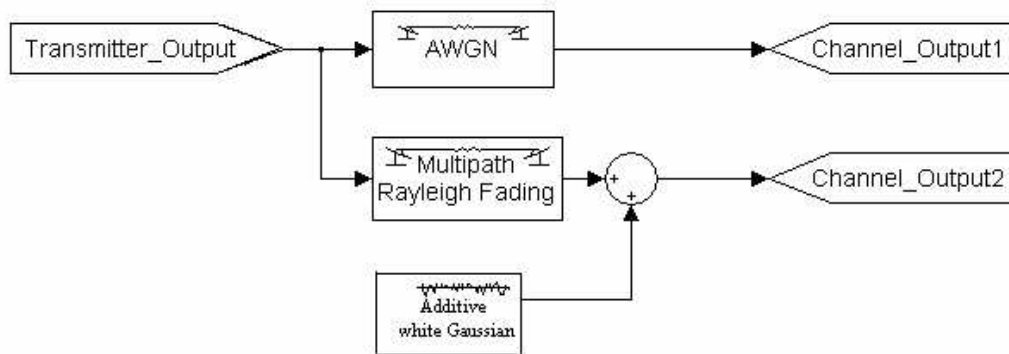
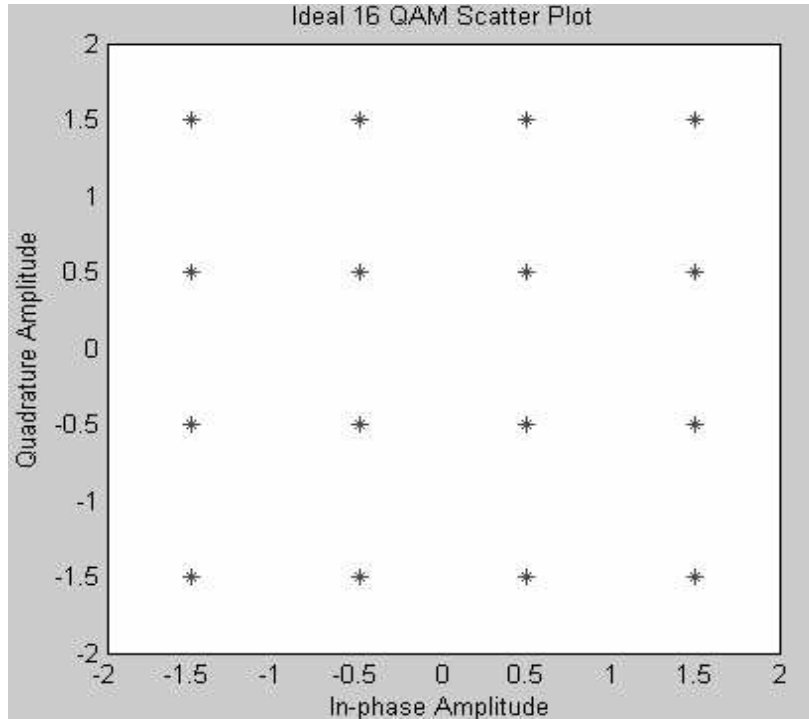
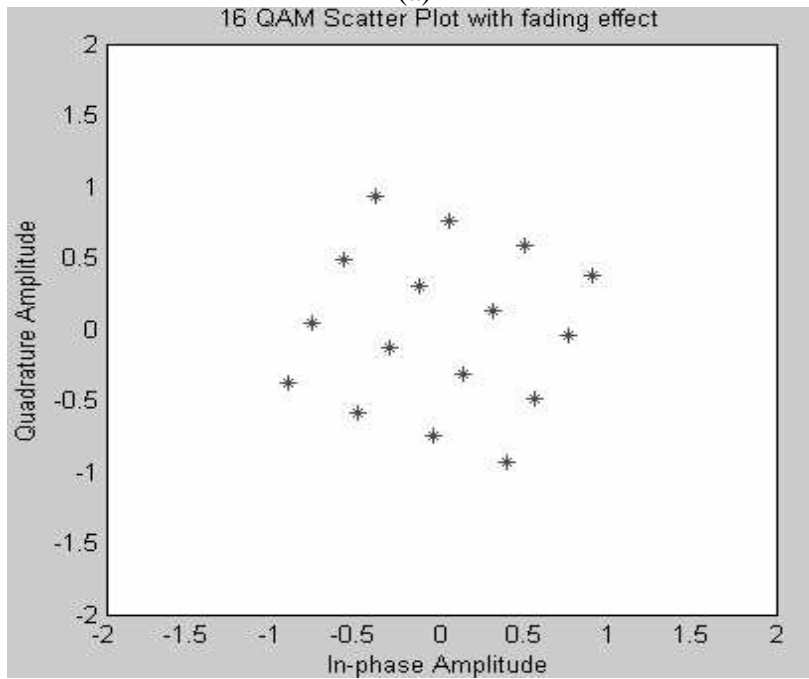


Fig. 4.8 Multi-path propagation channel

The ideal 16-QAM constellation is simulated and shown in Fig. 4.9 (a) and the received 16-QAM signal corrupted by a time-varying Rayleigh fading channel is shown in Fig. 4.9 (b).



(a)



(b)

Fig. 4.9 16-QAM signal corrupted by multi-path Rayleigh fading

The fading channel rotates the 16-QAM constellation and the magnitude is also changed. In Fig. 4.9 (b), it is clear that transmitted signal is severely attenuated by fading effect.

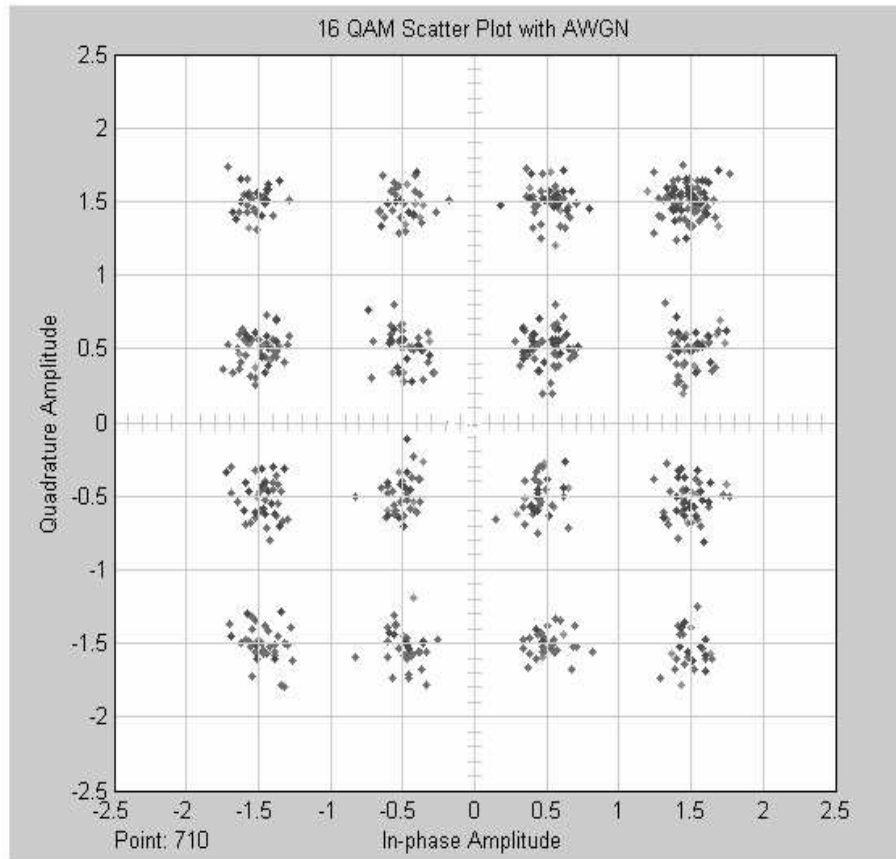


Fig. 4.10 16-QAM signal corrupted by AWGN channel

Fig. 4.10 shows the received signal 16-QAM scatter plot over an AWGN channel with 20 dB SNR. With this amount of noise, there are still very clear boundaries between symbols. As the noise level increases, the symbols are blurred more and decision errors become more frequent.

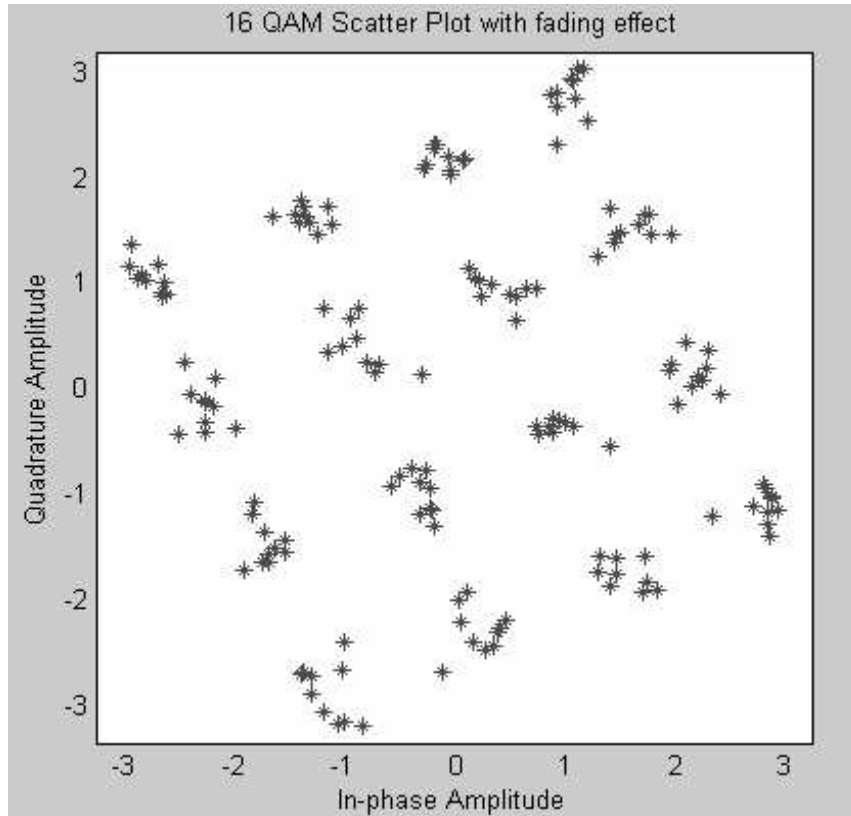


Fig. 4.11 16-QAM signal corrupted by multi-path Rayleigh fading and AWGN

In Fig. 4.11, Gaussian noise is added after the fading channel, and obviously the transmitted signal is corrupted more severely.

As we have discussed in the beginning of Section 4.2, the residual frequency error of carrier recovery has great impact on the received signal. Carrier frequency offset is introduced before the received signal is processed in the receiver. According to equation (A.5), the received discrete signal with carrier frequency offset can be expressed as: $r(k) = c(k)e^{j2\pi f_0 T_s k} s(k) + n(k)$, where f_0 is the frequency offset. Small carrier frequency errors multiply with the output signal of transmission channel. Fig. 4.12 depicts this process, in which “Channel_Output” can be either “Channel_Output 1” or “Channel_Output 2” in Fig. 4.8 depending on the channel model. By this way, the carrier frequency offset is emulated and introduced into simulation system, which makes the simulation system close to a real situation.

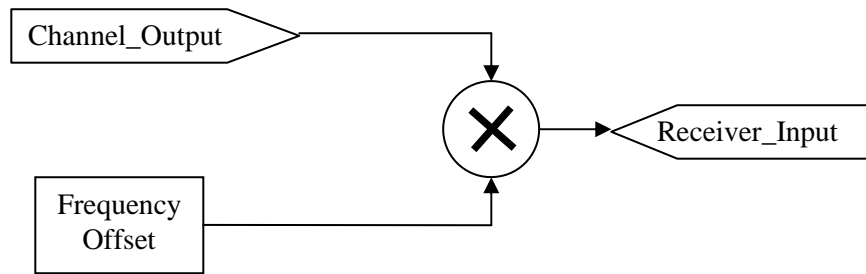


Fig. 4.12 Simulation of frequency offset

The frequency offset rotates the output signal of the fading and noisy channel and makes reception of received signal a more challenging work. The effect of frequency offset can be viewed in the scatter output of the received signal. This is shown in Fig. 4.13.

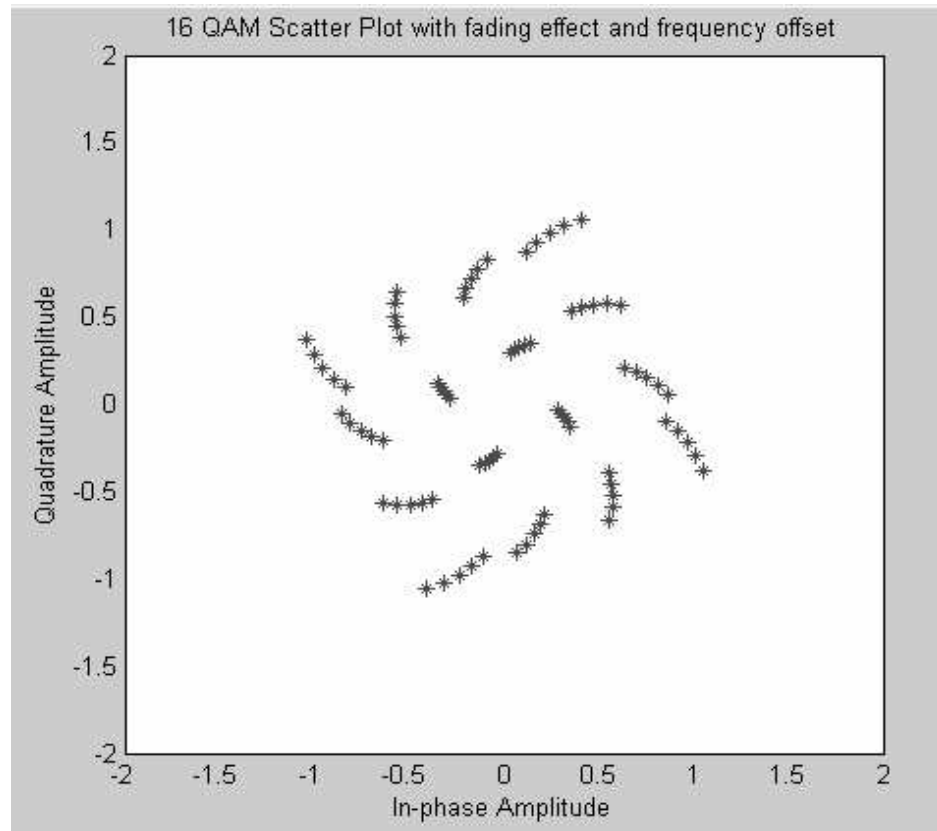


Fig. 4.13 Effect of fading and frequency offset to 16-QAM points

Comparing Fig. 4.13 with Fig. 4.11, clearly the signal was rotated by the frequency offset and phase information of received signal is changed because of the introduction of the multiplicative factor $e^{j2\pi f_0 T_s k}$.

4.2.3 Receiver Overview

The receiver consists of a matched filter and symbol sampler. As discussed in Chapter 2, a square root cosine filter (SRRC) is used in transmitter as a pulse shaping filter and then, correspondingly in the receiver another SRRC filter is used as a matched filter to demodulate the received signal from channel. The parameters in the receiver SRRC filter are set the same as the ones in the transmitter. Because the output signal of matched filter is at a much higher sample rate, we need a down-sampler to recover the signals to the same symbol rate as the input signals. The down-sampling rate here is 16 times the input symbol rate. The block diagram of a receiver is shown in Fig. 4.14.

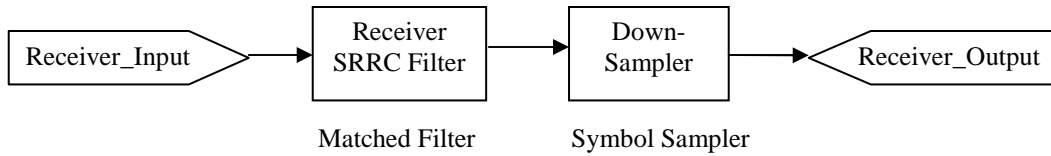


Fig. 4.14 Simulink receiver block diagram

4.2.4 Frame Synchronizer Overview

The objective of this study is to develop a frame synchronization scheme to identify the time position of pilot symbols in the combined pilot and data signal. The frame synchronizer works in a non-coherent manner as discussed in Chapter 3. It ignores phase information of signals and simply detects the specified amplitude information. In Simulink, the frame synchronizer begins by taking the squared magnitude of the “Receiver_Output” in Fig 4.14, i.e., the incoming symbol samples.

The first part of the frame synchronizer is the channel fading estimation filter that roughly estimates the magnitude of the channel state information based on the received signal from “Receiver_Output”. Symbols are transmitted with squared magnitude of 0.5, 2.5 and 4.5 and with probabilities of 0.25, 0.5 and 0.25 respectively when they are transmitted randomly. Channel gain is estimated by taking the average symbol energy over a period that is less than the fading interval but large enough to mitigate the effect of random variation in the data. Note that uniform utilization of all 16-QAM states results in an average energy of 2.5 and that increased channel noise will also introduce a bias in the squared magnitude. This noise bias can be compensated if the SNR is known. By dividing by 2.5, the channel fading signal is normalized to unity. Squared magnitude samples are delayed by an amount that corresponds to the delay in estimation of channel fading signal. Delayed magnitude squared received signal samples and the channel fading estimate are fed into frame synchronizer together in order to apply the frame synchronization algorithms developed in Chapter 3. The timing position of pilot symbols is finally decided by the frame synchronization algorithms.

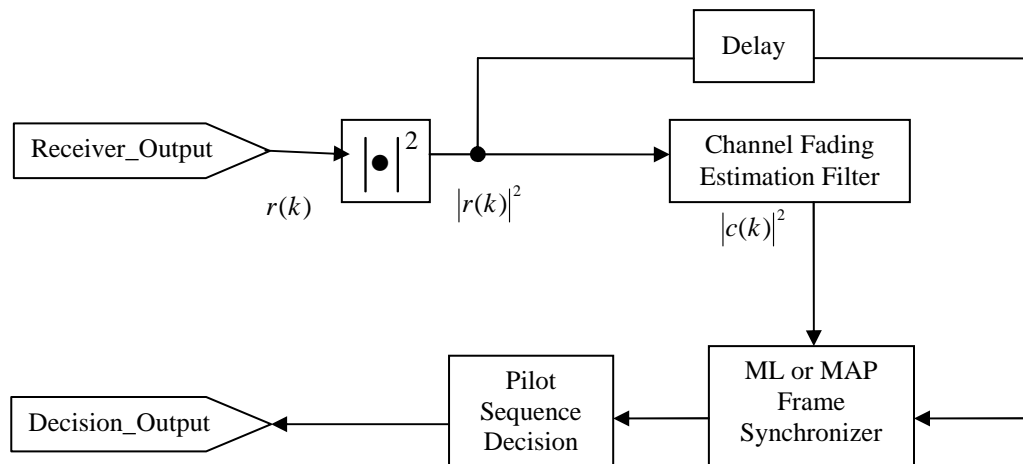


Fig. 4.15 Simulink block diagram of non-coherent frame synchronizer

According to the previous introductions, we illustrate the complete simulation processes of two frame synchronization techniques (ML and MAP) in block diagrams Fig. 4.16. and Fig. 4.17 respectively.

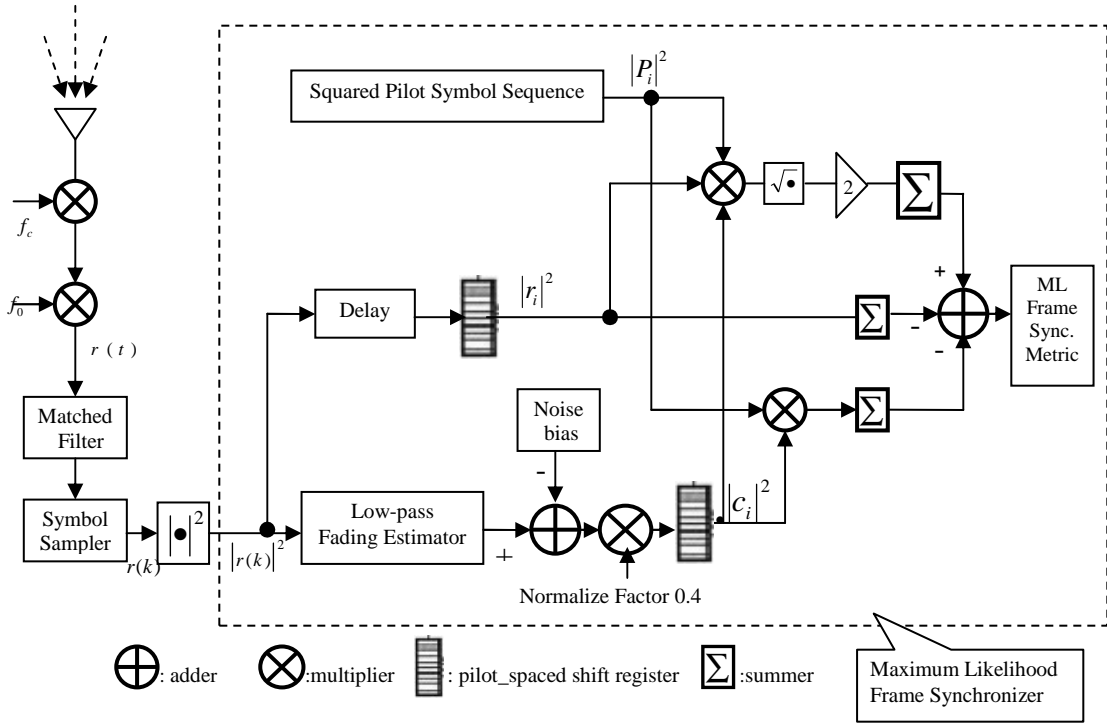


Fig. 4.16 ML frame synchronization simulator

It is pretty simple to implement maximum likelihood (ML) frame synchronization scheme since the mathematical expression is simple. The equations of maximum likelihood frame synchronization techniques is repeated here as

$$\hat{\mu}_{ML_AWGN} = \arg \max \left(\sum_{i=0}^{N-1} 2|r_i||P_i| - |r_i|^2 - |P_i|^2 \right)$$

$$\hat{\mu}_{ML_Fading} = \arg \max \left(\sum_{i=0}^{N-1} (2|r_i||c_i||P_i| - |r_i|^2 - |c_i|^2|P_i|^2) \right)$$

signal squared magnitude samples, quantized hard decision samples and channel fading samples are placed into shift register of length $L_p \times N$ with taps at interval of L_p . The pilot spaced taps yield N element pilot-spaced vectors (N is the length of pilot sequence) that are used to calculate the maximum a Posteriori (MAP) probability frame synchronization algorithms with reference pilot symbol squared magnitude samples which are N element vectors as well. Note that as the registers are shifted, the received squared magnitude vector \mathbf{r}^P , whose notation is introduced in Chapter 3, will correspond to the pilot sequence, a shifted version of the pilot sequence, or most probably, a random data sequence. All the pilot-spaced shifted vectors are fed into the MAP synchronization mathematic metric. The location of the pilot symbol P_0 can be decided then. This is the working process of MAP frame synchronizer. It is a little bit complicated compared with ML frame synchronizer, however, it is still simple to implement.

The maximum a posteriori probability frame synchronization approaches in AWGN and Rayleigh fading channels are expressed as:

$$\hat{\mu}_{MAP_AWGN} = \arg \max \left\{ \sum_{i=0}^{N-1} (|s_i|^2 - |P_i|^2) + 2|r_i| (|P_i| - |s_i|) - LnP(|s_i|^2) \right\}$$

$$\hat{\mu}_{MAP_Fading} = \arg \max \left\{ \sum_{i=0}^{N-1} |c_i|^2 (|s_i|^2 - |P_i|^2) + 2|c_i||r_i| (|P_i| - |s_i|) - LnP(|s_i|^2) \right\}$$

Pilot symbols can be identified using either of these two decision methods. Both decision methods are based on the high SNR approximation.

Chapter 5 Simulation Results and Discussions

In this chapter, the simulated performances of the proposed frame synchronizers are examined. The chapter begins with a description of the simulation system and follows with how the parameters are set. The chapter concludes with performance evaluations.

5.1 Simulation System Description

The objective of this project is to develop frame synchronization techniques for a PSAM system. Although PSAM is mainly used in the wireless communication systems to mitigate fading effects, it is still insightful for us to also consider frame synchronization problems in an AWGN channel. In Chapter 3, we have developed the frame synchronization techniques for both AWGN and fading channels. It is also reasonable to include carrier frequency offset in the simulation system. Therefore, four channel situations will be tested in our simulations: (1) an AWGN channel without frequency offset, (2) an AWGN channel with small frequency offset, (3) a frequency non-selective slow Rayleigh fading channel without receiver frequency offset, (4) a frequency non-selective slow Rayleigh fading channel with small frequency offset. Similar to the mathematical development of the data model in Chapter 3, the matched filter and symbol sampler outputs corresponding to these channels can be expressed respectively as

$$\left\{ \begin{array}{l} r(k) = s(k) + n(k) \\ r(k) = e^{j(2\pi f_0 k)} s(k) + n(k) \\ r(k) = c(k)s(k) + n(k) \\ r(k) = e^{j(2\pi f_0 k)} c(k)s(k) + n(k) \end{array} \right. \quad \begin{array}{l} (5.1) \\ (5.2) \\ (5.3) \\ (5.4) \end{array}$$

where $s(k)$ is a pilot symbol or a data symbol, $n(k)$ is the zero mean complex AWGN with variance N_0 , f_0 is a random small value frequency offset and the fading term $c(k)$ is a zero mean complex multiplicative distortion whose magnitude has a Rayleigh distribution. The frequency offset, additive noise, data symbols and the multiplicative fading are statistically independent of each other.

In the simulation process, data symbols are from the 16-QAM constellation data set. Pilot sequences are 7-bit Barker sequence (BK7), 11-bit Barker sequence (BK11), 13-bit Barker sequence (BK13), 13-bit Neuman-Hoffman (NH13) code and 15-bit pseudo-random noise (PN) sequence (PN15), all of which have good autocorrelation properties. For these pilot sequences, the length of the frame format has 70, 110, 130 or 150 symbols respectively. The pilot insertion rate is $L_p = 10$ and the pilot symbols are placed in the first position of every subframe, as illustrated in Fig. 2.8. The fading channel is modeled by the Simulink integrated block “Multipath Rayleigh Fading Channel”. In Simulink, this block can define the number of paths, gain of each path, time delay and Doppler shift. The channel fading has zero mean and the variance is set to unity. Path delay is set to much less than the symbol time as is compliant with the definition of frequency non-selective fading. Fading rate is set to 1%, 2% and 5% of the symbol rate to test the performance under different fading conditions (in Gansman’s work [9] only fading rate 1% is tested in simulation). In the whole simulation process, 100,000 trials (full frames) are run to test the statistical performance. In simulation, 1000 symbols (about 10 frames) were simulated prior to recording the performance data. This

“start up” time was to allow a reasonable estimate of $c(t)$ prior to the performance analysis.

5.2 Simulation Test Bench

To facilitate verification of the performance of the frame synchronization design, we build a test bench which is illustrated in Fig. 5.1.

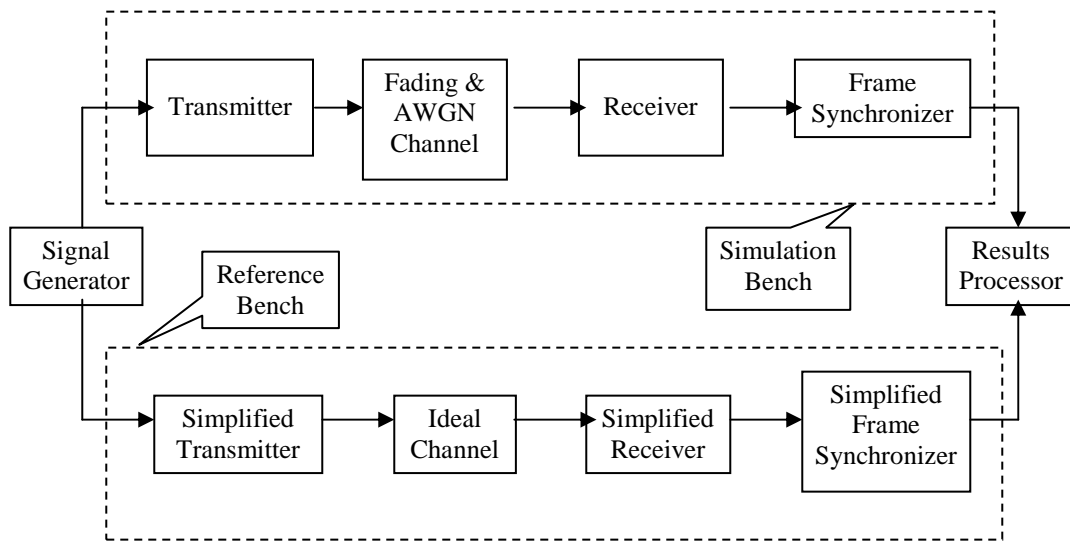


Fig. 5.1 Test bench for simulation

In this test bench, the input signal is generated for the transmitter, a reference signal is also needed to compare with the output of frame synchronizer decisions, and then the results processor collects the output of frame synchronizer to generate the desired simulation statistics and evaluate the performance of the frame synchronization design.

In order to generate a reference signal at the receiver, a reference transmission system is built, which is almost the same as the simulation system model discussed in the beginning of Chapter 4 except that there is no distortion and noise. System delay must be taken account, therefore the reference transmission system has

exactly the same time delay as the simulation transmission system in every process and this ensures the simulation transmission system and reference transmission system are working in a synchronous mode. It is very simple to build such a reference transmission system. All that we need to do is just to copy and paste the simulation system model in the simulation bench and simplify it by deleting all the distortion caused by noise and fading.

In this simulation test bench, the system in the simulation bench emulates a real land mobile communication condition, while in the reference bench it works in an ideal condition. Thus, the simplified frame synchronizer in reference bench can correctly detect the location of pilot symbol P_0 .

The results processor compares the output of the frame synchronizer to that of the simplified frame synchronizer and counts the number of P_0 symbols that are falsely detected during 100,000 full frame observations. The ratio of the number of falsely detected frames by frame synchronizer in the simulation bench to the number of total simulated frames from simplified frame synchronizer in the reference bench is thought as the probability of false acquisition.

The probability of selecting the wrong time location of the pilot symbol is known as false acquisition. The probability of false acquisition vs. SNR will be examined in computer simulation and, since SNR is generally not known, a range of values are explored. As shown in test bench Fig. 5.1, the signal generator continuously generates a pseudo-random sequence until 100,000 full frame observations are received at the frame synchronizer. The transmitter of the simulation bench and the simplified transmitter of the reference bench work in a synchronous mode, so that they insert the same pilot symbol at exactly the same location in the symbol stream at the same time. For each full frame observation, the frame synchronizer generates an estimate of the location of pilot symbol P_0 .

Once the probability of false acquisition is obtained, it is easy to calculate the mean time to acquisition vs. SNR. Mean time to acquisition is obtained based on

full frame observations and a verification stage that declares synchronization after two identical frame location estimates in succession. Assuming that has been adapted to $c(t)$, the mean time to acquisition can be calculated using the mathematical expression adapted from [33] and it is given as

$$\bar{T}_{acq} = T_f \left(\frac{1}{p_d^2} + \frac{1}{p_d} - \frac{1}{2} \right) + T_f p_f \left(1 + \frac{p_f}{(1-p_f)^2} \right) \left(\frac{1}{p_d^2} - \frac{1}{2} \right) \quad (5.5)$$

where $T_f = L = N \times L_p$ is one full frame period, p_d is the probability of correctly detecting the true pilot symbol detection and p_f is the probability of false alarm, i.e. detection of a non-pilot symbol instead of the true pilot symbol.

5.3 Simulation Results and Performance Analysis

5.3.1 Performance in AWGN Channel

This study finds that the maximum likelihood (ML) synchronizers have good performance over a wide range of SNR (signal to noise ratio) in AWGN channels. Fig. 5.2 (a) illustrates the probability of false acquisition of ML frame synchronizer in the AWGN channel without frequency offset. The simulation results show that with the increase of the frame observation length, the probability of true pilot symbol detection increases, which is consistent with theoretical analysis. However, in this plot, NH13 is better than PN15 when SNR is equal to 8 dB. It is an unexpected result. But with the SNR is increased, PN15 shows stable and better performance than NH13 and it is still consistent with the theoretical analysis. To test the robustness of the synchronizer to frequency offset, we set frequency offset $f_0 = 0.02 f_{sy}$ the same as the value used by Gansman in [9]. The probability of false acquisition in the AWGN channel with this frequency offset is shown in Fig. 5.2 (b). The performance of synchronizer has very little effect by this frequency offset. This is mainly due to the non-coherent scheme we proposed. The computed mean time to

acquisition under these two AWGN conditions are shown in Fig. 5.2 (c) and Fig. 5.2(d) respectively. When the frame length is smaller, the synchronizer converges to synchronization faster. The computer simulation shows that although the proposed frame synchronization method assumes high SNR, it also works well in moderate SNR.

The similar performance evaluations of the maximum a posteriori probability (MAP) frame synchronization technique are tested as we have done with the ML frame synchronization technique. 100,000 simulation trials are used to get desired statistical evaluations. Fig. 5.3 shows the probability of false acquisition of the MAP frame synchronizer under the AWGN channel without frequency offset. In this MAP frame synchronization metric, we use threshold detection to obtain the hard decision of data symbol first and then use this hard decision to help the detection of pilot symbols. Considering the range of SNR > 6 dB as appropriate for 16-QAM transmission, and comparing Fig. 5.2 with Fig. 5.3, we find that the simulation results of the MAP frame synchronizer show slightly better performance than those of ML.

We further investigate the immunity of the non-coherent frame synchronization schemes to a range of frequency offsets up to 60% of the symbol rate. As introduced in Chapter 4, carrier frequency error happens after carrier recovery stage and because of the carrier frequency error; the receiver signal frequency is shifted. The mismatch between the shifted signal frequency and the band limits of the receiving square root cosine filter results in performance degradation. Our purpose is to examine the effect of carrier frequency error, not fading or noise. Therefore in the simulation process, SNR and fading factor are fixed and different values of carrier frequency error are used to investigate the performance degradation.

Fig. 5.4 (a), (b) and (c) show the results of performance degradation in the AWGN channel, where SNR is set to 10 dB and the 11-bit Barker sequence is the pilot symbol sequence. In Fig. 5.4 (a), the probability of performance degradation of ML and MAP synchronizers is plotted based on the roll-off factor 0.5. Roll-off

factor has been introduced in Chapter 2. The acquisition performance degradation is obtained by dividing the probability of true acquisition under different carrier frequency offset values to the probability of true acquisition under zero frequency offset. This plot shows that in the presence of different frequency offset, MAP synchronizer has better performance than ML synchronizer. Fig. 5.4 (b) and (c) are the acquisition performance degradation of the ML and MAP frame synchronizers under different roll-off factors respectively. It is clear that from the simulation results, the large roll-off factor allows operation with large local carrier frequency error.

5.3.2 Performance in Fading Channel

The performance in the frequency non-selective slow Rayleigh fading channel is more complicated than the performance in the AWGN channel. However, based on the high SNR signal processing approximations, the frame synchronization criteria for fading channel, equations (3.42) and (3.69), are as easy to be implemented as those in the AWGN channel. The simulation results shown in Fig. 5.5 (a) illustrate the probability of false acquisition of maximum likelihood (ML) synchronizer in Rayleigh fading channel when Doppler shift and SNR are known. The design parameters were $f_d = 0.01$ of symbol rate, frequency offset $f_o = 0$, and a range of different SNRs values are used to test the performance. The probability of false acquisition of ML synchronizer with carrier frequency offset which is set to 2% of symbol rate is plotted in Fig. 5.5 (b). The performance of synchronization is poor under low SNR; however it becomes quite good in moderate to high SNR range due to the high SNR approximations. In Fig. 5.5 (c) and Fig. 5.5 (d), the mean times to acquisition calculated based on the probabilities of false acquisition from Fig. 5.5 (a) and (b) are illustrated as well. It is apparent that the longer the pilot sequence is used, generally the better the performance of correct pilot symbol detection, however the longer time is taken to converge to synchronization.

Similarly, the performance of MAP frame synchronizer in fading channel is investigated as well. The probability of false acquisition under Rayleigh fading channel without frequency offset is depicted in Fig. 5.6 (a) and the probability of false acquisition with a small frequency offset $f_0 = 0.02 f_{sy}$ is depicted in Fig. 5.6 (b). In the simulation, the fading rate f_d was set to 1% of the symbol rate. Mean times to synchronization vs. SNR are computed using equation (5.5) and plotted in Fig. 5.6 (c) and (d) correspondingly.

These two proposed frame synchronizers are working based on the pilot-spaced observation instead of the observation symbol by symbol, thus they are suboptimum synchronizers theoretically, however their performances to synchronization show that the pilot-spaced suboptimum synchronizers are working properly under moderate to high SNR range. Also, comparing the simulation results without frequency offset with those with frequency offset, it is clear that this small frequency offset $f_0 = 0.02 f_{sy}$ has very little effect on the performance of the synchronizers and this is largely attributed to the non-coherent signal processing used in the development of the frame synchronization metrics.

As discussed in the last section, the mismatch between the signal frequency shifted by carrier frequency offset and the band limits of the receiving square root cosine filter results in performance degradation of the frame synchronizer. The performance degradation due to carrier frequency offset is also tested in fading channel.

In the fading channel verification, SNR is set to 10 dB and the fading rate is fixed and set to 1% of the symbol rate to be consistent with [9]. Fig. 5.7 (a), (b) and (c) show the acquisition performance degradation of ML and MAP frame synchronizers in fading channel, where 11-bit Barker sequence is used as the pilot symbol sequence. In Fig. 5.7(a), the probabilities of performance degradation of ML and MAP synchronizers are plotted where the performance is tested when a fixed roll-off factor is set to 0.5. The probability of performance degradation is defined same as it is in the AWGN channel, which is discussed in last section. Fig. 5.7 (b)

and (c) are the probability of performance degradation of the ML frame synchronizer and the MAP frame synchronizer under a range of roll-off factors respectively. The larger roll-off factor shows better tolerance to local carrier frequency error. Comparing the performance in the fading channel with the performance in the AWGN channel, it is obvious that in AWGN channel the frame synchronization system works better than in fading channel. It is easy to understand that, in the analysis of the performance of a communication system, AWGN is always used to give an upper bound performance, because the AWGN condition is the simplest case in wireless communication environment.

In the above-mentioned simulations, the fading rates were all set to 1% of the symbol rate to be consistent with that in [9] in order to conveniently compare the performance of these two frame synchronization methods. However, it is important to consider other fading conditions to further test the robustness of our proposed frame synchronization techniques. In Fig. 5.8 and Fig. 5.9, the probability of false acquisition of the ML and the MAP frame synchronizers without carrier frequency offset under different fading rates is illustrated respectively. In these simulations, 11-bit Barker sequence was used as pilot symbol sequence. Fading rates are set to 1%, 2% and 5% of symbol rate respectively. These plots show that with the increasing of fading rate, the performance of frame synchronization becomes worse. The frame synchronizer with fading rate 5% failed. According to the definition of non-selective slow fading stated in Chapter 2, if the fading rate is too large, then the data model (equation (3.17)) used in this study is not valid anymore. Thus the frame synchronization algorithms developed based on this equation are not working properly. Also in larger Doppler shift situations, the transmitted signal are distorted more dramatically and this makes the performance of synchronization degrade very quickly. In such cases, high SNR is needed to improve the performance and more accurate fading estimation is required to compensate for the severe fading effect.

5.3.3 Comparisons to Existing Synchronizers

In this section, Our ML and MAP synchronizers are compared through simulation to some existing synchronizers. They are the Gansman's ML frame synchronizer, the standard correlator and the non-coherent synchronizer of Liu & Tan [6]. The latter two are expressed respectively as,

$$\hat{\mu}_c = \arg \max_{\mu \in [0, L-1]} \left| \sum_{k=0}^{N-1} p_k^* x_{kL_p + \mu} \right| \quad (5.6)$$

$$\hat{\mu}_{lt} = \arg \max_{\mu \in [0, L-1]} \left| \sum_{k=0}^{N-1} p_k^* x_{kL_p + \mu} \right| - f(x_{k+\mu}) \quad (5.7)$$

where $f(x_k)$ is a data correction term which we have chosen to be the magnitude of received signal $|r|$ in our simulations. Fig. 5.10 compares the simulated performance of synchronizers in AWGN channels without frequency offset and shows that our synchronizers and Gansman's synchronizer perform much better than the standard correlator and Liu & Tan, where COR denotes the standard correlator. The standard correlator failed and Liu & Tan is ok in the AWGN channel. Our MAP is slightly better than Gansman and our ML synchronizer has slightly less performance than Gansman in the low SNR, but ours have better performance in the high SNR than Gansman. In each case, 11-bit Barker sequence was used as pilot symbol sequence. Fig. 5.11 shows the comparison of the performance of our ML and MAP frame synchronizers with Gansman with frequency offset = 0.02 of the symbol rate in an AWGN channel. It is obvious that our techniques are very robust under this frequency offset; however, Gansman's synchronizer fails in the presence of this frequency offset. This is mainly because the non-coherent scheme is applied in our study. Fig. 5.12 compares the performance of different synchronizers in fading channel with fading rate $f_d = 0.01$ of the symbol rate. Our proposed ML and MAP frame synchronizers and Gansman's synchronizer perform well, while the standard correlator (COR) and Liu & Tan failed in the fading environment. It is seen that Gansman's synchronizer has

better performance than ours in low SNR, and has slightly less performance when SNR becomes high. This mainly is attributable to the approximation rule used in the development of the frame synchronization criterions. In Gansman, a low SNR rule is applied, while in our study, a high SNR rule is used.

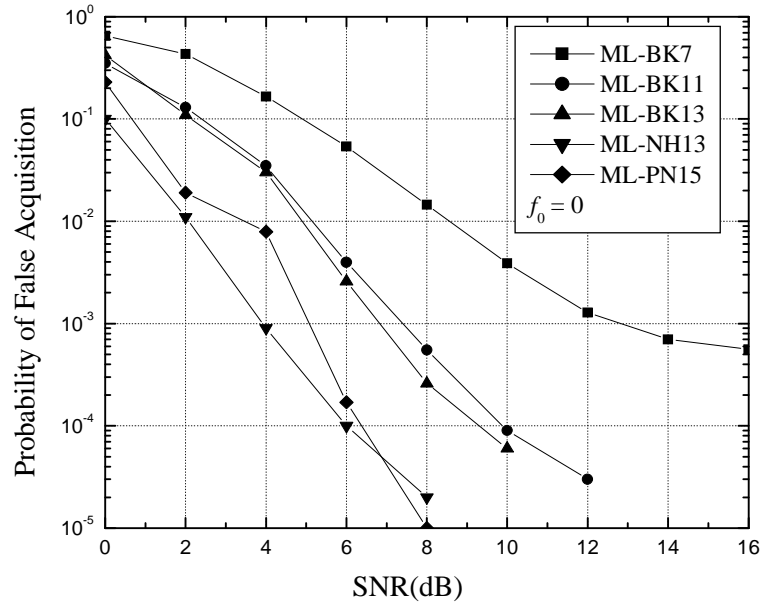


Fig. 5.2 (a) ML, false acquisition in AWGN channel without frequency offset

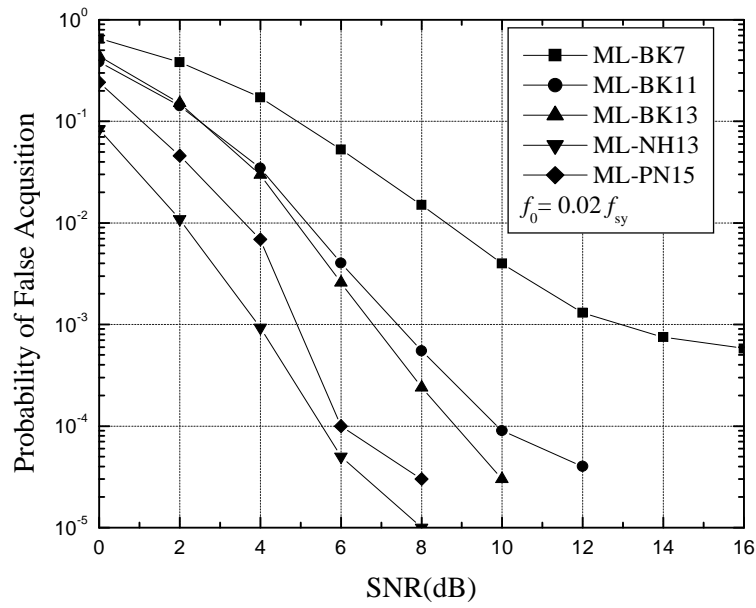


Fig. 5.2 (b) ML, false acquisition in AWGN channel with frequency offset = $0.02 f_{sy}$

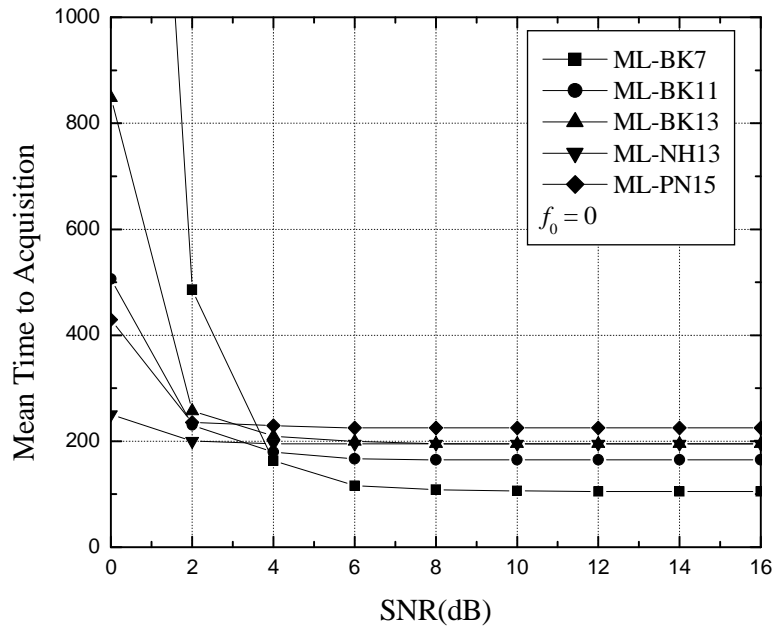


Fig. 5.2 (c) ML, mean time to acquisition in AWGN channel without frequency offset

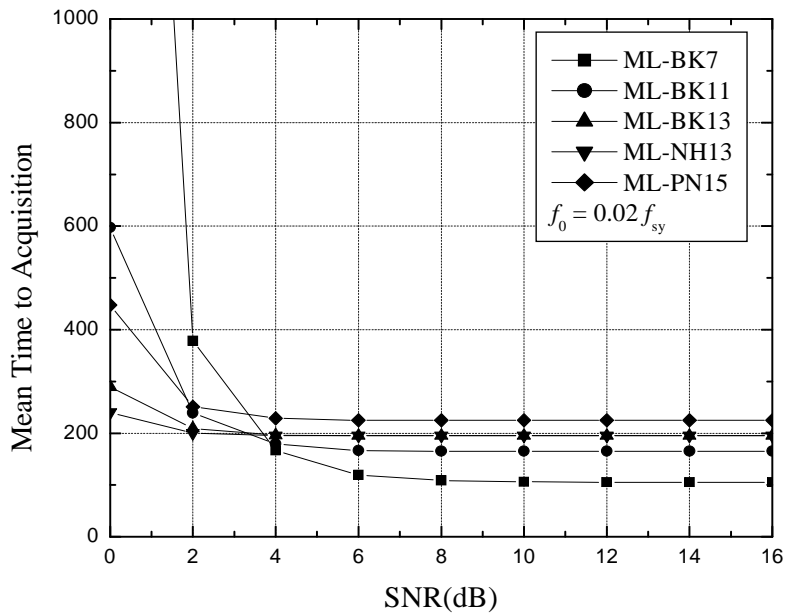


Fig. 5.2 (d) ML, mean time to acquisition in AWGN channel with frequency offset = $0.02 f_{sy}$

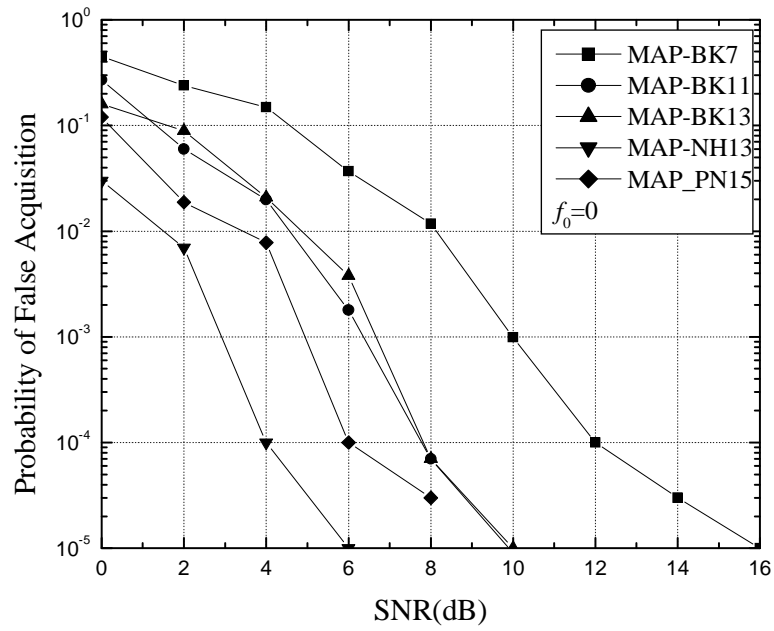


Fig. 5.3 (a) MAP, false acquisition in AWGN channel without frequency offset

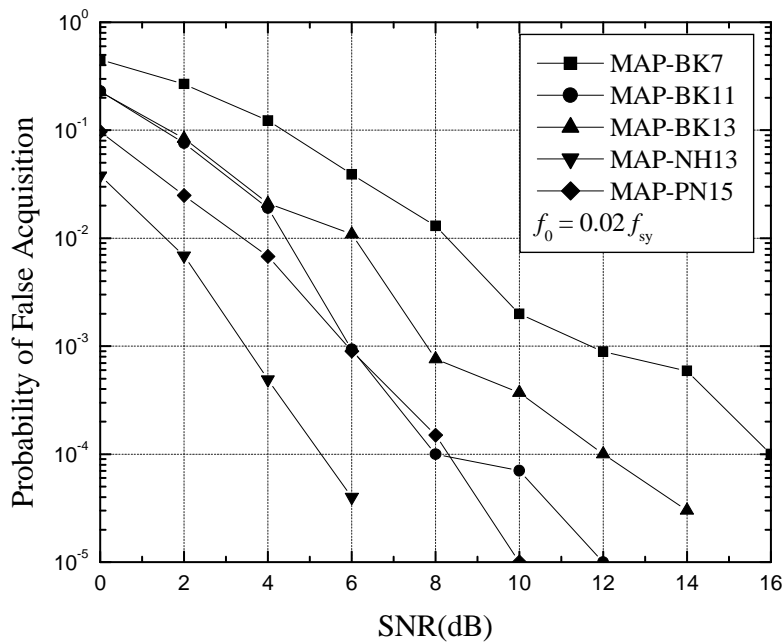


Fig. 5.3 (b) MAP, false acquisition in AWGN channel with frequency offset = $0.02 f_{sy}$

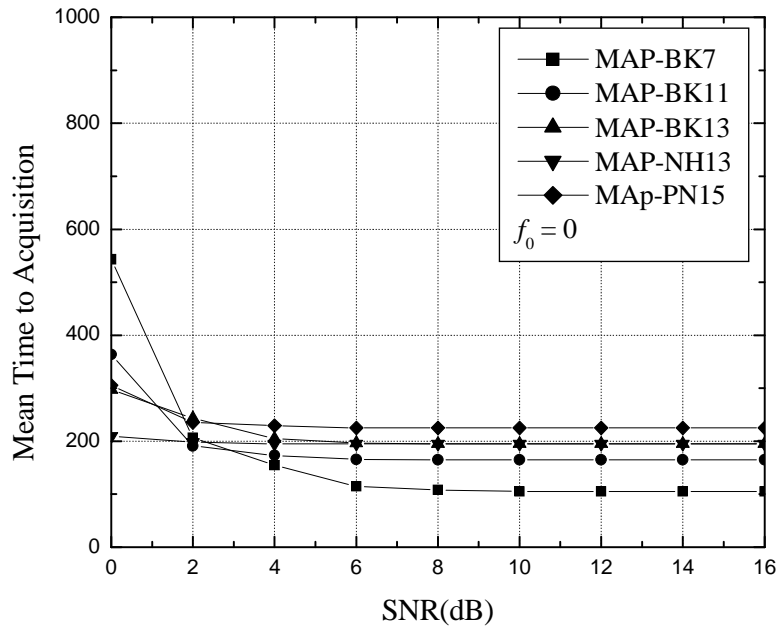


Fig. 5.3 (c) MAP, mean time to acquisition in AWGN channel without frequency offset

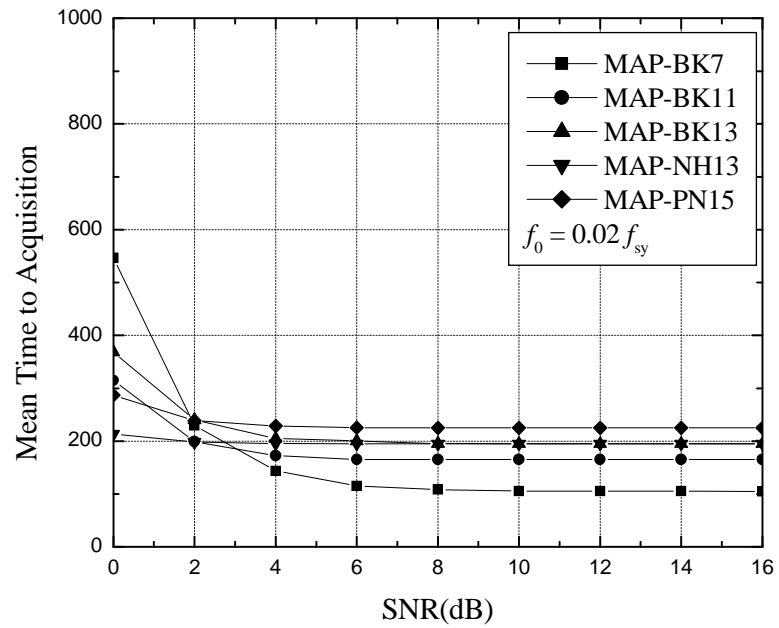


Fig. 5.3 (d) MAP, mean time to acquisition in AWGN channel with frequency offset = $0.02 f_{sy}$

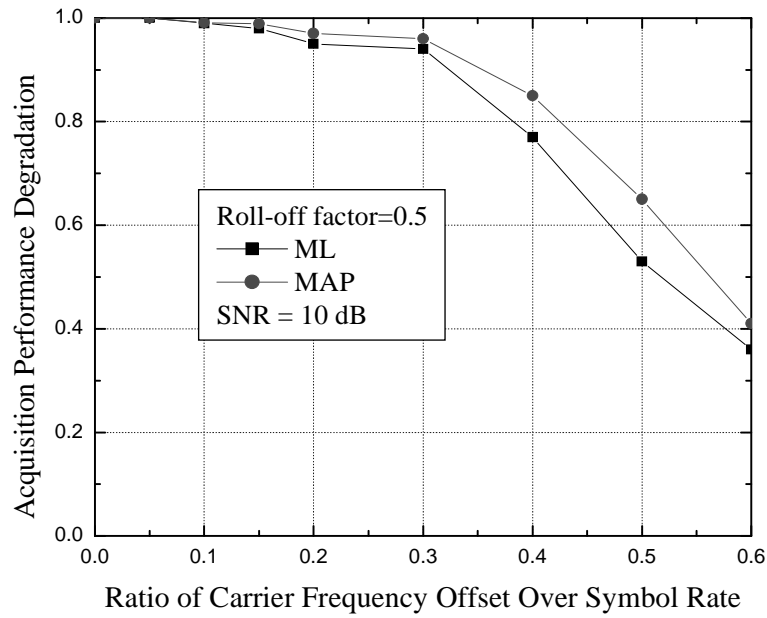


Fig. 5.4 (a) AWGN performance degradation of ML and MAP synchronizers vs. f_0

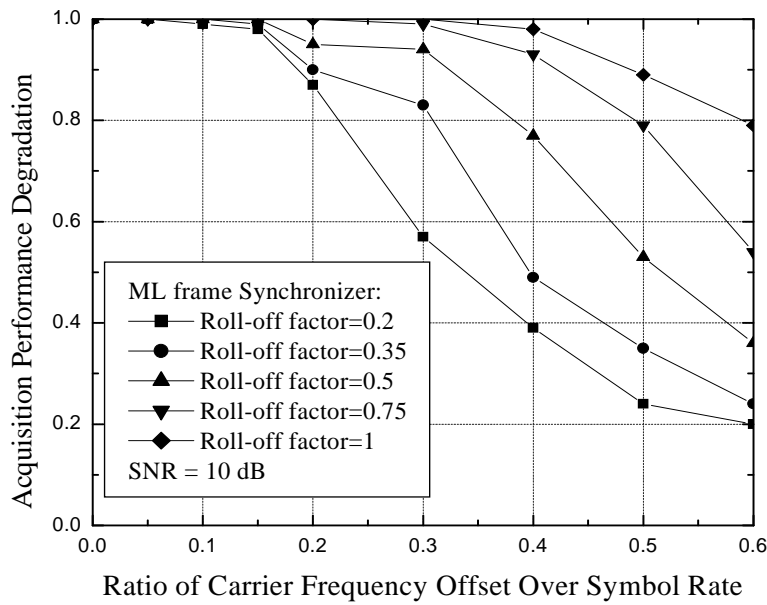


Fig. 5.4 (b) AWGN performance degradation of ML synchronizer vs. f_0

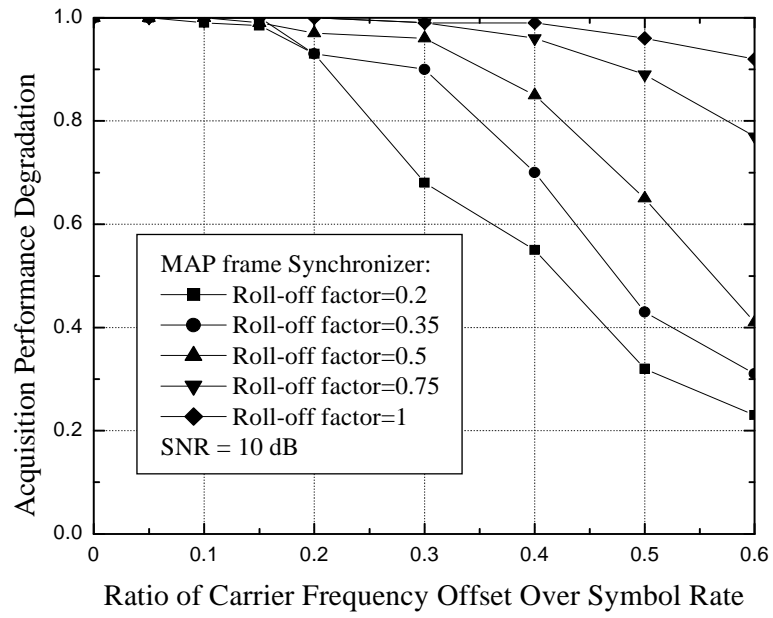


Fig. 5.4 (c) AWGN performance degradation of MAP synchronizer vs. f_0

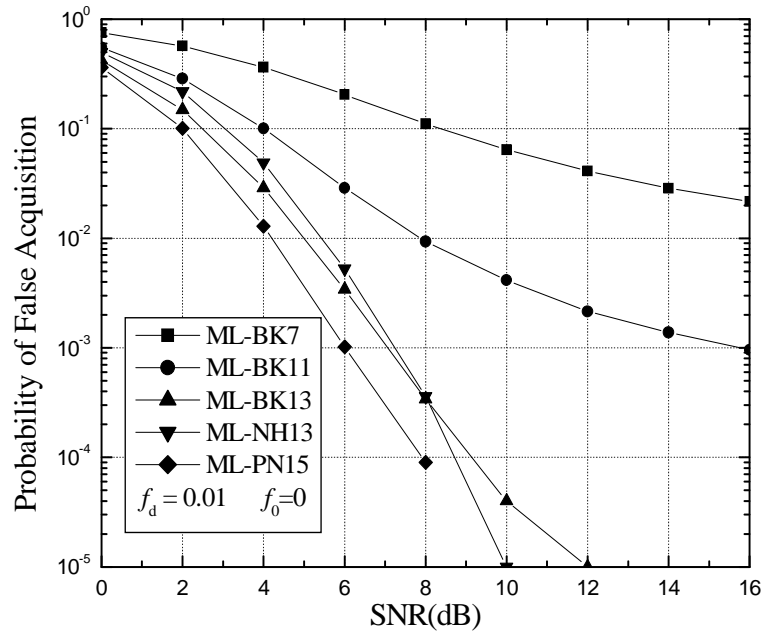


Fig. 5.5 (a) ML, false acquisition in fading channel with $f_d = 0.01$ and $f_0 = 0$

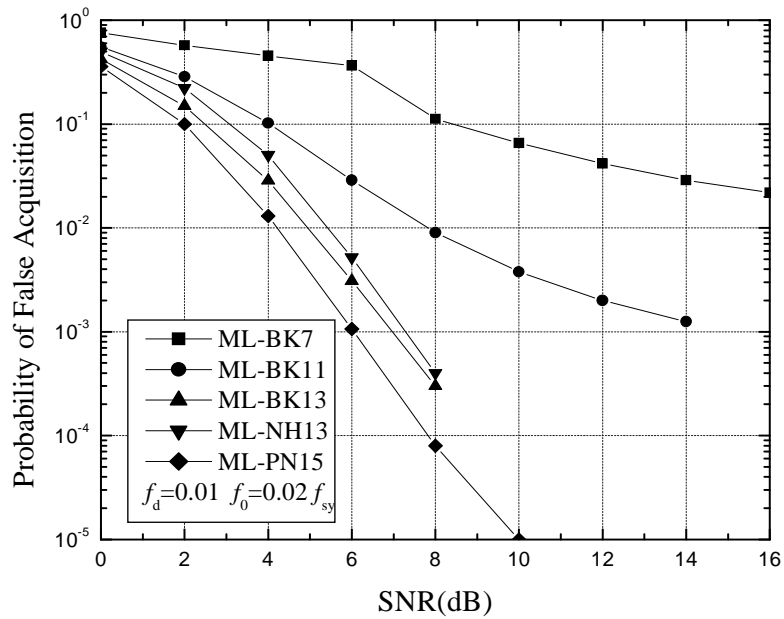


Fig. 5.5 (b) ML, false acquisition in fading channel with $f_d = 0.01$ and $f_0 = 0.02 f_{sy}$

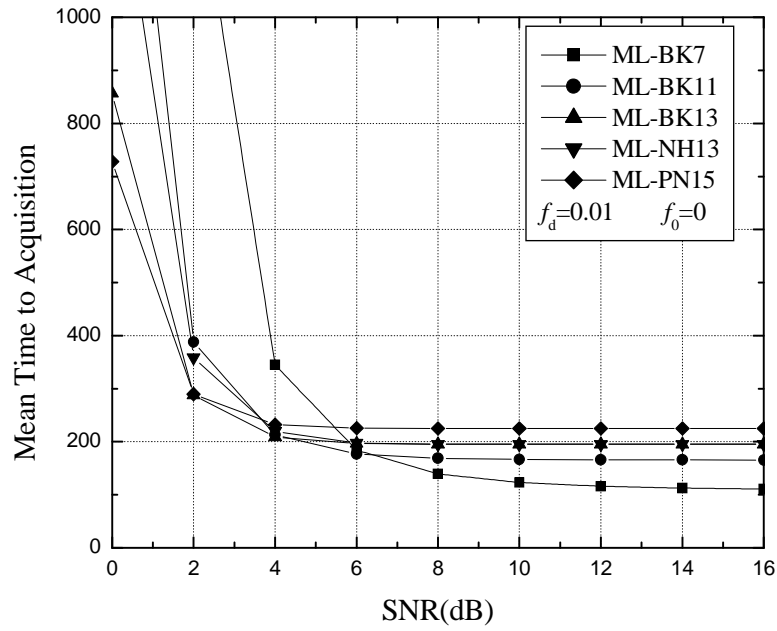


Fig. 5.5 (c) ML, mean time to synchronization in fading channel with $f_d = 0.01$ and $f_0 = 0$

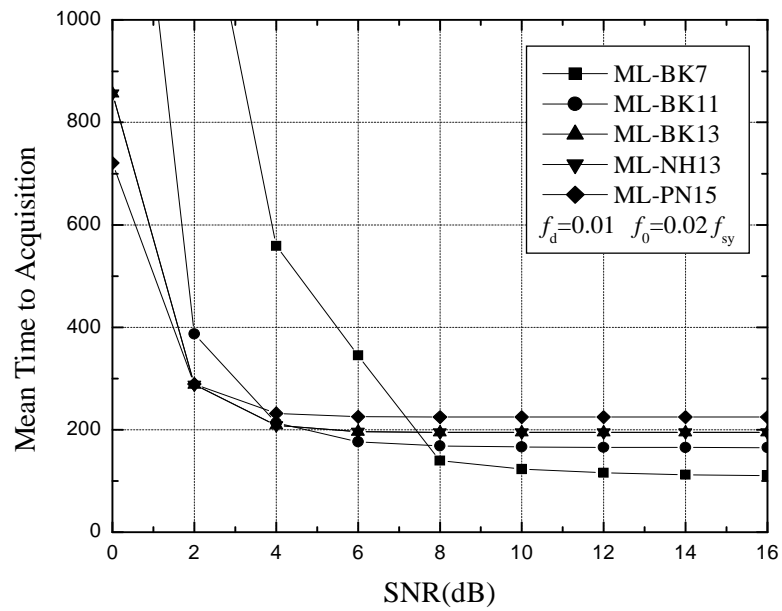


Fig. 5.5 (d) ML, mean time to synchronization in fading channel with $f_d = 0.01$ and $f_0 = 0.02 f_{sy}$

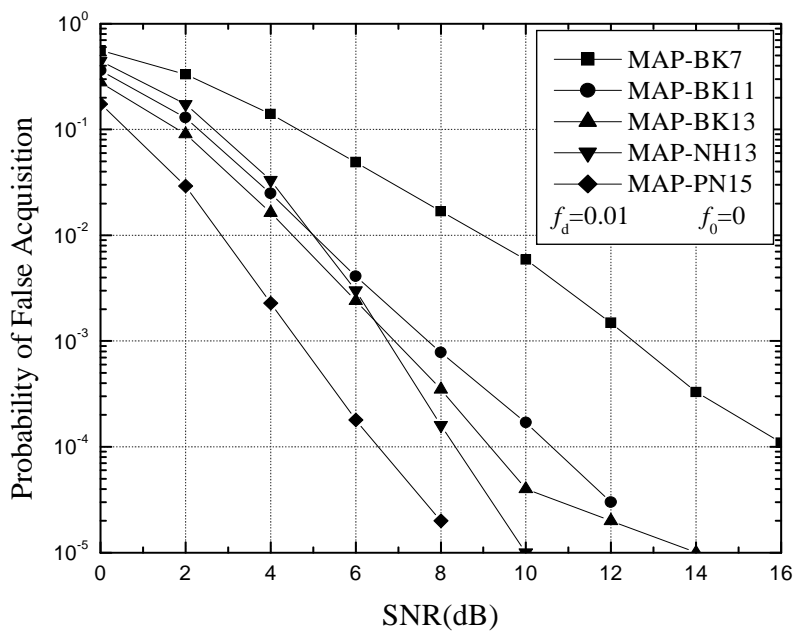


Fig. 5.6 (a) MAP, false acquisition of in fading channel with $f_d = 0.01$ and $f_0 = 0$

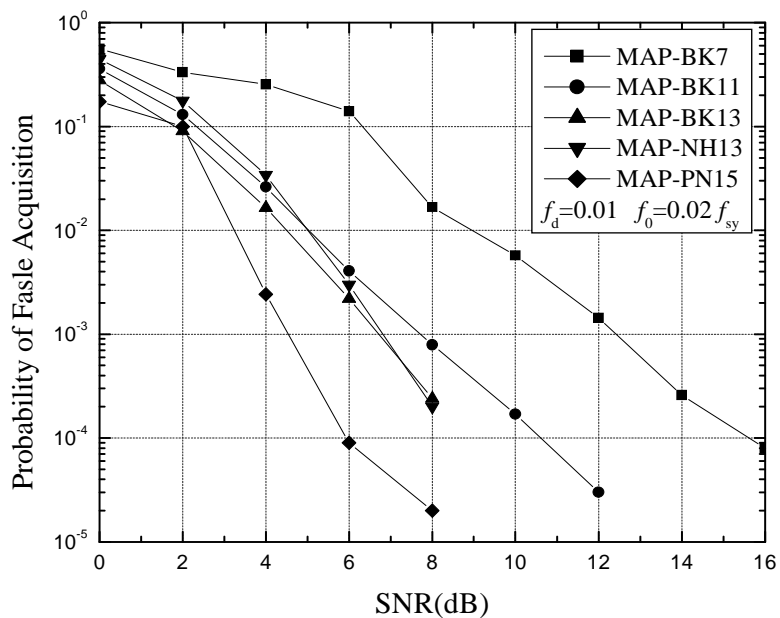


Fig. 5.6 (b) MAP, false acquisition in fading channel with $f_d = 0.01$ and $f_0 = 0.02 f_{sy}$

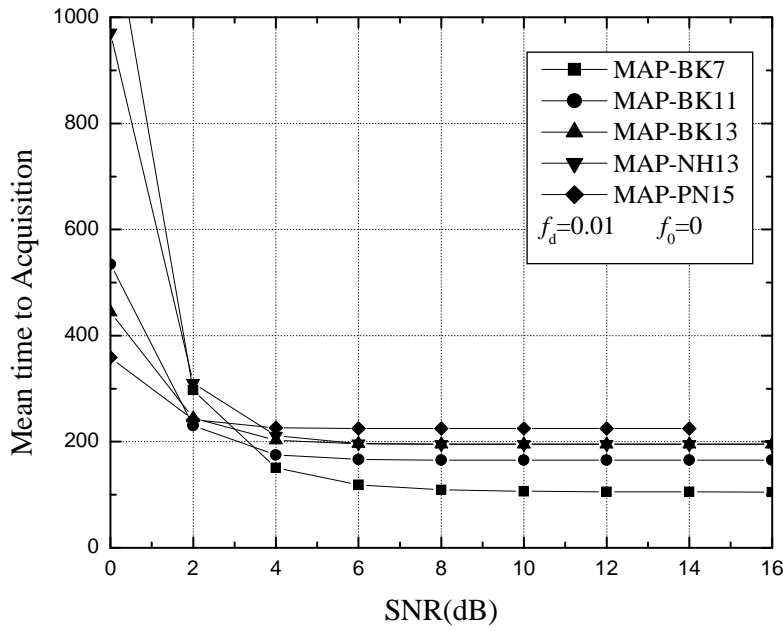


Fig. 5.6 (c) Mean time to synchronization of MAP frame synchronizers in fading channel no freq. offset

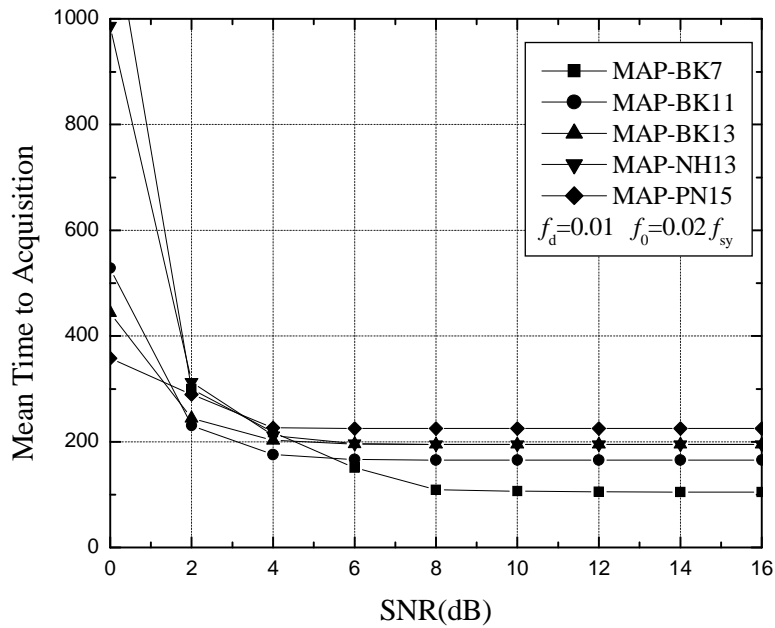


Fig. 5.6 (d) Mean time to synchronization of MAP frame synchronizers in fading channel with freq. offset

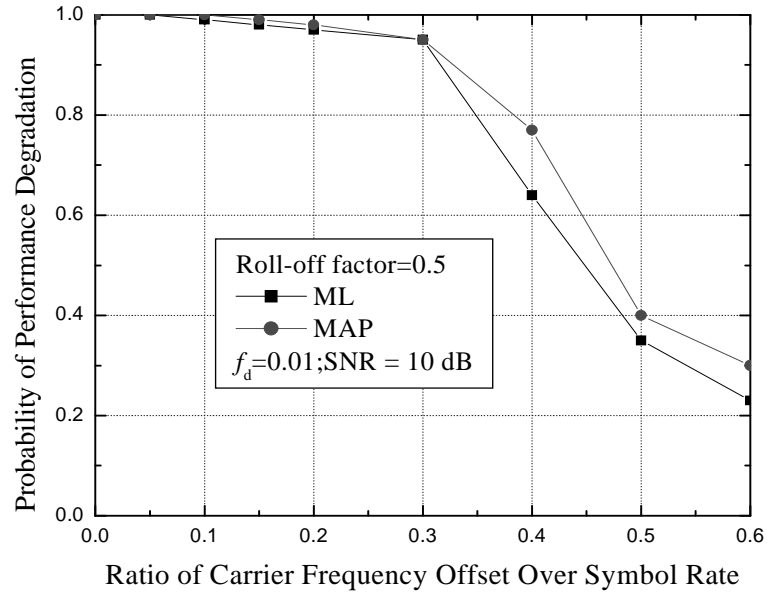


Fig. 5.7 (a) Performance of ML and MAP synchronizers in fading channel vs. f_0

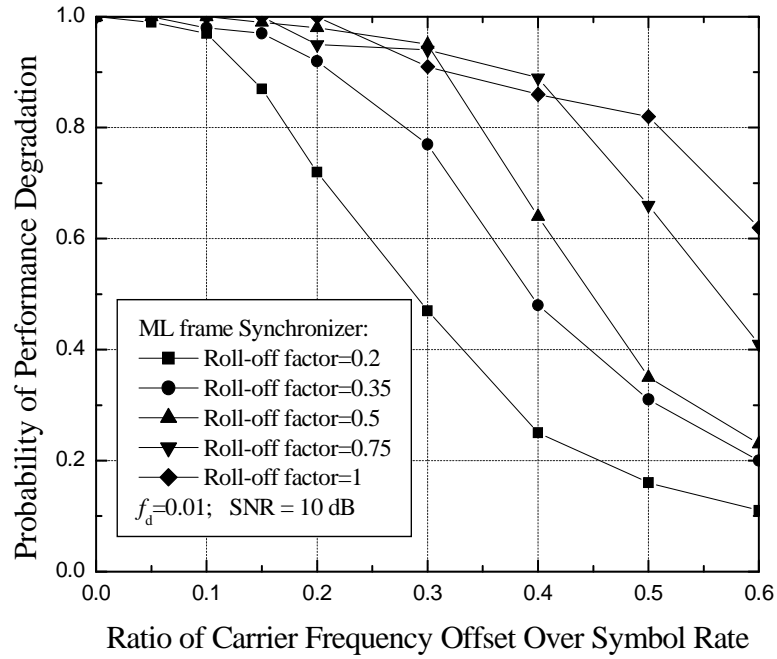


Fig. 5.7 (b) Performance of ML synchronizer in fading channel vs. f_0 and β

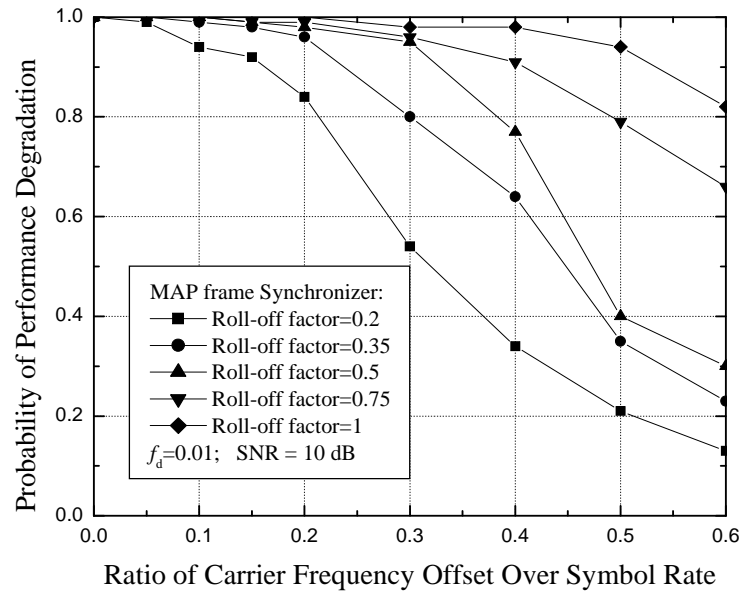


Fig. 5.7 (c) Performance of MAP synchronizer in fading channel vs. f_0 and β

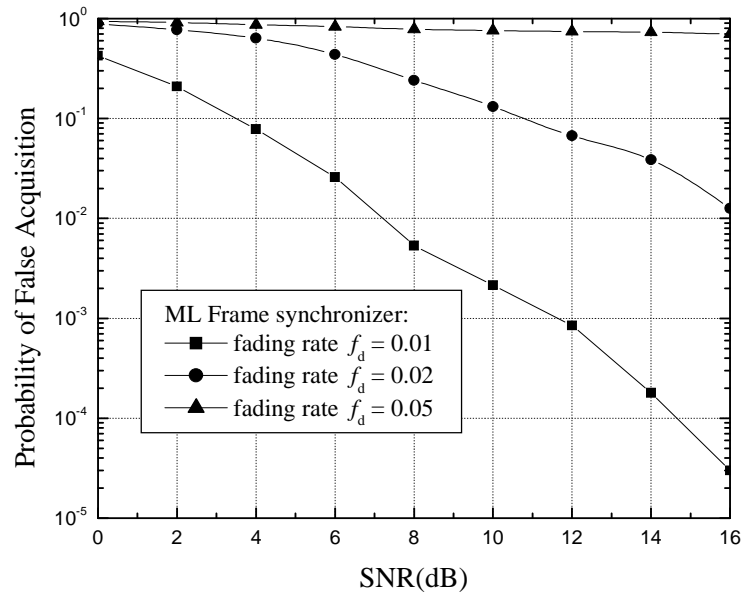


Fig. 5.8 ML frame synchronizer under different fading rates

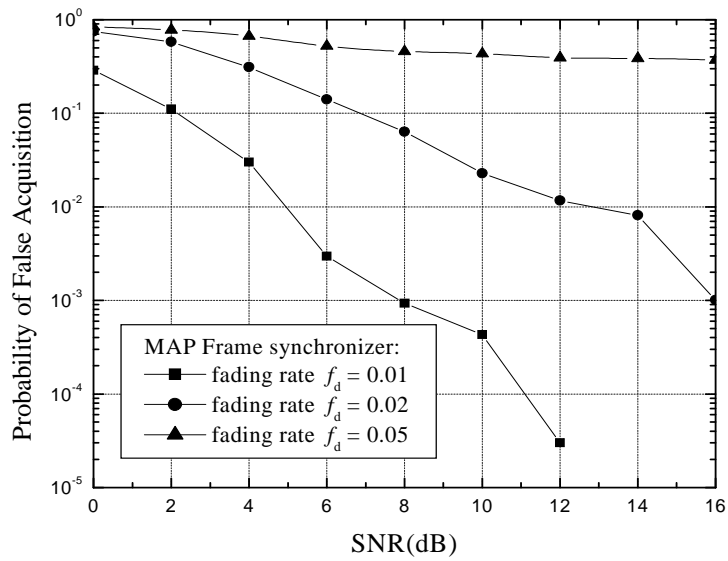


Fig. 5.9 MAP frame synchronizer under different fading rates

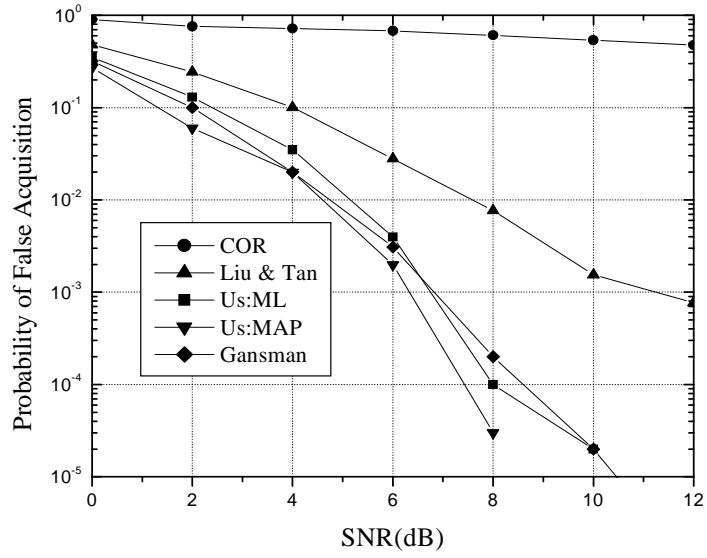


Fig. 5.10 Comparison of synchronizers in AWGN channel without carrier frequency offset and pilot sequence BK11

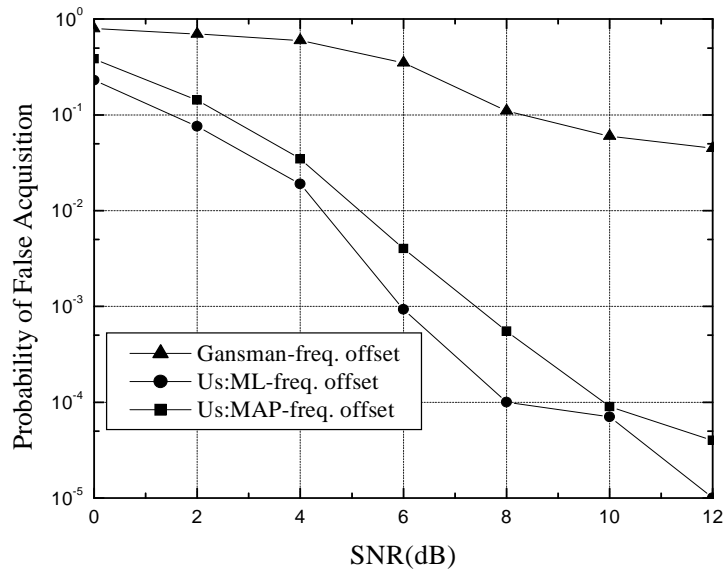


Fig. 5.11 Comparison of synchronizers in AWGN channel with frequency offset = 2% and pilot sequence BK11

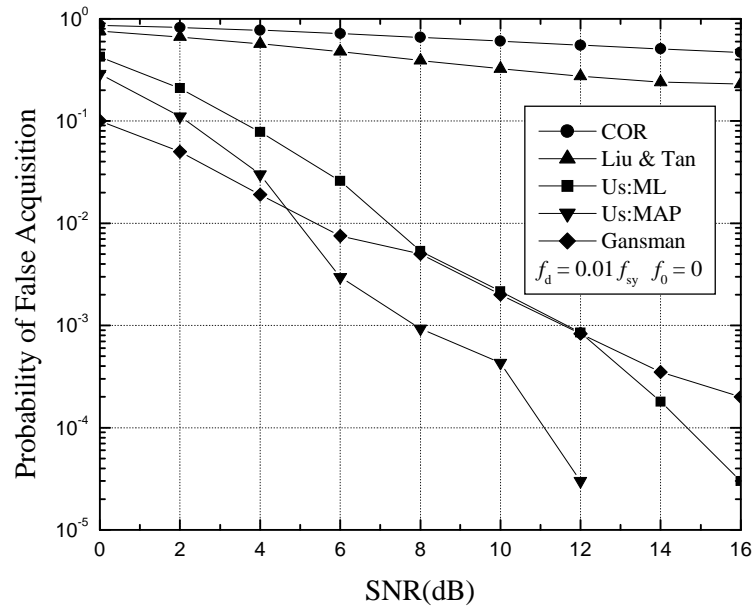


Fig. 5.12 Comparison of synchronizers in fading channel with $f_d = 1\%$ of the symbol rate and no frequency offset. Pilot sequence is BK11

Chapter 6 Conclusions and Future Work

6.1 Conclusions

In this study, frame synchronization techniques for PASM were developed for both AWGN and frequency non-selective Rayleigh fading channels. Compared with Gansman's work [9], in which frame synchronization techniques were obtained based on the coherent detection, this study extends the work by introducing two non-coherent frame synchronization approaches that are tolerant to the frequency offset. In this non-coherent approach, only the magnitude of the received signal is used to obtain the timing of pilot symbols.

One frame synchronization approach is based on a maximum likelihood (ML) estimation algorithm. The other frame synchronization approach is maximum a Posteriori probability (MAP) criterion depending on threshold detection. Both synchronization methods are computed based on pilot-spaced observations. The models implement the ML and the MAP decision criteria - an "argmax" structure indicates the most likely position of the pilot symbol P_0 within a window length of L .

Signal processing in the receiver uses simplifying approximations that rely on relatively high SNR as consistent with the reception of 16-QAM. Computer simulation has been used to test the probability of false acquisition, the mean time to acquisition and the performance degradation for both AWGN and fading channel conditions. Several different lengths and patterns of pilot symbol sequences were used to investigate these synchronizers' performances where every 10th symbol was

a pilot symbol and all the other symbols were randomly selected 16-QAM data symbols.

The simulation results show that proposed MAP frame synchronizer has better performance than ML synchronizer in all cases. With the increase of the length of one full frame, i.e. the different pilot sequences are used, the performance of synchronization becomes better. However, the longer the frame length, the slower the synchronizer converges to synchronization and the mean time to acquisition is longer correspondingly. Compared with the simulation results of some other existing synchronizers, results from this study show somewhat better performance in both AWGN and fading channels. The standard correlator fails in the AWGN and fading channel no matter if there is frequency offset or not. The Liu & Tan synchronizer is good in the AWGN channel, but failed in fading conditions. Gansman's synchronizer works well in AWGN and fading channels when there is no frequency offset. Gansman's synchronizer has better performance than ours in lower SNR conditions and ours has better performance than his in higher SNR conditions. This is due to the difference between the approximations rules used to develop the frame synchronization criteria. In Gansman's method, the low SNR rule was used, while in our methods, the high SNR rule was used. The frequency offset is limited primarily by the bandwidth of transmitter and receiver Nyquist filters. While all the other synchronizers failed in the presence of frequency offset, our proposed synchronizers have significantly better performance in presence of larger carrier frequency offsets. This is due to the non-coherent system proposed in this study. Moreover, our methods lead to simple analysis and these methods are somewhat simpler to implement.

6.2 Future Work

The work presented in this thesis shows a novel scheme of frame synchronization for PSAM. However, it is by no means the definitive work on this

study. In this section, a number of suggestions on future work based on this study include:

- PSAM frame structure design:

In this study, it is noted that pilot symbols in the PSAM frame structure are uniformly inserted and spaced. Hence, non-uniformly spaced pilot symbol frame structure could be explored in future to see that how non-uniform pilot symbols inserted frames will change the receiver structure, how they will affect the frame synchronization performance and if an optimum structure exists for the PSAM system.

- Low SNR approximation Rule

Another aspect that is worth serious investigation is the alternative approximation rule, the low SNR approximation rule. In this study, we used high SNR approximation rule to obtain our simple frame synchronization criterions. However, main difficulty in applying a low SNR approximation rule is that the resultant expressions are not similar to a Gaussian distribution, which prevents effective simplification in the subsequent development. Therefore it could result in a more complicated mathematical expression than the high SNR approximations rule.

- The effect of symbol timing error

In this study, symbol synchronization is assumed to be perfectly recovered before the investigation of frame synchronization. However, in real communication systems, symbol timing errors exist and become worse in low SNR conditions. It is important to further investigate the effect of this error to the performance of frame synchronizer by simulation and mathematical means.

- Frame synchronization evaluations:

A few minor extensions can be made to the frame synchronization evaluation. First it could be extended to a Rician fading model. Second it could be extended to

consider additive noise which is not white. However, it could be a difficult problem to deal with, because it is hard to simplify the non-white noise to an easy model.

- PSAM in frequency selective fading:

Typical PSAM system is used in frequency nonselective fading channels where the delay spread is small so the different multi-paths can be combined into one multiplicative distortion process. If the delay spread is large, intersymbol interference is induced and some type of blind equalization technique is used instead of PSAM. Therefore, a good project would be extended the frame synchronization of PSAM to frequency selective channels and compare its performance to that of the blind equalization.

- Implementation extensions:

In this study, we used 16-QAM to simplify our analysis and implementation. However, according to the characterization of the square constellations 16-QAM scheme, we think this non-coherent method could be extended to other larger constellations, such as 64-QAM scheme. There are different levels of magnitude on the constellation of 64-QAM. Therefore it is possible to use the similar idea we applied in this study on how to define the pilot symbols, we can map the binary pilot sequence into 64-QAM data set and thus design a frame synchronization scheme based on 64-QAM format.

References

- [1] R. A. Scholtz, "Frame synchronization techniques," *IEEE Transactions on Communications*, vol. COM-28, pp. 1204-1212, August, 1980.
- [2] J. J. Stiffler, *Theory of Synchronous Communications*. Englewood Cliffs, New Jersey, Prentice Hall, 1971.
- [3] H. Meyr and G. Ascheid, *Synchronization in Digital Communications*. New York, Wiley, 1990.
- [4] R. H. Barker, "Group synchronization of binary digital system," in *Communication Theory*, W. Jackson, Ed., London, England, Butterworth, pp. 273-287, 1953.
- [5] J. L. Massey, "Optimum frame synchronization," *IEEE Transactions on Communications*, vol. COM-20(2), pp. 115-119, April, 1972.
- [6] G. L. Lui and H. H. Tan, "Frame synchronization for Gaussian channels," *IEEE Transactions on Communications*, vol. COM-35, pp. 818-829, August, 1987.
- [7] B. H. Moon and S. S. Soliman, "ML frame synchronization for the Gaussian channel with ISI," in *Proceedings of IEEE International Conference on Communications*, pp. 1698-1702, Denver, June, 1991.

- [8] P. Robertson, "Maximum likelihood frame synchronization for flat fading channels," in *Proceedings of IEEE International Conference on Communications*, pp. 1426-1430, Chicago, June, 1992.
- [9] J. A. Gansman, M. P. Fitz and J. V. Krogmeier, "Optimum and suboptimum frame synchronization for Pilot-Symbol-Assisted-Modulation," *IEEE Transactions on Communications*, vol. COM-45, pp. 1327-1337, October, 1997.
- [10] J. P. McGeehan and A. J. Bateman, "Phase locked transparent tone-in-band (TTIB): A new spectrum configuration particularly suited to the transmission of data over SSB mobile radio networks," *IEEE Transactions on Communications*, vol. COM-32, pp. 81-87, January, 1984.
- [11] A. J. Bateman et al., "Speech and data communications over 942 MHz TAB single sideband mobile radio systems incorporating feed-forward signal regeneration," *IEEE Transactions on Vehicular Technology*, vol. VT-34, pp. 13-21, February, 1985.
- [12] F. Davarian, "Mobile digital communications via tone calibration," *IEEE Transactions on Vehicular Technology*, vol. VT-36, pp. 55-62, May, 1987.
- [13] P. M. Martin et al., "The implementation of a 16-QAM mobile data system using TTIB-based fading correction technique," in *Proceedings of IEEE Transactions on Vehicular Technology Conference*, pp. 71-76, Philadelphia, June, 1988.
- [14] J. H. Lodge and M. L. Moher, "Time diversity for mobile satellite channels using trellis coded modulations," *IEEE Global Telecommunications Conference*, Tokyo, December, 1987.

- [15] M. L. Moher and J. H. Lodge, "TCMP-A modulation and coding strategy for Rician fading channels," *IEEE Journal on Selected Areas in Communications*, vol. 7, pp. 1347-1355, December, 1989.
- [16] J. K. Cavers, "An analysis of pilot symbol assisted modulation for Rayleigh fading channels," *IEEE Transactions on Vehicular Technology*, vol. VT-40, pp. 686-693, November, 1991.
- [17] S. Sampei and T. Sunaga, "Rayleigh fading compensation for QAM in land mobile radio communications," *IEEE Transactions on Vehicular Technology*, vol. VT-42, pp. 137-147, May, 1993.
- [18] W. T. Webb and L. Hanzo, "Modern quadrature amplitude modulation: Principles and applications for fixed and wireless channels," *IEEE Press-John Wiley co-publication*, pp. 557, 1994.
- [19] Ian A. Glover and Peter M. Grant, *Digital Communications, 2nd edition*. Person Education, 2004.
- [20] J. G. Proakis, *Digital Communications, 3rd edition*. McGraw-Hill, 1995.
- [21] N. Gerein, "A special diversity scheme for fixed point indoor wireless communication," M. Sc. thesis, University of Saskatchewan, SK, 2004.
- [22] A. Papoulis, *Probability, Random Variables and Stochastic Processes*. McGraw-Hill, 1991.
- [23] J. K. Cavers, "On the validity of the slow and moderate fading models for matched filter detection of Rayleigh fading signals," *Canadian Journal of Electrical and Computer Engineering*, vol. 17 (10), pp. 183-189, November, 1992.

- [24] W. C. Jakes, *Microwave Mobile Communications*. IEEE Press, 1974.
- [25] J. R. Barry, Edward A. Lee and David G. Messerschmitt, *Digital Communication, 3rd edition*. Kluwer Academic Publishers, Boston, 1988.
- [26] M. S. Roden, *Digital Communication Systems Design*. Prentice Hall, New Jersey, 1988.
- [27] J. G. Proakis, *Communication Systems Engineering*. Prentice Hall, New Jersey, 1994.
- [28] Q. Zhang, "Frame synchronization for pilot symbol assisted modulation," M. Sc. thesis, University of Saskatchewan, SK, 2002.
- [29] H. Jia and D. E. Dodds, "Frame synchronization for PSAM in AWGN and Rayleigh fading channels," *Proceedings of IEEE Canadian Conference on Electrical and Computer Engineering*, pp. 2290-2296, Saskatoon, May, 2005.
- [30] M. Abramowitz and Irene A. Stegun, *Handbook of Mathematical Functions with Formulas, Graphs, and Mathematical Tables*. National Bureau of Standards, 1964.
- [31] D. E. Dodds, K. Takaya and Q. Zhang, "Frame synchronization for pilot symbol assisted modulation," *Proceedings of IEEE Canadian Conference on Electrical and Computer Engineering*, pp. 52-58, Edmonton, May, 1999.
- [32] User Manual of Matlab and Simulink, available on company website: <http://www.mathworks.com>, The MathWorks, Inc.

- [33] B. Persson, D. E. Dodds and R. J. Bolton, "A segmented matched filter for CDMA code synchronization in systems with Doppler frequency offset," *Proceedings of IEEE Global Telecommunications Conference*, vol. 1, pp. 648-653, San Antonio, November, 2001.

Appendix A: Fading Channel with Frequency and Phase Error

The channel model in equation (2.15) is the simplest based on the assumptions made in Chapter 2. However, there is a quite significant problem neglected in the previous discussion. This problem is the local carrier frequency offset and phase error.

Although good carrier recovery is assumed before the frame synchronization stage, it is not possible for a real communication system to have perfect carrier synchronization. It is hard to tune the local oscillator in receiver exactly to match the oscillator in transmitter, because both oscillators in transmitter and receiver cannot be made exactly the same physically, and thus the frequencies generated by both oscillators are not exactly the same. Therefore it is difficult for the receiver to coherently demodulate the received signal precisely. To account for the effect of carrier frequency offset and phase error in the frame synchronization scheme, it is necessary to include it in the channel model.

According to the 16-QAM receiver in Fig 2.1 (b), the received signal can be conveniently expressed as

$$x(t) = \text{Re}[s(t)a(\tau ; t)e^{j\theta(t)}e^{j2\pi f_c t}]. \quad (\text{A.1})$$

where $\text{Re}[A]$ means the real part of a complex signal, $x(t)$ is the bandpass received signal, $s(t)$ is the complex continuous time baseband signal, and factor $a(\tau ; t)e^{j\theta(t)}$ is the continuous time expression of the multiplicative fading distortion corresponding to the discrete time expression in equation (2.13), f_c is the carrier frequency at the transmitter.

After coherent demodulation and low-pass square root raised cosine receiver filter, the baseband signal is obtained as

$$r(t) = s(t)a(\tau ; t)e^{j\theta(t)}e^{j(2\pi f_0 t + \phi)}. \quad (\text{A.2})$$

where f_0 is the frequency offset of carrier recovery and ϕ is a constant phase error which is uniformly distributed over $[0, 2\pi]$. Note that both f_0 and ϕ are slow time varying signals, they are approximated by constants because the variations are negligible compared to that of the channel fading.

According to the discussion in Section 2.3.2, the statistical model of fading is considered as Rayleigh fading, which means that envelope of $a(\tau ; t)$ has a Rayleigh probability density distribution (PDF) and phase $\theta(t)$ is uniformly distributed over $[0, 2\pi]$. Since the phase error ϕ has the same uniform probability density distribution over $[0, 2\pi]$ as that of $\theta(t)$, the sum of these two random variables $\theta(t) + \phi$ also has uniform probability density distribution because the summation of phases is modulo of 2π . The sum of $\theta(t)$ and ϕ is denoted as $\hat{\theta}(t)$. Thus, equation (A.2) changes to

$$r(t) = s(t)a(\tau ; t)e^{j\hat{\theta}(t)}e^{j2\pi f_0 t}. \quad (\text{A.3})$$

The baseband fading channel is denoted by $c(t)$ in the channel model (equation 2.15) and here we use $c(t)$ to replace $a(\tau ; t)e^{j\hat{\theta}(t)}$ for channel fading. Adding the Gaussian noise that is ignored initially for the simplicity of analysis, the received baseband signal finally becomes

$$r(t) = c(t)e^{j2\pi f_0 t}s(t) + n(t). \quad (\text{A.4})$$

The continuous time baseband received signals are then sampled by the symbol sampler and fed into frame synchronizer to be processed to identify the timing position of pilot symbols.

In the beginning of this thesis, it is assumed that symbol timing is perfectly recovered. In Section 2.3, we have discussed the fading channel is assumed to be frequency non-selective and slow fading for this study, therefore it can be approximated as constant during one symbol period. Hence the continuous time fading signal can be approximated as a discrete time function, which has constant value during a symbol interval and only changes its value at symbol boundaries. To derive the discrete expression of the received samples, the frequency offset represented by f_0 is assumed to be small and within limits that is determined by the square root raised-cosine filter and symbol sampler [9]. When the frequency offset is very small compared with symbol rate, during each symbol interval, the phase change is negligible. Thus we can approximate the frequency offset as discrete phase change that occurs at the boundaries between symbols. Based on all these assumptions and approximations, the discrete received signal after symbol sampler can be expressed as

$$r(k) = c(k)e^{j2\pi f_0 T_s k} s(k) + n(k). \quad (\text{A.5})$$

where $c(k)$ is the discrete time approximation of the multiplicative fading distortion $c(t)$, T_s is the symbol time.

It is noted that although the $c(k)$ is assumed to be circular symmetric, and so is $c(k)e^{j2\pi f_0 T_s k}$, however, $e^{j2\pi f_0 T_s k}$ and $c(k)$ can't be combined together and easily simplify the product to $c(k)$ as in the discussion of the phase offset. This is because that $c(k)e^{j2\pi f_0 T_s k}$ shifts the power spectrum of $c(k)$ and represents another random process that is distinct from the original random process.

The equation (A.5) is important for the non-coherent detection scheme discussion and is important for the performance evaluation in the computer simulations.

Appendix B: Power Spectrum of the Squared Magnitude of Received Signal

In this appendix, the power spectrum of the squared magnitude of the received signal $|r(k)|^2$ is developed. Some assumptions are introduced before detailed development:

- $c(k)$, $s(k)$ and $n(k)$ represent fading signal, transmitted signal and noise respectively. They are baseband complex stationary random processes and can be expressed in complex forms as

$$c(k) = c_I(k) + jc_Q(k), \quad s(k) = s_I(k) + js_Q(k), \quad n(k) = n_I(k) + jn_Q(k).$$

where I denotes the in-phase components and Q denotes the quadrature components. The in-phase and quadrature components of a baseband complex random process have independent and identical distribution (i.i.d).

- $c(k)$, $s(k)$ and $n(k)$ have variance 1, σ_s^2 and σ_n^2 respectively. In this study, fading signal $c(k)$ is modeled as a Rayleigh fading, which is a zero-mean complex-valued random process and its variance is normalized to unity. $s(k)$ is from the 16-QAM data symbol set, which has zero mean as discussed in Section 2.1. Noise term $n(k)$ is the zero-mean additive white Gaussian noise throughout the study. Therefore $c(k)$, $s(k)$ and $n(k)$ are all zero-mean random process and each component random process, i.e. in-phase component or quadrature component, is zero mean. Thus we obtain $E(c_I^2) = E(c_Q^2) = 0.5$, $E(s_I^2) = E(s_Q^2) = 0.5\sigma_s^2$, and $E(n_I^2) = E(n_Q^2) = 0.5\sigma_n^2$.
- $s(k)$ and $n(k)$ are independent identical distributed (i.i.d) random variables for different values of k . This implies that their power spectrums are constants over the frequency range of bandwidth.

Besides above assumptions, the following notations are defined to simplify the discussion.

$$R_{r^2}(l) = E\{|r(k)|^2|r(k-l)|^2\} \text{ Denotes the autocorrelation of } |r(k)|^2$$

$$R_{c^2}(l) = E\{|c(k)|^2|c(k-l)|^2\} \text{ Denotes the autocorrelation of } |c(k)|^2$$

$$R_{s^2}(l) = E\{|s(k)|^2|s(k-l)|^2\} \text{ Denotes the autocorrelation of } |s(k)|^2$$

$$R_{n^2}(l) = E\{|n(k)|^2|n(k-l)|^2\} \text{ Denotes the autocorrelation of } |n(k)|^2$$

and $\sigma_c^2 = E(|c(k)|^2)$, $\sigma_s^2 = E(|s(k)|^2)$ and $\sigma_n^2 = E(|n(k)|^2)$ denote the variance of signal $c(k)$, $s(k)$ and $n(k)$ correspondingly.

Before starting with the discussion of $|r(k)|^2$, we need to know $R_{c^2}(l)$, $R_{s^2}(l)$ and $R_{n^2}(l)$. According to the definition of autocorrelation function, for a complex-valued stationary process $c(k)$

$$\begin{aligned} R_c(l) &= \frac{1}{2} E\{c(k)c^*(k-l)\} \\ &= \frac{1}{2} E\{[c_I(k) + jc_Q(k)][c_I(k-l) - jc_Q(k-l)]\} \\ &= \frac{1}{2} E\{[c_I(k)c_I(k-l)] + [c_Q(k)c_Q(k-l)] + j[c_I(k)c_Q(k-l)] - [c_Q(k)c_I(k-l)]\} \\ &= \frac{1}{2} \{R_{c_I}(l) + R_{c_Q}(l) + j[R_{c_Ic_Q}(l) - R_{c_Qc_I}(l)]\} \\ &= R_{c_I}(l), \end{aligned} \tag{B.1}$$

where $R_{c_I}(l)$ and $R_{c_Q}(l)$ are autocorrelation functions of the in-phase component $c_I(k)$ and the quadrature component $c_Q(k)$ respectively; $R_{c_Ic_Q}(l)$ and $R_{c_Qc_I}(l)$ are the cross-correlation of these two components. The results of (B.1) is obtained based on the assumption that $c_I(k)$ and $c_Q(k)$ are independent, identically distributed, zero-mean Gaussian random process.

Therefore, the autocorrelation function of $|c(k)|^2$ is given as

$$\begin{aligned}
R_{c^2}(l) &= \mathbb{E}\{|c(k)|^2|c(k-l)|^2\} \\
&= \mathbb{E}\{[c_I^2(k) + c_Q^2(k)][c_I^2(k-l) + c_Q^2(k-l)]\} \\
&= \mathbb{E}\{c_I^2(k)c_I^2(k-l) + c_Q^2(k)c_Q^2(k-l) + c_I^2(k)c_Q^2(k-l) + c_Q^2(k)c_I^2(k-l)\} \\
&= 2\mathbb{E}\{c_I^2(k)c_I^2(k-l)\} + \mathbb{E}\{c_I^2(k)c_Q^2(k-l)\} + \mathbb{E}\{c_Q^2(k)c_I^2(k-l)\} \\
&= 2\mathbb{E}\{c_I^2(k)c_I^2(k-l)\} + 2\mathbb{E}\{c_I^2(k)\}\mathbb{E}\{c_Q^2(k)\} \\
&= 2R_{c_I^2}(l) + 2\left(\frac{1}{2}\sigma_c^2\right)^2 \\
&= 2R_{c_I^2}(l) + \frac{1}{2}. \tag{B.2}
\end{aligned}$$

Equation (B.2) is obtained based on the assumptions that $\sigma_c^2 = 1$ and the in-phase and the quadrature components are i.i.d. and zero mean.

According to Papoulis in [22], if random variable \mathbf{v} is a normal stationary process with zero mean and autocorrelation $R_v(\tau)$, and $R_v(0) = \sigma_v^2$, for another random process $z = \mathbf{v}^2$, the autocorrelation of z is expressed as

$$R_z(\tau) = R_{v^2}(\tau) = R_v^2(0) + 2R_v^2(\tau). \tag{B.3}$$

So we have

$$R_{c_I^2}(l) = R_{c_I}^2(0) + 2R_{c_I}^2(l). \tag{B.4}$$

Substituting (B.4) into (B.2) gives

$$R_{c^2}(l) = 4R_{c_I}^2(l) + 1 \tag{B.5}$$

and when $l = 0$, we get $R_{c^2}(0) = 2$.

In the similar way, the autocorrelation function for $|s(k)|^2$ and $|n(k)|^2$ are given as

$$\begin{aligned}
R_{s^2}(l) &= E\{|s(k)|^2 |s(k-l)|^2\} \\
&= E\{[s_I^2(k) + s_Q^2(k)][s_I^2(k-l) + s_Q^2(k-l)]\} \\
&= E\{s_I^2(k)s_I^2(k-l) + s_Q^2(k)s_Q^2(k-l) + s_I^2(k)s_Q^2(k-l) + s_Q^2(k)s_I^2(k-l)\} \\
&= 2R_{s^2}(l) + 2\left(\frac{1}{2}\sigma_s^2\right)^2 \\
&= 2[R_{s_I^2}(0) + 2R_{s_I^2}(l)] + \frac{1}{2}\sigma_s^4 \\
&= \frac{1}{2}\sigma_s^4 + 4\left[\frac{1}{2}\sigma_s^2\delta_l(l)\right]^2 + \frac{1}{2}\sigma_s^4 \\
&= \sigma_s^4\delta_l(l) + \sigma_s^4.
\end{aligned} \tag{B.6}$$

and

$$\begin{aligned}
R_{n^2}(l) &= E\{|n(k)|^2 |n(k-l)|^2\} \\
&= \sigma_n^4\delta_l(l) + \sigma_n^4.
\end{aligned} \tag{B.7}$$

In equation (3.3), the squared magnitude of received signal $|r(k)|^2$ is expressed as

$$|r(k)|^2 = |c(k)|^2 |s(k)|^2 + |n(k)|^2 + 2\operatorname{Re}[c(k)s(k)n^*(k)], \tag{B.8}$$

and thus the autocorrelation of $|r(k)|^2$ is expressed as

$$\begin{aligned}
R_{r^2}(l) &= E\{|r(k)|^2 |r(k-l)|^2\} \\
&= E\left\{\left[|c(k)|^2 |s(k)|^2 + |n(k)|^2 + 2\operatorname{Re}[c(k)s(k)n^*(k)]\right]\right. \\
&\quad \left.\times \left[|c(k-l)|^2 |s(k-l)|^2 + |n(k-l)|^2 + 2\operatorname{Re}[c(k-l)s(k-l)n^*(k-l)]\right]\right\}
\end{aligned}$$

$$\begin{aligned}
&= E \left\{ \underbrace{\left\{ |c(k)|^2 |c(k-l)|^2 |s(k)|^2 |s(k-l)|^2 \right\}}_{\text{Term 1-1}} + \underbrace{\left\{ |n(k)|^2 |n(k-l)|^2 \right\}}_{\text{Term 1-2}} \right. \\
&\quad + \underbrace{\left\{ |c(k)|^2 |s(k)|^2 |n(k-l)|^2 \right\} + \left\{ |c(k-l)|^2 |s(k-l)|^2 |n(k)|^2 \right\}}_{\text{Term 1-2}} \\
&\quad + \underbrace{4 \operatorname{Re}[c(k)s(k)n^*(k)] \operatorname{Re}[c(k-l)s(k-l)n^*(k-l)]}_{\text{Term 2}} \\
&\quad + \underbrace{2 \operatorname{Re}[c(k)s(k)n^*(k)] \left\{ |c(k-l)|^2 |s(k-l)|^2 + |n(k-l)|^2 \right\}}_{\text{Term 3}} \\
&\quad \left. + \underbrace{2 \operatorname{Re}[c(k-l)s(k-l)n^*(k-l)] \left\{ |c(k)|^2 |s(k)|^2 + |n(k)|^2 \right\}}_{\text{Term 4}} \right\}. \tag{B.9}
\end{aligned}$$

Term 3 and Term 4 in the above equation equal to zero after being taken ensemble average, because the random processes $s(k)$ and $n(k)$ are zero mean. Term 2 is expanded using the real and imaginary parts of random signal as

$$\begin{aligned}
&E \left\{ 4 \operatorname{Re}[c(k)s(k)n^*(k)] \operatorname{Re}[c(k-l)s(k-l)n^*(k-l)] \right\} \\
&= 4E \left\{ \left\{ c_I(k)s_I(k)n_I(k) - c_Q(k)s_Q(k)n_I(k) + c_Q(k)s_I(k)n_Q(k) + c_I(k)s_Q(k)n_Q(k) \right\} \right. \\
&\quad \times \left\{ c_I(k-l)s_I(k-l)n_I(k-l) - c_Q(k-l)s_Q(k-l)n_I(k-l) \right. \\
&\quad \left. \left. + c_Q(k-l)s_I(k-l)n_Q(k-l) + c_I(k-l)s_Q(k-l)n_Q(k-l) \right\} \right\} \\
&= 4E \left\{ c_I(k)s_I(k)n_I(k)c_I(k-l)s_I(k-l)n_I(k-l) \right. \\
&\quad + c_Q(k)s_Q(k)n_I(k)c_Q(k-l)s_Q(k-l)n_I(k-l) \\
&\quad + c_Q(k)s_I(k)n_Q(k)c_Q(k-l)s_I(k-l)n_Q(k-l) \\
&\quad \left. + c_I(k)s_Q(k)n_Q(k)c_I(k-l)s_Q(k-l)n_Q(k-l) \right\} \\
&= 4 \left\{ R_{cI}(l)R_{sI}(l)R_{nI}(l) + R_{cQ}(l)R_{sQ}(l)R_{nI}(l) \right. \\
&\quad \left. + R_{cQ}(l)R_{sI}(l)R_{nQ}(l) + R_{cI}(l)R_{sQ}(l)R_{nQ}(l) \right\} \\
&= 16R_{cI}(l)R_{sI}(l)R_{nI}(l), \tag{B.10}
\end{aligned}$$

In the above equation, $c_I(k)$, $s_I(k)$ and $n_I(k)$ are in-phase components of complex $c(k)$, $s(k)$ and $n(k)$ respectively; $c_Q(k)$, $s_Q(k)$ and $n_Q(k)$ are quadrature components. Let $R_{xy}(l)$ denote the autocorrelation function for the y components of \mathbf{x} signal, where \mathbf{x} represents c , s or n and y represents I or Q . For instance, $R_{cI}(l)$ is the autocorrelation function for the in-phase component of fading signal $c(k)$. If we further assume $s(k)$ and $n(k)$ are white random processes with variance σ_s^2 and σ_n^2 respectively, and $c(k)$ has unit variance, then B.10 can be further reduced to

$$16R_{cI}(l)R_{sI}(l)R_{nI}(l) = 2\sigma_s^2\sigma_n^2\delta_l(l), \quad (\text{B.11})$$

Term 1-1 is equal to

$$R_{c^2}(l)R_{s^2}(l) + R_{n^2}(l) = R_{c^2}(l)[\sigma_s^4\delta_l(l) + \sigma_s^4] + [\sigma_n^4\delta_l(l) + \sigma_n^4], \quad (\text{B.12})$$

Term 1-2 in B.9 can be simplified to

$$\begin{aligned} & E\left\{\left\{|c(k)|^2|s(k)|^2|n(k-l)|^2\right\} + \left\{|c(k-l)|^2|s(k-l)|^2|n(k)|^2\right\}\right\} \\ &= 2E\left\{|c(k)|^2\right\}E\left\{|s(k)|^2\right\}E\left\{|n(k)|^2\right\} \\ &= 2\sigma_s^2\sigma_n^2, \end{aligned} \quad (\text{B.13})$$

Substituting equations (B.11), (B.12) and (B.13) into equation (B.9), the expression of $R_{r^2}(l)$ is finally given as

$$\begin{aligned} R_{r^2}(l) &= R_{c^2}(l)[\sigma_s^4\delta_l(l) + \sigma_s^4] + [\sigma_n^4\delta_l(l) + \sigma_n^4] + 2\sigma_s^2\sigma_n^2 + 2\sigma_s^2\sigma_n^2\delta_l(l) \\ &= R_{c^2}(l)\sigma_s^4 + [R_{c^2}(0)\sigma_s^4 + 2\sigma_s^2\sigma_n^2 + \sigma_n^4]\delta_l(l) + 2\sigma_s^2\sigma_n^2 + \sigma_n^4 \\ &= [R_{c^2}(l) - 1]\sigma_s^4 + (2\sigma_s^4 + 2\sigma_s^2\sigma_n^2 + \sigma_n^4)\delta_l(l) + (\sigma_s^2 + \sigma_n^2)^2. \end{aligned} \quad (\text{B.14})$$

Taking Fourier transform on both sides of (B.14), we obtain the power spectrum of $|r(n)|^2$ as

$$S_{r^2}(f) = \sigma_s^4 [S_{c^2}(f) - \delta(f)] + (2\sigma_s^4 + 2\sigma_s^2\sigma_n^2 + \sigma_n^4) + (\sigma_s^2 + \sigma_n^2)^2 \delta(f). \quad (\text{B.15})$$

This equation plays a key role in development of the fading signal estimation in Chapter 3. The spectrum of $|r(k)|^2$ is illustrated in Fig. 3.1.

Taking discrete time Fourier transform of (B.5), i.e. the autocorrelation of $|c(k)|^2$, we obtain the power spectrum of $|c(k)|^2$,

$$\begin{aligned} S_{c^2}(f) &= \text{F}\{4R_{cl}^2(l) + 1\} \\ &= 4S_{cl}(f) * S_{cl}(f) + \delta(f) \\ &= 4S_c(f) * S_c(f) + \delta(f). \end{aligned} \quad (\text{B.16})$$

where $\text{F}[A]$ means the Fourier transform of A and the symbol $*$ represents the convolution operation. Equation (B.15) shows that the power spectrum of $|c(k)|^2$ is made of two components, covariance spectrum and a spectral line at $f = 0$. The covariance spectrum is a self-convolution of the power spectrum for $c(k)$ and it represents the variation in $|c(k)|^2$. Due to the convolution operation, the bandwidth of spectrum $S_c(f) * S_c(f)$ is twice the bandwidth of $S_c(f)$. That means the highest frequency components in $|c(k)|^2$ is two times of the maximum Doppler shift in $c(k)$, and this is due to the nonlinear effect of the square law device. The spectral line at dc frequency indicates the mean value of $|c(k)|^2$.